S
FACULTY OF SCIENCE AND TECHNOLOGY
MASTER THESIS

Study programme / specialisation: Structural Engineering and Materials Science/ Offshore structures	The spring semester, 2022 Open
Author: Mondir Mohammed Alani	*Mondir M Alani* (Signature author)
Course coordinator: Sudath C. Siriwardane Supervisor(s): Associate Professor, Yanyan Sha	
Thesis title: Analysis and design of floating bridge subjected to seismic motion and seismic-induced tsunami	
Credits (ECTS): 30	
Keywords: K12 Floating bridge Orcaflex Time-domain Analysis Ground motion Seismic motion Time history Seismic-induced tsunami	Pages: 107 + appendix: 16 Stavanger, 14/06/2022

Abstract

The objective of this master's thesis is to examine one of the bridge designs suggested by the Norwegian Public Road Administration (NPRA) for the Bjørnafjorden crossing. The main goal for NPRA is to build a continuous coastal roadway from Kristiansand to Trondheim, eliminating the need for ferries.

AMC (Aas-Jakobsen, Multiconsult and Cowi) proposed bridge concept (K12) is a curving end-anchored floating bridge with 38 steel pontoons spaces around 125 meters from each other. The bridge is elevated at its southern end, allowing ships to pass. According to NPRA, if the project is finished, this bridge will be the longest of its kind.

The scope of study in this thesis is to mimic the AMC model in Orcaflex and do a time-domain analysis of the bridge when it's subjected to seismic motion and seismic-induced tsunami. Dr. Kaiming Bi created the seismic ground motions, and the spatially correlated time histories were created using the design spectrum from Eurocode 8-2.

During the thesis, the bridge modelled in Orcaflex is utilized to do numerical assessments on the bridge, which has been subjected to seismic excitations and seismic induced tsunami. The bridge's motion and forces are gathered through simulations to see how the bridge reacts to the external motions.

The floating bridge's simulation indicates that it is viable when subjected to seismic excitations and tsunamis with low to moderate seismicity. To put it another way, seismic excitations with PGA=0.08g have little to no effect on the K12 floating bridge.

Acknowledgments

Table of contents

List of figures

List of tables

Abbreviations

EC	Eurocode
NPRA	Norwegian Public Road Administration
TLP	Tension leg platform
MSL	Mean surface level
SDOF	Single degree of freedom
MDOF	Multiple degree of freedom
PSD	Power spectral density
RC	Reinforced concrete
SFT	Submerged Floating Tunnels
TLP	Tension leg platform
PGA	Peak Ground Acceleration
KN	Kilonewton
MN	Meganewton
CHPO	Constant-height pushover
TH	Time-history
VHPO	Variable-height pushover

Symbols

A	Cross-section area
A_{Ed}	design seismic action
C	Damping matrix
E_{Edi}	Component of ground motion in direction i
E	Elastic modulus
G_k	characteristic permanent action
I_x	Moment of inertia (x-axis)
I_y	Moment of inertia (y-axis)
I_z	Moment of inertia (z-axis)
L_{lim}	Limited length of the continuous bridge deck
L_{tot}	Total length of the continuous bridge deck
L_g	Distance between which the ground motions may be considered as completely correlated NS-EN 1998-2:2005
M_{rd}	Moment resistance
P_k	characteristic value of prestressing
Q_k	characteristic variable action
S	Soil factor for ground types defined in NS-EN 1998-1:2004, Cl 3.2.2.2
$S_e(T)$	Horizontal elastic response spectrum
$S_{ve}(T)$	Vertical elastic response spectrum
$S_d(T)$	Spectral acceleration of the design spectrum
T	period of the fundanlental nlode of vibration for the direction under consideration
T_B	Lower limit of the period of the constant spectral acceleration branch NS-EN 1998-1:2004
T_C	Upper limit of the period of the constant spectral acceleration branch NS-EN 1998-1:2004
T_D	Value defining the beginning of the constant displacement response range of the spectrum; NS-EN 1998-1:2004
$W_{i,eff}$	Effective Plastic section modulus about i axis
a_g	Design ground acceleration for ground type A NS-EN 1998-1:2004

a_{gR}	Reference peak ground acceleration for ground type A	
f_y	Yielding strength	
γ_1	importance factor	
γ_M	Material partial factor	
ψ_{21}	Combination factor	
G	Modulus of rigidity	
J	Polar moment of inertia	
K	Stiffness matrix	
M	Mass matrix	
g	Acceleration of gravity (9.81m/s2)	
t	time	
ρ	Water density	

Chapter 1: General

1.1 Introduction

The Norwegian Public Roads Administration (NPRA) aims to achieve a ``ferry-free E39``. The project stretches around 1100 km, starting from the south in Kristiansand to the Trondheim.

Currently, traveling from Kristiansand to Trondheim involves taking eight boats, which adds up to a total travel time of approximately 21 hours. By implementing the proposed improvements to the existing E39, the total amount of time spent traveling across the length of the project will be cut in half. Along this route are also important urban centers such as Stavanger, Ålesund, and Molde. As a result, the amount of time needed to travel between the cities along the route will be cut down, which will benefit the commercial regions and the housing, labor, and service markets.

The project contains several fjord crossings such as Vartdalsfjorden, Bjørnafjorden, Nordfjorden and Sulafjorden to mention a few. These fjords are suggested to be crossed by either tunnel or bridge. Bjørnafjorden has been selected as the object of this thesis and is marked with a red circle in Figure 1-1.

Figure 1-1: Ferry-Free E39 [1]

1.2   Floating bridges

When crossing a vast body of water with a significant amount of depth, floating bridges are an excellent option. When compared to the cost of constructing a long-span fixed bridge, tube, or tunnel, the typical cost of constructing a floating bridge for a crossing that is a couple of kilometers long and has a water depth of more than 60 meters is projected to be three to five times lower. [2]

Rather than permanently installed support pillars, Pontoons are used to construct floating bridges, which can be built on waterways like rivers and fjords. Since they are so sturdy and can span expansive and lengthy bodies of water, bridges of this type are extremely common all over the world. Floating bridges are an option worth considering in areas that have both deep water and a sandy bottom. [3].

The use of floating bridges, also known as pontoon bridges, has been around for quite some time. They were beneficial during times of war when armies needed to be transported across rivers. According to Watanabe [4], Floating Bridges can be traced back to the far past, about the year 2000 B.C.

Figure 1-2: Proposed K12 floating bridge crossing of Bjørnafjorden [5]

There are many different configurations that one might choose for a floating bridge. A few of the possibilities are illustrated down below. Still, in the real world, the only types of pontoon bridges that are used are continuous pontoon bridges and divided pontoon bridges. Although

TLP-supported bridges and submerged floating tunnels have not yet been put into use to cross waterways, plans are now being developed to do so.

1.2.1 Pontoon bridges

Pontoon bridges, continuous and separated, are among the most common bridges utilized for pedestrian and vehicle traffic. These are some of the most up-to-date designs for floating bridges, which feature reinforced, prestressed concrete pontoons or steel pontoons. This bridge may feature an elevated section that is available for use as a passageway for boats.

A continuous pontoon floating bridge is made up of individual pontoons that are connected to form a continuous framework. The size of each individual pontoon is determined by the design requirements, construction facilities, and transportation route limits. The pontoons' tops could be used as a highway, or another structure might be built on top of them.

Separated pontoon bridges are structures that are supported by floating pontoons that are not physically joined to one another, as the name of this type of bridge would imply. The structure needs to be strong and stable to maintain the position of the pontoons. Pontoon bridges with separation between them were used to construct Norway's two new floating bridges.

1.2.2 TLP-supported Floating Bridge

The second idea is a floating bridge that is supported by pillars. A tension leg platform, or TLP for short, supports the bridge pillars. Tethers attach a tension leg platform to the ocean floor. These are lengthy steel pipes that have been pre-tensioned such that the tension forces impart stiffness to the platform, minimizing movements greatly. The tension wires must be able to withstand loads in both the transverse and longitudinal directions, such as wind and waves. This type of bridge technology makes it possible to reduce the number of pontoons without leading to an increase in the number of dynamic impacts. Reducing the number of pontoons also reduces the risk of ship collisions. The proposed bridge would provide an alternative means of transport across the Bjørnafjorden.

Figure 1-3: Section concept suspension bridge [6]

1.2.3 Submerged Floating Tunnels (SFT)

The idea of a submerged floating tunnel (SFT) has grown in popularity to cross the straits. In this design, the structural solution involves buoyancy force on the tunnel body as well as tension in the mooring tethers [7]. Either pontoons are used to keep the structure floating after it has been lowered into the water and fixed in place with mooring tethers attached to the seabed, or the structure is lowered into the water and secured in place with mooring tethers. The SFT solution is shown in Figure 1-4 below. SFT can be a useful solution in situations where conventional crossing methods are impractical due to environmental constraints, such as when the water is deep. Submerged tunnels can be utilized whenever there is a need to cross deep bodies of water. Although this type of passage is not usually referred to as a bridge, it still serves the same function as a bridge would. This style of crossing has never been utilized in the past.

Figure 1-4: Submerged floating tunnel illustration [6]

1.3 Objectives

To model the floating bridge and perform a nonlinear finite element analysis of floating bridges that have been subjected to seismic excitations and seismic induced tsunami is the fundamental objective of this research. Additionally, to being able to withstand the dynamic stresses. A structure that is going to be shaken by earthquakes needs to have a certain level of safety that comes from its strength, ductility, and ability to absorb energy. Because of the unpredictability of the bridge's reaction to the activity, it is important to conduct nonlinear dynamic assessments of the structure. Throughout the course of this thesis, we will make use of Orcaflex to examine how the bridge will react to earthquake excitations and the subsequent tsunami.

A model of the floating bridge is modelled using the Orcaflex software. Before using the program to carry out seismic excitation assessments, one must first have a solid understanding of both the model and the program. With the help of this application, one may observe how the floating bridge responds to different types of ground motions that are produced.

1.4 Problem

Build a model in Orcaflex as close as possible to the NPRA report. Also, familiarize with floating bridge design.

The response of the bridge to various ground vibrations must be evaluated, and design principles for general bridges must be discussed according to various design codes. For floating bridges, the reaction to seismic excitations is unknown, and there are no established design recommendations.

1.5 Scope and Limits

The primary goal of this thesis is to acquire a greater understanding of the structural dynamics of the K12 floating bridge when subjected to seismic excitation and tsunami. The main report that was prepared by AMC will serve as the benchmark against which the model of the bridge will be evaluated. Because of the limited amount of time, most of the information regarding the bridge's properties came from the consultant's report. The primary focus is on gaining an understanding of the modelling of the structure in Orcaflex, as well as observing and comprehending the reaction that the simulations produce in terms of the global response. A time-domain simulation of the model subjected to seismic excitations, and the tsunami that follows the excitation is the main task in this thesis.

Chapter 2: Earthquake and tsunami

2.1 Seismology

Every day, roughly 50 earthquakes strong enough to be felt locally occur around the planet, and every few days, an earthquake capable of causing structural damage happens. Each incident generates seismic waves that travel around the globe, and numerous earthquakes every day produce distant ground vibrations that, while too small to be felt, may be detected with current technology anywhere on the planet. Seismology is the study of these waves and what they reveal about the structure of the Earth and earthquake physics. It is also directly concerned with gaining a better knowledge of the physical mechanisms that create earthquakes and finding ways to tackle the devastating effects they have on humanity. [8]

2.1.1 Plate

Tectonic earthquakes are triggered when plate tectonic boundaries in the crust or lithosphere of the earth shift. As a result of the plates' persistent motion, a few of them eventually become stuck to one another because of friction and become immobile. The other plates will continue to move, which will subject the locked plates to an increased amount of pressure and strain. After some time, the strain energy will become greater than its resistance, and the enormous pressure will push the plates to move extremely quickly, which will ultimately result in a tectonic earthquake. The constant movement of tectonic plates is generated by the convective motion of material in the earth's mantle, which is caused by the heat in the earth's core. This motion is caused by the heat in the earth's core. An earthquake on a tectonic plate releases its stored energy in the form of seismic waves.

2.1.2 Seismic Waves

There is a wide range of sizes and shapes that can be produced by seismic waves, and each of these waves travels in a unique manner. Waves can be broken down into two main groups: body waves and surface waves. However, body waves can only move across the surface of the planet, whereas surface waves, which are similar to ripples on water, can travel through the Earth's interior layers. Seismic energy is released by earthquakes as both body and surface waves.

Body waves travel through the Earth's interior before reaching the surface waves created by an earthquake. The frequency of these waves is higher than that of surface waves. Body waves has two kinds of waves, the primary and secondary waves.

The main type of body wave is known as the P wave, which also goes by the name primary wave. The seismic waves from this type of earthquake travel the farthest and arrive at seismic stations the earliest. P waves are also known as compressional waves since they push and pull in opposite directions. When a P wave is acting on particles, those particles will move in the same direction as the wave. This is referred to as the "direction of wave propagation," and it indicates the path that the energy will take.

The S wave, also known as a secondary wave, is the second wave to come following an earthquake. It's easy to remember because it's the second wave to arrive after an earthquake. A P wave travels at a pace that is 1.7 times that of a S wave. The fact that S waves are unable to move through liquids is the main difference between the two types.
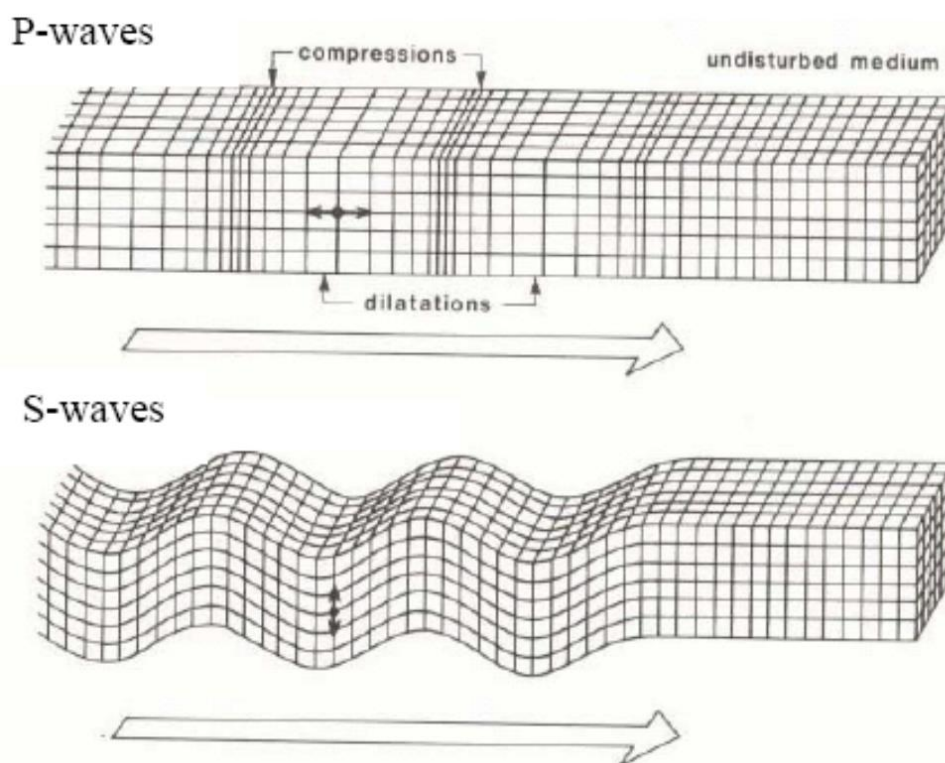
Figure 2-1: : Particle motions associated with P-waves (upper caption) and S-waves (lower caption) [9]

Surface waves travel more slowly and have a lower frequency than body waves because they travel through Earth's material at the planet's surface. On a seismogram, they may be easily differentiated as illustrated in Figure 2-2. Deeper earthquakes produce weaker surface waves, whereas shallow earthquakes produce stronger surface waves.
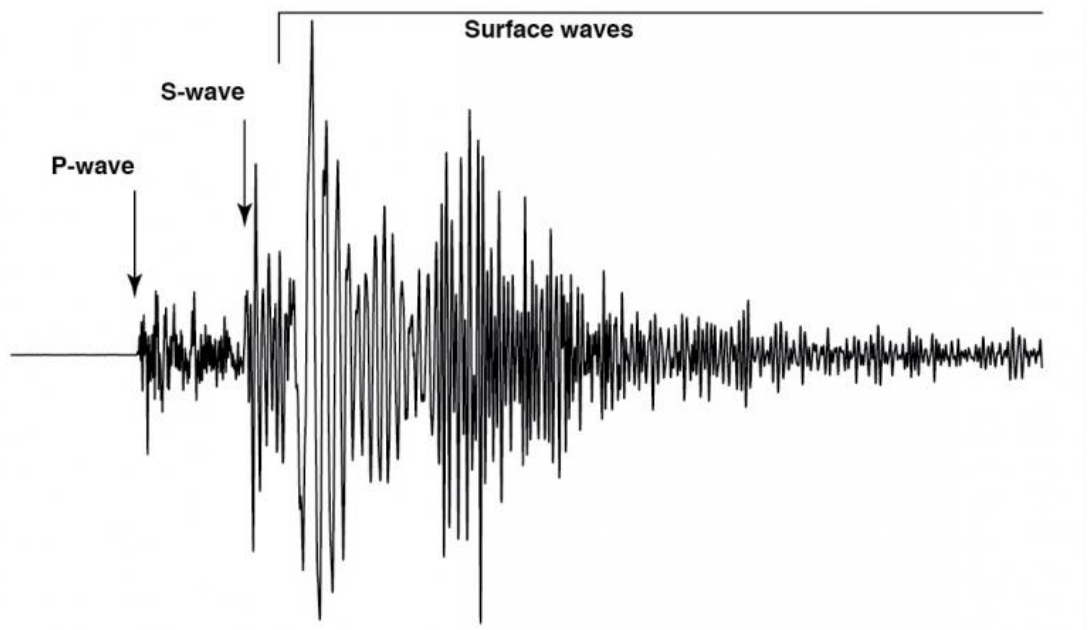
Figure 2-2: Body waves (P and S) and surface waves

2.2 Tsunami

The word tsunami is derived from two Japanese words: "harbor" (tsu) and "wave" (nami). The phenomena were previously known as a tidal wave. Waves caused by abrupt vertical motions of the ocean floor, triggered by massive earthquakes, volcanic eruptions, or undersea explosions, are what this term refers to in the scientific world.

Because of their impulsive nature, tsunamis can be considered transitional events. They have a long period and have a long wavelength. Tsunamis can travel for thousands of kilometers across the open ocean at speeds of 600–800 km per hour, and their effects can be seen hours later on shores [10]

2.2.1 Seismic induced tsunami

An earthquake that occurs on the ocean floor has the potential to cause an abrupt rise or fall in the level of the earth's crust. This movement has the potential to induce the water above it to rise or fall, which will result in the formation of tsunami waves.

2.2.2 Landslides

The same processes that cause landslides to happen on land can also happen on the seafloor. It is more likely for an underwater landslide to happen in areas of the seafloor that are steep and have a lot of sediment, such as the edge of the continental slope. When an underwater landslide takes place, it is possible for a significant quantity of sand, mud, and gravel to move down the slope (possibly following a nearby earthquake). This movement will cause the water level to drop, which may result in a tsunami that spreads over the ocean.

Chapter 3: Literature review

3.1   Available Standards

There are multiple standards to choose from regarding the seismic analysis for bridges. The Eurocode 8 is the main standard for design of structures for earthquake resistance. Part 1 of Eurocode 8: EN 1998-1 [11] targets the general rules, seismic actions and rules for buildings subjected to earthquake. While for Part 2 of Eurocode 8: NS-EN 1998-2 [12], is used as design code for bridges against seismic actions. The United States uses ASCE/SEI7-16 for seismic design criteria and requirements [13] among other standards. The NPRA has its own criteria for design of bridges, ferry quays and other load-bearing structures in the public road [14]. A mix of N400, European standard and the ASCE standard will be used in this thesis.

3.1.1   European Standard

EN 1998-2:2005 specifies specific Performance Requirements, Compliance Criteria, and Application Rules for earthquake resistance on traditional bridges. Design of floating bridges is not included in the scope of EN 1998-2:2005, according to clause 1.1.1(4). The design code's purpose is to keep the bridge operable after an earthquake or to enable considerable damage to the bridge without it collapsing. When building a bridge to withstand earthquake loads, it's crucial to keep human lives in mind. Simplified criteria may be devised in the case of low seismicity. According to Tabell NA.2(904) of NS-EN 1998-2 the design method depends on the seismic class and $a_s S$. Table 3-1 shows Tabell NA.2 translated to English.

Note: The abbreviations EC8-1 stands for NS-EN 1998-1 and EC8-2 stands for NS-EN 1998-2

Table 3-1: Requirements for analysis method (Tabel NA.2(904) [12])

Seismic class	$a_s S > 1.2\,m/s^2$	$0.5\,m/s^2 < a_s S < 1.2\,m/s^2$	$a_s S < 0.5\,m/s^2$
I	0	0	0
II	1	0	0
III	2	1	0
IV	2	2	1
0: There are no special requirements for the choice of analysis method 1: Method for analysis with a degree of freedom in accordance with section 4.2.2 or equivalent simplified methods of analysis may be used where this is considered sufficient in accordance with NS-EN 1998. Otherwise, Multi-degree-of-freedom analysis according to the response spectrum method shall be used 2: Multi-degree-of-freedom Analysis according to the response spectrum method shall be used. Socially important road bridges with $L_{tot} < 50m$ and $a_s S < 1.2\,m/s^2$ can be analysed according to method 1			

In NS-EN 1998-2, bridges are categorized into importance classes based of collapse in the case of earthquake. Table 3-1 shows indicative table for selection of seismic class for road bridges, and Table 3-2 shows the separate importance factor depending on the importance classes. The importance factor value is also used to calculate the design ground acceleration a_g.

Table 3-2: Seismic factor for bridges [12]

Importance class	Importance factor,γ_1
I	0.7
II	1.0
III	1.4
IV	2.0

In accordance with section 3.2.2.2 and 3.2.2.3 in NS-EN 1998-2, there are two types of elastic spectrum shapes, each depending on the magnitude of the earthquake. It is recommended that if the surface-wave magnitude (M_s) is not greater then 5.5, than it is recommended to

adopt the Type 2 spectrum. For the ground types, it is divided into A, B, C, D and E with parameters S, T_B, T_C and T_D.

The seismic action is represented by three translational components, according to NS-EN 1998-2, and the earthquake motion must be measured in terms of response spectrum or time-history representation. Each of the three components will be evaluated separately as one-component actions utilizing the response spectrum. Clause 3.2.2, which refers to the application of clauses 3.2.2.2 and 3.2.2.3 of NS-EN 1998-1, specifies the horizontal and vertical components.

Section 3.3 in NS-EN 1998-2 stats that spatial variability shall be considered if L_{lim} exceeds an appropriate length defined as $L_{lim} = L_g/1.5$ where L_g is defined in Table 3-3.

Table 3-3: Recommended length of L_g (Tabel NA.3.1 [12])

Ground type	A	B	C	D	E
L_g (m)	600	500	400	300	500

With a dampening of 5%, the elastic response spectra are represented in time-history representation according to NS EN 1998-2 clause 3.2.3 (S_e (T)). The seismic action of bridges is determined by the natural period of vibration $- T_1$, where T_1 is the natural period of the basic mode of the structure in the case of a ductile bridge. For the time domain and spectrum to be consistent, Clause 3.2.3(3)P must be fully satisfied. For periods between $0.2T_1$ and $1.5T_1$, the SRSS (square root of sum squares) of the spectra of each component of the accelerogram should be more than $1.3S_e$ (T) [12].

There are four types of analysis mentioned, and the option is based on section 4.2 of the EC8 part 2 standard [12]. The Response Spectrum Method (Linear), Fundamental Mode Method, non-linear dynamic time-history analysis, and static nonlinear analysis (Pushover Analysis) are the analytical methodologies offered to conduct the reaction of an earthquake occurrence.

3.2 Handbooks

In collaboration with the Directorate for Public Roads, the Norwegian Public Roads Administration creates Handbooks. Level 1 handbooks include standards and manuals, whereas Level 2 handbooks provide recommendations. The Directorate for Public Roads oversees developing and maintaining the standards and manuals; however, the rules and manuals must be approved by the higher authority.

3.2.1 N400

The Handbook N400, is a standard that governs the structural design, control, and authorization of bridges, ferry docks, and other load-bearing structures in or near public roads. Where the standards are insufficient or unspecific, the handbook incorporates extra requirements. These regulations are expected to be applicable throughout the design, construction, and service life of the structure, as well as any repairs or maintenance work that may influence the structure's load-bearing capacity. The standard also specifies safety criteria for temporary bridges, formwork structures, scaffoldings, and other supporting structures.

Bridges, ferry quays, and other load-bearing structures in the public road network are designed using the standard N400 [14]. Bridges and other existing structures with private construction sites that go over, under, or along the public road network are likewise covered by the N400.

Chapter 4 of N400 sets the requirements for special bridges such as arch bridges, floating bridges, pipe bridges etc.

3.3 Reports

A quick review of the used journals in this thesis will be mentioned in this section. The three main journals are `*Fragility functions for a reinforced concrete structure subjected to earthquake and tsunami in sequence*`, `*Fragility assessment of a RC structure under tsunami actions via nonlinear static and dynamic analyses*` and `*Modelling and simulation of spatially varying earthquake ground motions at sites with varying conditions*`. Where the first two journals mentioned focuses on earthquake induced tsunami, while the last one is for earthquake ground motion simulation and the spatially variations.

3.3.1 Fragility assessment for reinforce concrete structure subjected to tsunami

The reaction of a seismically engineered reinforced concrete frame structure to tsunami inundation alone, as well as earthquake ground motion and tsunami inundation in tandem, is investigated in this study. By comparing these evaluations, it is possible to determine the impact of the prior ground motion on the structure's subsequent tsunami reaction. A seismic source representative of the M9 2011 Tohoku earthquake was used to create realistic ground motion and wave inundation time histories. [15]

3.3.2 Fragility assessment of RC structures subjected to tsunami

In estimating tsunami impact on buildings, the article compared distinct nonlinear static models to dynamic assessments. Three different analytical approaches were examined in terms of their ability to forecast structural reaction and accuracy in analyzing collapse fragility curves for tsunami actions: constant-height pushover (CHPO), variable-height pushover (VHPO), and time-history (TH) studies. The case study for the comparison study was a reinforced concrete frame tsunami evacuation facility that was subjected to simulated 2011 Tohoku tsunami inundation flows. To define a series of tsunami inundation time-histories in terms of inundation depth and flow velocity at different sites in Japan's Tohoku region, a tsunami inundation simulation was used. Tsunami force was calculated using a recently developed formula that was tweaked in this study to fit a typical tsunami inundation trace. To disperse the tsunami force along the height of the building, two different load patterns were used: triangular and trapezoidal. The initial step was to conduct a load sensitivity analysis in order to determine how to discretize the tsunami loads on the modelled structure. With a good discretization method, it was proved that the tsunami load should be spread throughout the height of the structure. [16]

3.3.3 Modelling and simulation of EGM and the spatially variations

Kaiming Bi and Hong Hao published a journal called `*Modelling and simulation of spatially varying earthquake ground motions at sites with varying conditions*`.

This work proposes a two-step method to predict and simulate spatially variable ground motions on an uneven terrain. First, base rock vibrations at different sites are assumed to have the same intensity and modelled by a filtered Tajimi–Kanai power spectral density function or other stochastic ground motion attenuation models. Empirical coherency loss function models base rock ground motion spatial variation. The power spectral density functions of surface

motions on a site with multiple soil layers are derived based on deterministic 1D wave propagation theory, neglecting wave scattering on the uneven canyon surface, and assuming that the base rock motions consist of out-of-plane SH wave or in-plane combined P and SV waves propagating into the site with an assumed incident angle. Second, a stochastic method to construct spatially variable time histories consistent with non-uniform spectral densities and a coherency loss function is devised. Two numerical examples illustrate the method. Any two of the generated ground motion time histories are compatible with a model coherency loss function.

3.4 Methodology

Due to the time-dependent earthquake load, this thesis will apply dynamic analysis of the bridge structure. The earthquake load is determined by the magnitude, direction, and position of the earthquake, all of which change over time. There are numerous approaches of assessing a bridge's resistance to earthquake loads. For this thesis, the main analyzing approach will follow the Eurocode 8 and N400 Handbook.

Because single degree of freedom (SDOF) analysis is not appropriate for a complicated bridge like the Bjørnafjorden floating bridge, multiple degree of freedom (MDOF) analysis will be employed. The seismic zone, geometry, and importance class of the bridge structure all play a role in determining the best analysis approach. This section will provide a brief overview of the various methods for studying long, flexible bridges. It's worth noting that the techniques are designed for general bridges.

The realistic response of irregular bridges can be calculated using dynamic nonlinear time-history analysis, according to clause 4.1.9.(2) of EC8-2 [12].The response of the bridge will be determined utilizing the time-history technique and direct numerical integration of its non-linear equation of motion. As ground motion time-histories, accelerograms will be used.

This type of analysis has limitations. It's the most computationally intensive analysis. This method needs numerous ground motion records because the calculated response depends on ground motion. As mentioned in section 3.1.1 EC8-2 specifies three sets of horizontal ground motion recordings for new bridges.

The calculated response from both nonlinear dynamic time-domain analysis and response spectrum analysis will be used in this thesis.

Chapter 4: Theory

4.1   The equation of motion of multi-degree-of-freedom systems

The equation of motion is given by matrices since the bridge cannot be expressed as an SDOF, but rather as an MDOF system. The equation of motion for an MDOF bridge with numerous supports and distinct ground excitations, according to Orcaflex is:

$$M(P,a) + C(p,v) + K(p) = F(p,v,t)$$ <div style="text-align:right">*(Eq 4-1)*</div>

Where:

$M(P,a)$ is the system inertia load

$C(p,v)$ is the system damping load

$K(p)$ is the system stiffness load

$F(p,v,t)$ is the external load

$p, v\ and\ a$ are the position, velocity, and acceleration vectors respectively

t is the simulation time

OrcaFlex implements both explicit and implicit time domain dynamic integration techniques. Both techniques recalculate the system geometry at each time step, ensuring that the simulation accounts for all geometric nonlinearities, such as the spatial variation of both wave and contact loads.

For implicit integration, OrcaFlex employs Chung and Hulbert's [17] generalized-integration approach. Forces, moments, damping, mass, and other parameters are determined similarly to the explicit technique. At the end of each time step, the system equation of motion is solved.

4.2   Natural modes of a system

A modal analysis determines a system's undamped natural modes, which are defined by their modal frequency and shape. These modes are numbered in order of increasing frequency, starting with 1. Modal analysis is well-known approach with extensive documentation. A quick overview of the theory is provided here.

For a single degree of freedom system (SDOF) consisting of mass m and a linear spring of stiffness K. The undamped equation of motion is shown in (Eq 4-2).

$$m\ddot{x}(t) = -kx(t)$$

(Eq 4-2)

Where $x(t)$ is the offset at time t from the mean position and $\ddot{x}(t)$ is the acceleration. The term undamped modes neglect any damping in the analysis.

This equation's solution is known to be simple harmonic, that is, of the form

$$x(t) = a\sin(\omega t)$$

(Eq 4-3)

Where a and ω is unknown.

Differentiating (Eq 4-3) twice gives

$$\ddot{x}(t) = -\omega^2 a\sin(wt) = -\omega^2 x(t)$$

(Eq 4-4)

And substituting into (Eq 4-2)we obtain

$$-m\omega^2 x(t) = -kx(t)$$

(Eq 4-5)

Rearranged (Eq 4-5)we get a more familiar result

$$\omega = \sqrt{\frac{k}{m}}$$

(Eq 4-6)

however, for a simple harmonic oscillator shown in (Eq 4-3) to (Eq 4-6) corresponds to the single degree of freedom. For multiple degree of freedom, the above equations need to account for infinite number of undamped natural modes. We need to interpret the equations about as matrix equations.

We now have vectors a, x, and $\ddot{x}$ each with n elements (one for each degree of freedom), and $n \times n$ matrices **M** and **K**, while ω and **T** remain scalars. (Eq 4-2) is now

$$\omega^2 M x = K x \qquad \text{(Eq 4-7)}$$

4.3 Rayleigh damping

Classical Rayleigh damping uses a system damping matrix C defined as

$$C = \mu M + \lambda K \qquad \text{(Eq 4-8)}$$

Where:

μ is the mass proportional Rayleigh damping coefficient

λ is the stiffness proportional Rayleigh damping coefficient

M is the system structural mass matrix

K is the system structural stiffness matrix

With this formulation the damping ratio is the same for axial, bending and torsional response. Classical Rayleigh damping results in different damping ratios for different response frequencies, according to the equation

$$\xi = \frac{1}{2}\left(\frac{\mu}{\omega} + \lambda\omega\right) \qquad \text{(Eq 4-9)}$$

Where:

ξ is the damping ratio (a value of 1 corresponds to critical damping)

ω is the response frequency in rad/s.

It can be seen from this that the mass proportional term gives a damping ratio inversely proportional to response frequency and the stiffness proportional term gives a damping ratio linearly proportional to response frequency. [18]

The contribution of the mass and stiffness damping terms to the overall damping ratio is represented in Figure 4-1
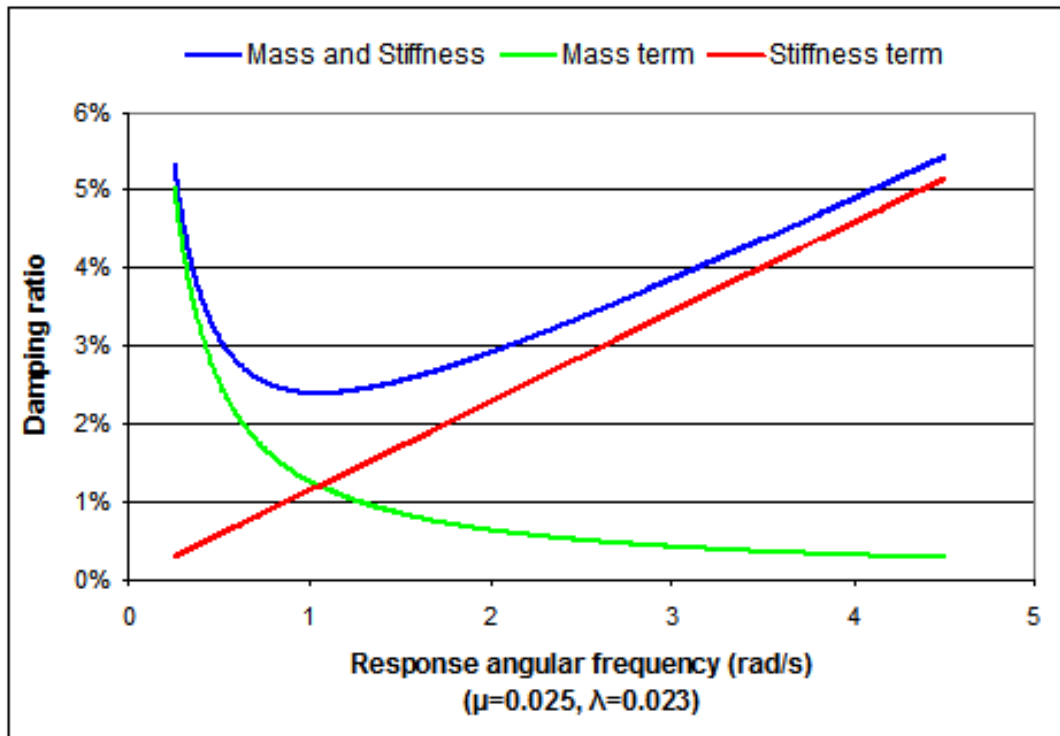
Figure 4-1: Variation of damping ratio with frequency [18]

Note that in Orcaflex, Rayleigh damping is used to modal structural damping for lines and turbine blades.

4.4   Earthquake motion

Accelerograms, which are recorded by high-powered motion accelerographs, offer the most accurate representation of the motion of an earthquake in the time domain. They record three components of ground acceleration at a given place, all of which are orthogonal to one another. An example of a typical accelerogram is shown in Figure 4-2. For the purposes of engineering, accelerograms are often captured on photographic paper or film before being converted to digital format. An accelerogram can be used to calculate the peak ground acceleration, the duration of an earthquake, and the frequency content of the shaking it causes. By integrating an accelerogram, one may determine the temporal shifts in ground velocity as well as ground displacement.
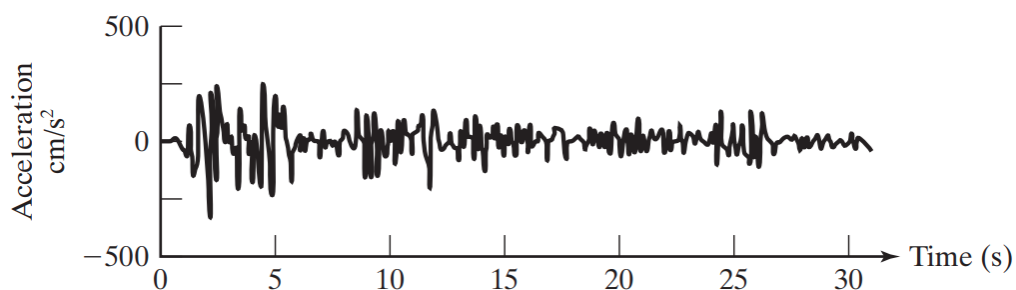
Figure 4-2: A typical accelerogram [19]

In order to provide the most accurate representation possible of the effect that an earthquake has on a building or piece of machinery, a response spectrum is utilized. The maximum response of a system with a single degree of freedom can be shown in terms of acceleration, relative pseudo velocity, and relative displacement by using logarithmic scales. The response spectrum illustrated in figure 4.18 is representative of the data found on four-way logarithmic paper. In this diagram, the spectral velocity is represented by the vertical axis, the horizontal axis represents the natural time period, the spectral displacement is represented by the 45-degree inclined axis, and the spectral acceleration is represented by the 135-degree inclined axis.
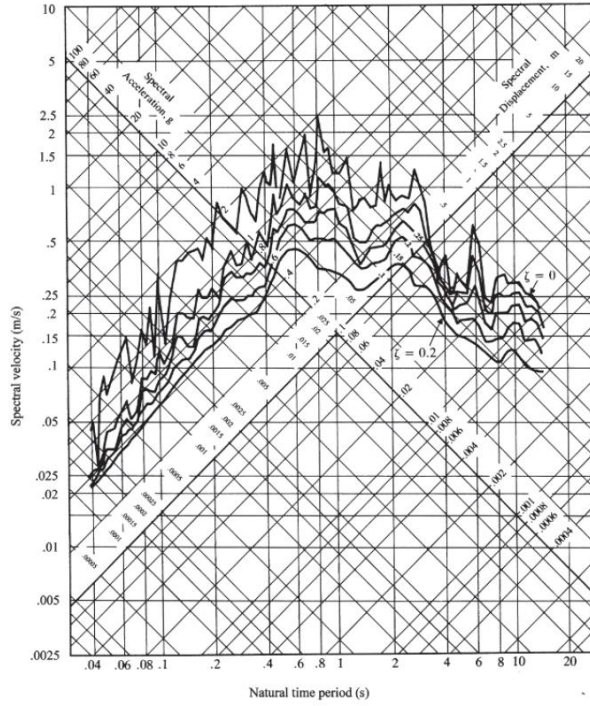
Figure 4-3: Response spectrum of a typical earthquake. (Imperial Valley Earthquake, May 18, 1940; z = 0, 0.02, 0.05, 0.10, and 0.20.) [19]
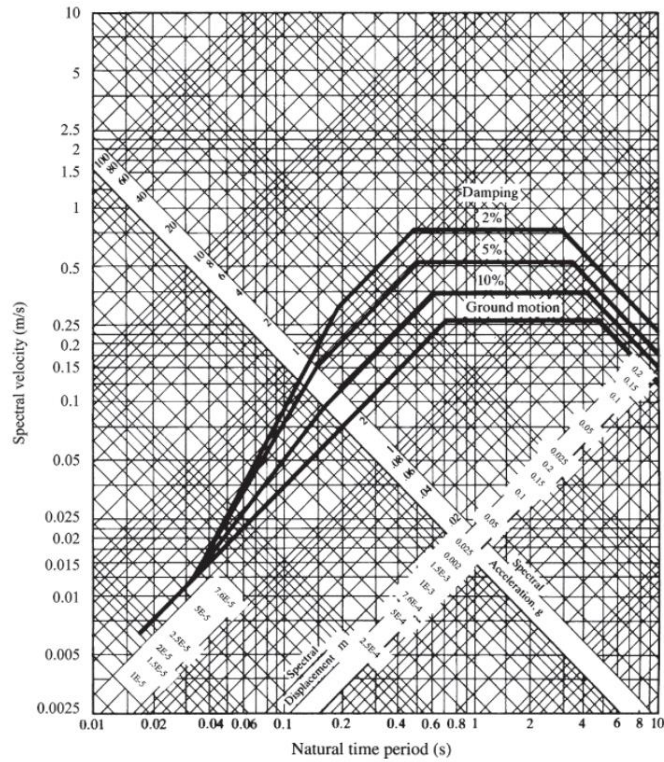
Figure 4-4: Design spectrum [19]

4.5 Tsunami

The most recent guidelines for tsunami design and assessment do not provide a formal definition of how to apply tsunami loads to offshore structures or which analysis approaches should be used in order to assess the structural response to tsunami loads.

Tsunami loading hitting the shore is well documented, however the methodology is not the same as for tsunami loads offshore. Hydrostatic and hydrodynamic forces, waterborne debris, and impact loads should all be included in the maximum tsunami event considering tsunami reaching the shore. The wave heights increase drastically when traveling the long distance from offshore to onshore. Therefor the loading will be significant higher when calculating tsunami loads hitting the shore.

In the event of an offshore seismic induced tsunami, the wave height won't have the distance and time to increase. Tsunami wave height usually doesn't exceed 1 meter offshore. As a result, the tsunami loading will be much reduced when compared to tsunami onshore. Offshore earthquake induced tsunami can also neglect debris, since the tsunami wave will not have travelled a distance, and therefore not been able to collect debris.

A simplified approach will be used to determine the tsunami loads as mentioned in section 3.3.2

4.6 Load combinations for seismic action

The maximum action effect due to seismic activity can be evaluated using the combination formulas (4.18) - (4.22) in EC8-1 {Standard, 2021 #16} according to EC8.2 {Standard, 2014 #19} clause 4.2.1.4. Sense the horizontal components of the seismic action is also relevant, the formulas (4.20) - (4.22) will be used:

$$E_{Edx} + 0.30E_{Edy} + 0.30E_{Edz} \qquad \textit{(Eq 4-10)}$$

$$0.30E_{Edx} + E_{Edy} + E_{Edz} \qquad \textit{(Eq 4-11)}$$

$$0.30E_{Edx} + 0.30E_{Edy} + E_{Edz} \qquad \textit{(Eq 4-12)}$$

Where E_{Edx} and E_{Edy} are the horizontal components and E_{Edz} are the vertical. The maximum action effect will be the most adverse combination of (Eq 4-10) - (Eq 4-12) according to clause 4.2.1.4(2) in EC8-2.

4.6.1 Load combination for seismic action with other loads

According to EC8-2 clause 5.5.(1)P, seismic action must be combined with other loads in accordance to EN 1990:2002 clause 6.4.3.4 and EC8-1 clause 3.2.4(1) resulting in the following function:

$$E_d = G_k + P_k + A_{Ed} + \psi_{21} Q_{1k} + Q_2 \qquad \textit{(Eq 4-13)}$$

Where:

G_k – are the permanent actions with their characteristic values

P_k – is the characteristic value of prestressing after all losses

A_{Ed} – is the design seismic action

ψ_{21} – is the characteristic value of the traffic load

Q_{1k} – is the combination factor for traffic loads in accordance with 4.1.2(3)P in EC8-2

Q_2 – is the quasi-permanent value of actions for long duration

Chapter 5: Ground motion and Tsunami loading

5.1 Seismic ground motion

When adopting the bridge's response spectrum method, the components of ground motions will be considered separately. According to paragraph 3.1.2(1)P in EC8-2, the seismic action is then represented by three one-component actions [12]

NS-EN 1998-1, clause 3.2.2.2, regulates the horizontal component in response spectrum methods [11]. If the soil type along the bridge supports changed, Clause 3.3 would have been employed. $S_e(T)$ the horizontal elastic response spectra, is described by equation 3.2-3.5, where T_B, T_C and T_D are the period values and S is the soil factor. When the ground type is determined, the values can be found. According to [20] the ground type for Bjørnafjorden is type A Because the bridge will be built where an earthquake's surface-wave magnitude is less than 5.5, the type 2 spectrum will be used, and table 1 displays the values for periods and soil factor for ground type A.

Table 5-1: Parameters for Type 2 elastic response for ground type A

Ground type	S	T_B	T_C	T_D
A	1.0	0.05	0.25	1.2

The vertical component shall be determined according to NS-EN 1998-1 clause 3.2.2.3 [11]. A vertical elastic response spectrum, $S_{ve}(T)$, will be used to represent the vertical component, which can be obtained using equation (3.8) - (3.11) in EC8 part 2. Table 2 shows the values for T_B, T_C and T_D, as well as the $\boldsymbol{a_{vg}}$.

Table 5-2: Parameters for Type 2 vertical elastic response for ground type A

Spectrum	$\boldsymbol{a_{vg}}$	T_B	T_C	T_D
Type 2	0.45	0.05	0.15	1.0

By using Table 5-1 and Table 5-2, we can obtain the acceleration response spectra by using (Eq 5-1) bellow.

$$a_g = \gamma_1 \cdot a_{gr}$$

where

a_{gr} is the peak ground acceleration

γ_1 is the importance factor.

Dr. Kaiming, created the ground motions utilized to analyze the bridge against seismic excitations. The motions include displacement and acceleration time histories based on the Eurocode's response spectrum and the location of the supports, including spatially variable ground motions. Six (6) separate sites will be subjected to the ground motion.

The ground motion spatial variation effect occurs when big dimensional structures, such as long span bridges, pipelines, and communication transmission systems, experience differing ground vibrations at different stations during an earthquake. Dr. Kaiming uses the Sobczyk model to represent the loss of coherency between ground motions at positions at points j' and k' $(j \neq k)$ at the base rock.

$$\gamma_{j'k'}(i\omega) = |\gamma_{j'k'}(i\omega)| \exp\left(-i\omega d_{j'k'} \cos \alpha \, / \, v_{app}\right)$$
$$= \exp\left(-\beta\omega d^2_{j'k'} \, / \, v_{app}\right) \cdot \exp\left(- i\omega d_{j'k'} \cos \alpha \, / \, v_{app}\right)$$

Where $|\gamma_{j'k'}(i\omega)|$ represents the lagged coherency loss, β is a coefficient (reflects the level of coherency loss), $d_{j'k'}$ is the distance between j' and k', α is the incident angle of the incoming wave to the site, and v_{app} is the apparent wave velocity at the base rock.

To account for ground motion variance, Dr. kaiming uses the Jennings envelope function that is multiplied by the simulated time histories. This is a shape function, and the equation is as follows:

$$\xi(t) = \begin{cases} (t/t_0) & 0 \le t \le t_0 \\ 1 & t_0 < t \le t_n \\ \exp[-0{,}155(t - t_n)] & t_n < t \le t_n \end{cases} \qquad \textit{(Eq 5-3)}$$

Where T is the duration of time. The generated time histories are given in section 5.1.1 below.

5.1.1 Ground motion generation

Here are the accelerations and displacements computed using the generating ground motion acquired by Dr. Kaiming. There are three separate load instances, including displacements, that are merged in the graphs to see if there are any large differences over time. In the response spectra, the theoretical peak ground acceleration (PGA) is $0.83\ m/s^2$. For more detailed showing of ground motion, see Appendix B: Ground motion generation.

The site location is shown below in Figure 5-1.
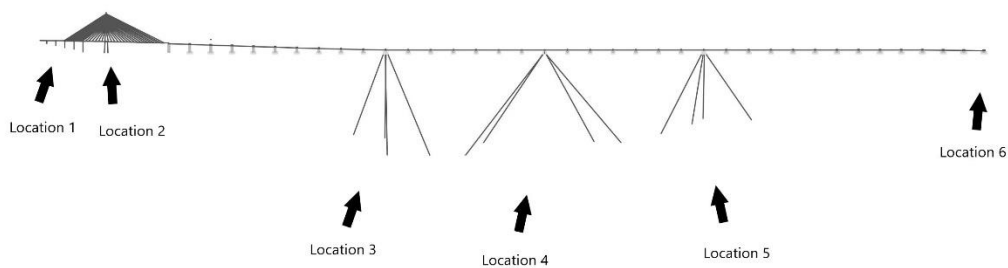
Figure 5-1: Ground motion locations

The three generated motion for each site location is summarized in Table 5-3 to Table 5-5. As we can see, the PGA's and PGD's for the horizontal (x-direction) motion for each set is 0.855, 0.784, 0.878 m/s^2 and 0.00799, 0.00752, 0.00851 m respectivaly

While the PGA's and PGD's for the horizontal (y-direction) motion is as following 0.815 0.832 0.745m/s^2 and 0.00748, 0.01005, 0.00785 m

And for the vertical (z-direction) motion the PGA's and PGD's is 0.810, 0.744, $0.788 m/s^2$ and 0.01036, 0.00749, 0.00805 m

Table 5-3: Peak ground motion acceleration and displacement for horizontal motions (x-direction)

	Locations											
	1		2		3		4		5		6	
	PGA	PGD	PGA	PGD	PGA	PGD	PGA	PGD	PGA	PGD	PGA	PGD
Set 1	0.8551	0.0080	0.7235	0.0072	0.7103	0.0071	0.6153	0.0053	0.6166	0.0040	0.6274	0.0049
Set 2	0.7454	0.0075	0.7839	0.0068	0.7327	0.0061	0.5353	0.0047	0.7543	0.0037	0.5301	0.0032
Set 3	0.7010	0.0079	0.8782	0.0085	0.7883	0.0076	0.6200	0.0041	0.5500	0.0034	0.5338	0.0042

Table 5-4: Peak ground motion acceleration and displacement for horizontal motions (y-direction)

	Locations											
	1		2		3		4		5		6	
	PGA	PGD	PGA	PGD	PGA	PGD	PGA	PGD	PGA	PGD	PGA	PGD
Set 1	0.8145	0.0060	0.7453	0.0070	0.7053	0.0075	0.6319	0.0043	0.6498	0.0041	0.5456	0.0044
Set 2	0.8325	0.0086	0.8259	0.0069	0.6652	0.0100	0.5937	0.0034	0.5975	0.0033	0.5343	0.0030
Set 3	0.7289	0.0061	0.7336	0.0079	0.7446	0.0058	0.5656	0.0041	0.6579	0.0047	0.5472	0.0042

Table 5-5: Peak ground motion acceleration and displacement for vertical motions (z-direction)

	Locations											
	1		2		3		4		5		6	
	PGA	PGD	PGA	PGD	PGA	PGD	PGA	PGD	PGA	PGD	PGA	PGD
Set 1	0.8005	0.0104	0.8104	0.0085	0.7925	0.0062	0.6393	0.0039	0.5494	0.0040	0.5808	0.0041
Set 2	0.7251	0.0072	0.7444	0.0067	0.6635	0.0075	0.6963	0.0044	0.6245	0.0036	0.5729	0.0038
Set 3	0.6700	0.0070	0.6060	0.0059	0.7877	0.0080	0.6898	0.0038	0.6516	0.0035	0.6049	0.0033
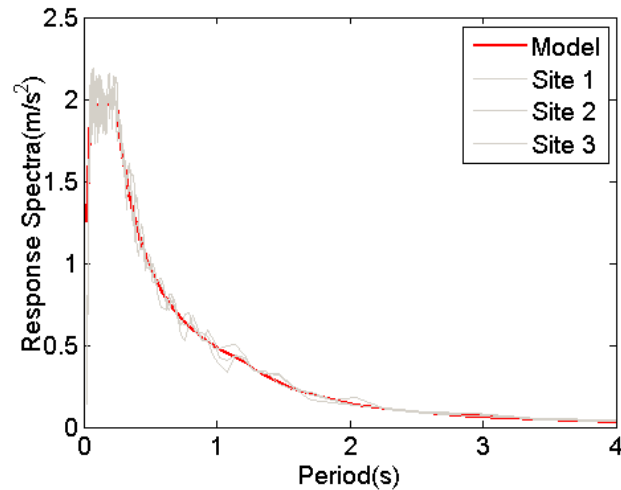
Figure 5-2: Comparison of PSD of the generated time histories

The actual site spectra and the target response spectra used to construct the ground movements are well-matched in Figure 5-2. The light plot is based on the synthetic accelerograms that were calculated.
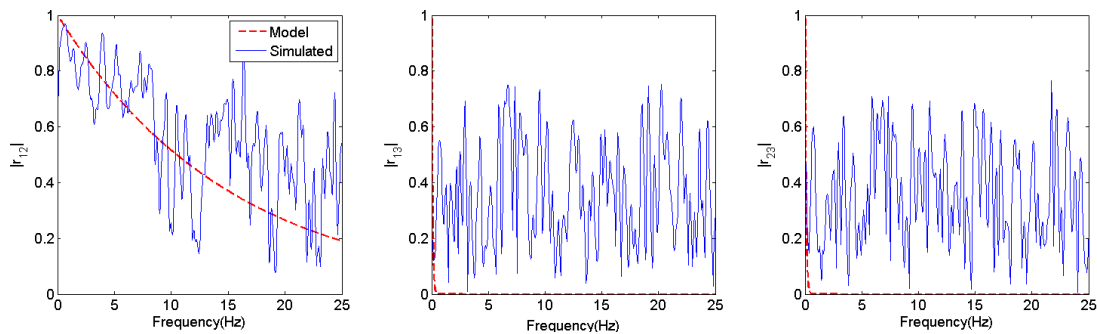
Figure 5-3: Comparison of coherency loss between genereted time histories

Figure 5-3 demonstrates the coherency loss functions between two seismic time histories. A good match can be observed for (r_{12}), while (r_{13}) and (r_{23}) isn't a good fit in the high frequency range, resulting in a poor coherence. This is to be expected, because as the distance increases, the coherency values decrease fast with frequency. And considering that the south end (r_{12}) is from the bridge tower (r_{13}) and the north side (r_{23}) the coherency decrease would be logical.

Ref has shown that a coherency value of about 0.3-0.4 is the cross-correlation threshold. Meaning that even when the model coherency function falls below this threshold value, the computed coherency loss between two simulated time histories remains around 0.4.

5.2 Tsunami load

It is widely known that tsunamis have an effect on humankind. Recent events have provided several examples of the devastation that can be brought on by these phenomena, highlighting the importance of understanding their dynamics. Because of a lack of in-situ expertise, the process of tsunami generation is the aspect of tsunamis that is understood the least. As a result, for numerical tsunami modelling, simplified source models are used.

$$F_\mathrm{T}(t)/b = sgn(u(t)) \begin{cases} 0.5C_\mathrm{D}\rho u(t)^2 h(t) & \text{if } F_r < F_{rc} \\ \lambda\rho g^{1/3} u(t)^{4/3} h(t)^{4/3} & \text{if } F_r \geq F_{rc} \end{cases} \qquad \textit{(Eq 5-4)}$$

Where:

    C_D is the drag coefficient

    ρ is the sea density

    F_r is the Froude number

    F_{rc} is the Froude number threshold

    λ is the leading coefficient

    g is the acceleration of gravity

    u is the flow velocity

    h is the inundation depth

Because of time limit and a lack of available tsunami load research, an assumption had to be made for an offshore structure. For example, the parameters F_{rc}, λ and C_D are dependent on the block ratio parameter b/w. In this context, b refers to the width of a rectangle, and w refers to the flume width, which can be difficult to get. Because of this, the block ratio that

was utilized in the research paper [16] will be utilized in this thesis as well. As a direct consequence of this, the parameters indicated in Table 4 1 are as follows:

Table 5-6: Tsunami load parameters

b/w	C_D	λ	F_{rc}
0.6	4.7	2.0	0.32

It is important to point out that the estimations for these parameters may be found in the publication [16] which relates to an onshore rectangular concrete building. On the other hand, it does not evaluate the impact of debris, which is a possibility for our structural integrity given that the earthquake would strike near the position of the bridge.

An estimation for the induration depth, *h(t)* and flow velocity, *u(t)*. Figure 5-4 and Figure 5-5 illustrates the time history of the induration depth and flow velocity.
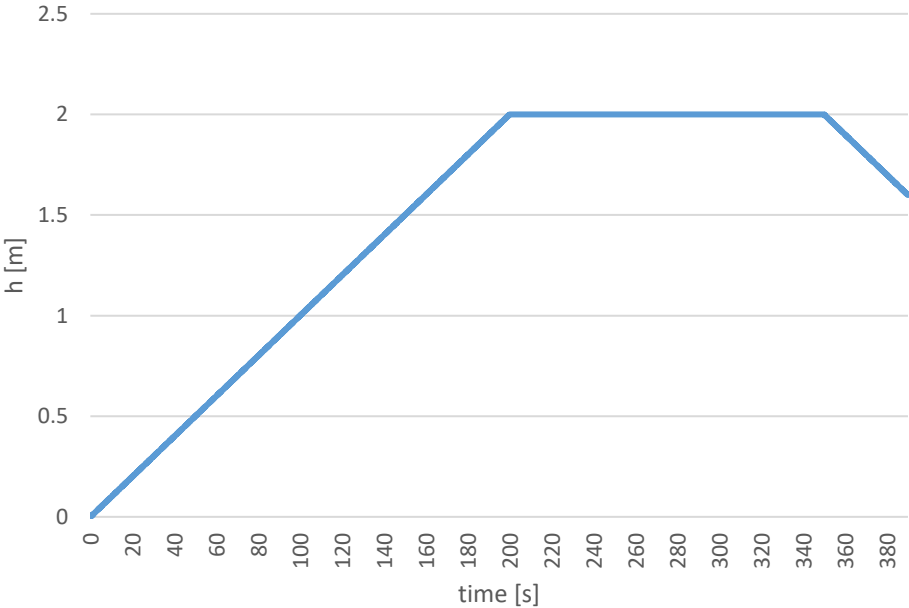
Figure 5-4: Induration depth time history
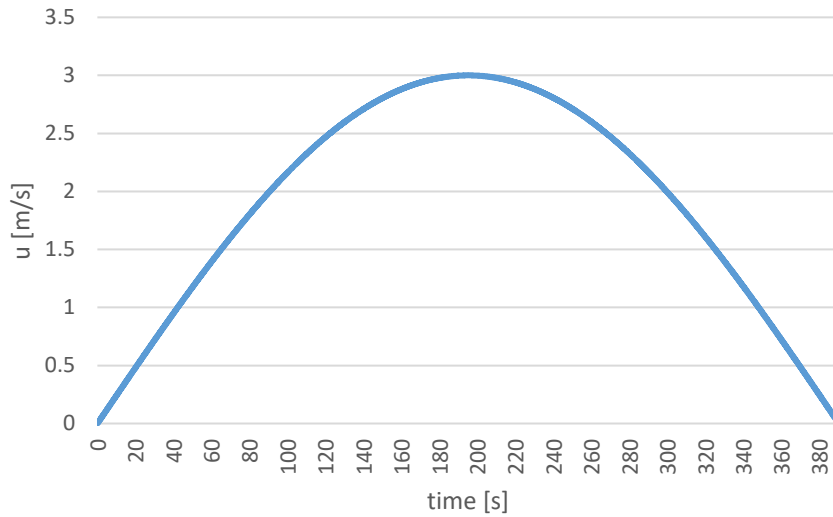
Figure 5-5: Flow velocity time history

To acquire the Froud number time history, (Eq 5-5 was used and the time history is illustrated in Figure 5-6.

$$F_\Gamma = u(t) \, / \, \sqrt{gh(t)}$$

(Eq 5-5)
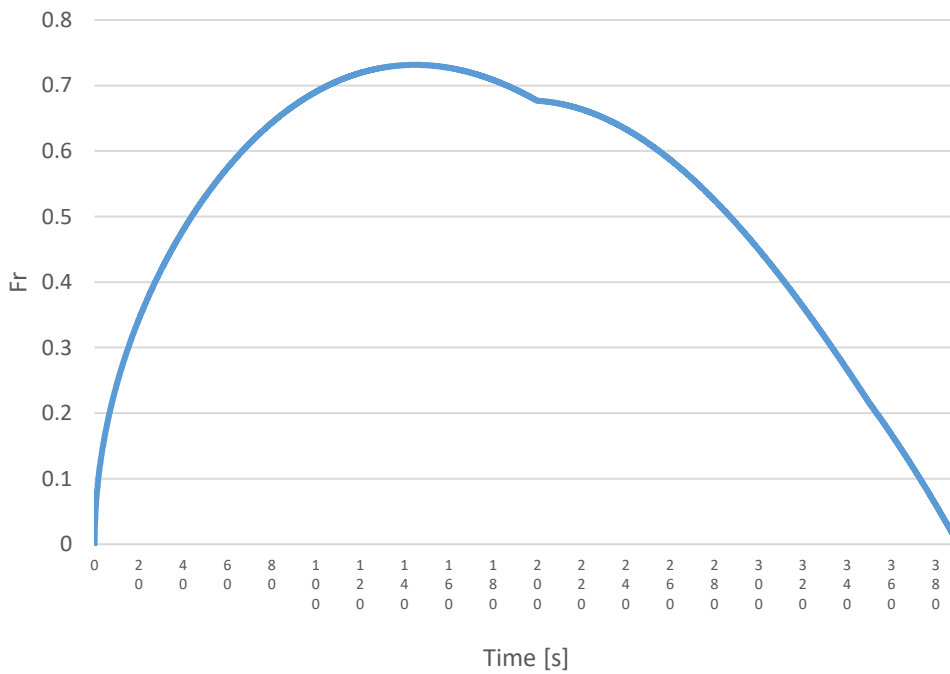
Figure 5-6: Froud number time history

Solving (Eq 5-4 we obtain the force acting on each pontoon. Figure 5-7 shows the tsunami force time history that will be utilized in this thesis.
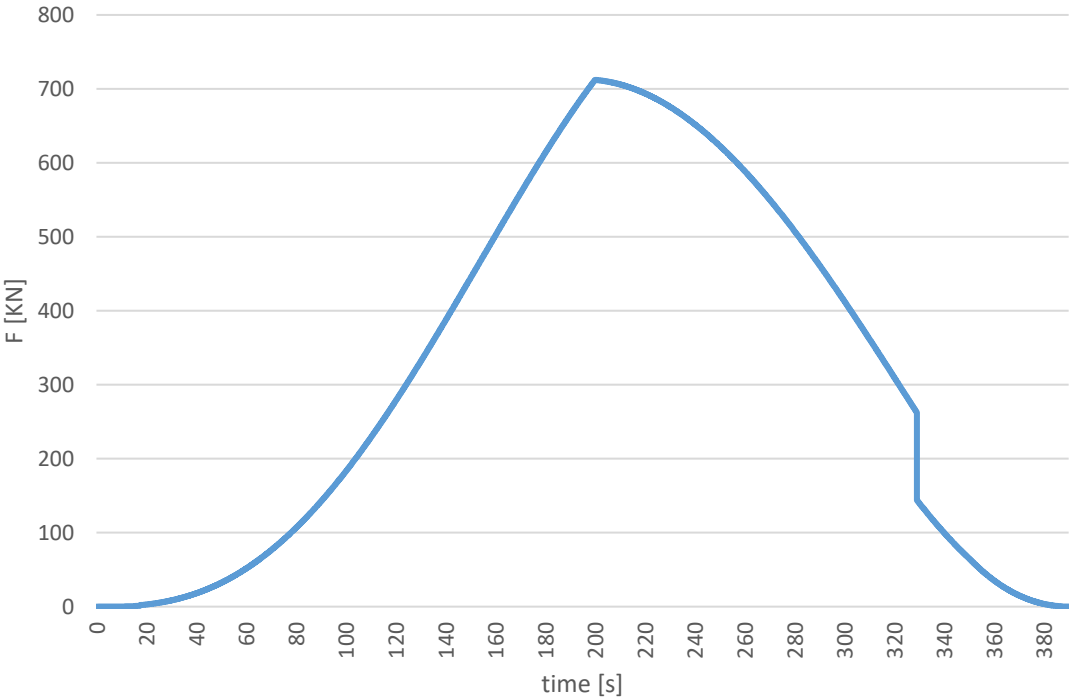
Figure 5-7: Tsunami force time history

Chapter 6: Bridge modelling in Orcaflex

6.1 Global Analysis

In this chapter, we will discuss the design of the K12 floating bridge in Orcaflex as well as conduct an analysis of the model with regard to seismic excitations and tsunami load. There will be a brief explanation of the modelling process for the pontoons, columns, bridge girder, mooring lines, tower, and tower cables that will be shown. The AMC description will serve as the basis for the model that will be created [21]. Figure 6-1 shows an illustration of the K12 floating bridge. However, it is important to note that the data presented here may not exactly match those in the main report. In that scenario, the modifications will be discussed and displayed.
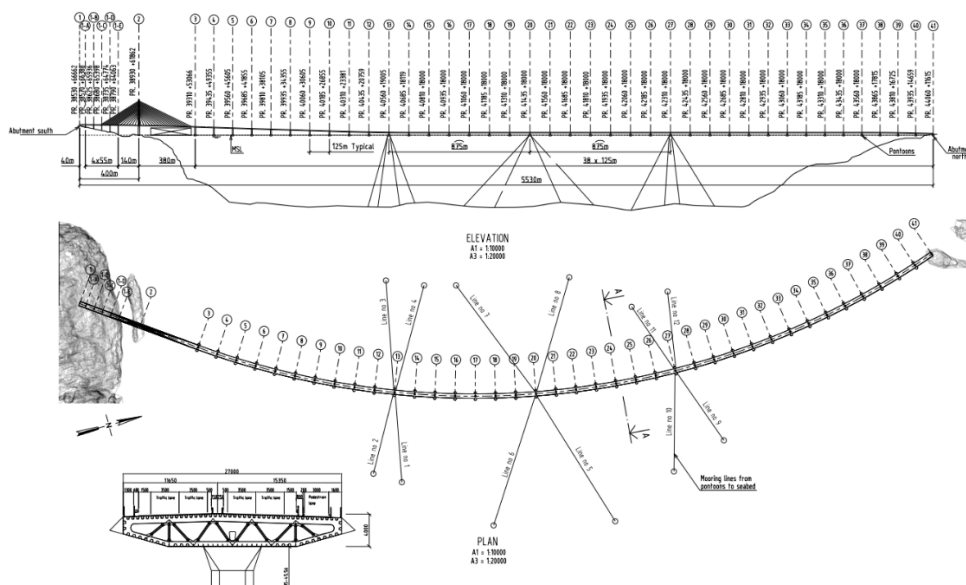
Figure 6-1: Overview of the K12 floating bridge [22]
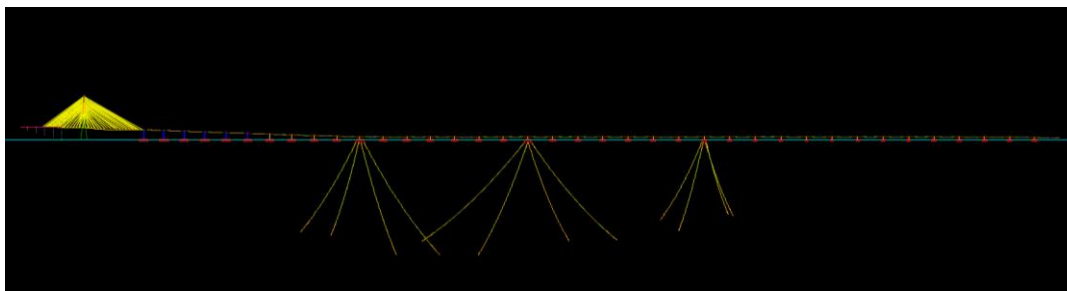
Figure 6-2: Overview of the model in Orcaflex

6.1.1 Orcaflex

Orcaflex (developed by Orinca) is a marine dynamics application. The application is used to perform static and dynamic analyses on a variety of offshore systems, including riser systems, mooring systems, lifting and installation activities, and towing systems. The user can examine custom-built systems in various environments. The user can extract motions, forces, stresses, and moments after establishing an appropriate model. As a result of this, Orcaflex is going to be an extremely helpful tool for the dynamic response of the model.

6.1.1.1 Coordinate system

The global coordinate system, which follows the right-hand rule and is shown in Figure 6-4, defines the coordinates of the bridge. The model's origin is at pontoon 20, the origin node starts coordinate is (0,0,0).

This model follows the same global modal coordinate system as defined in [23], which is defined as;

- X-axis points toward North
- Y-axis points towards West
- Z-axis points upwards
- The baseline (Z=0) is the mean surface level (MSL)
- The origin of the coordinate system is set at 6668744.33 N, 299215.63 E (UTM32) at MSL. Consequently, the positions of Axes 1 and 41 in the global coordinate system are:
  - Axis 1: x = -2581.00 m, y = 1267.77 m
  - Axis 41: x = 2587.25 m, y = 199.84 m
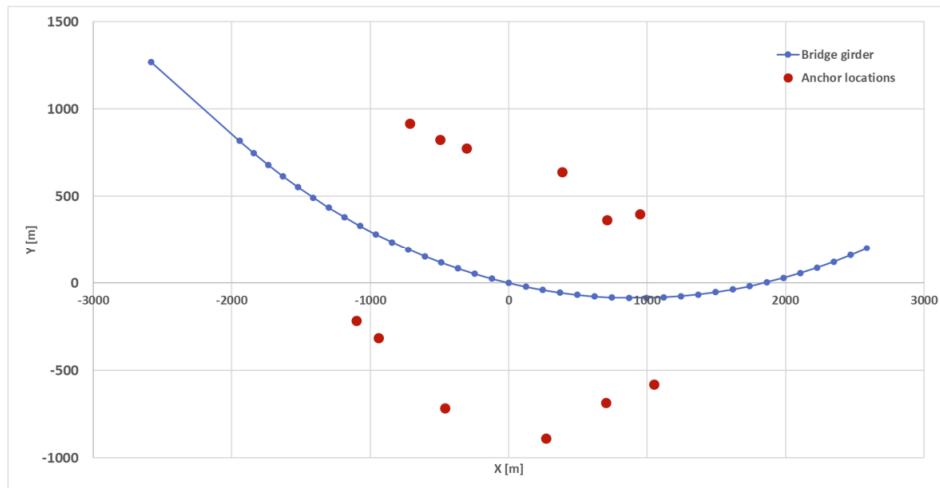
Figure 6-3: Coordinates of the model [23]
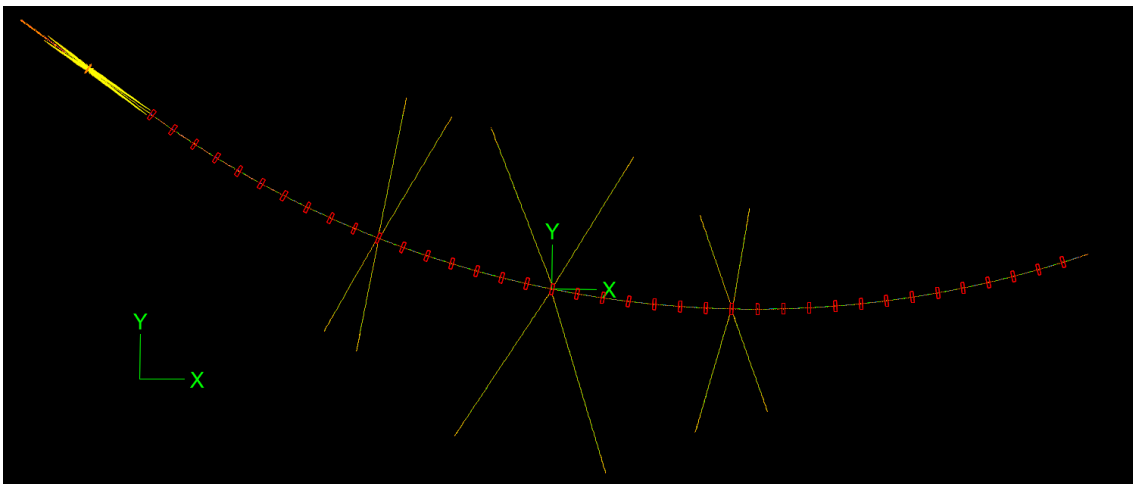
Figure 6-4: Global coordinate system in Orcaflex

6.1.1.2   Local orientation

Most of the elements differ in orientation and local coordinates. This subchapter will show the different local orientations.
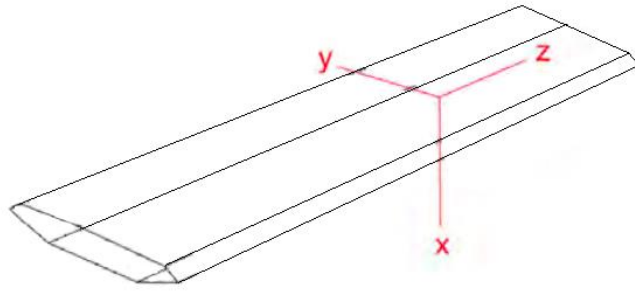
Figure 6-5: Local coordinate system bridge girder [21]
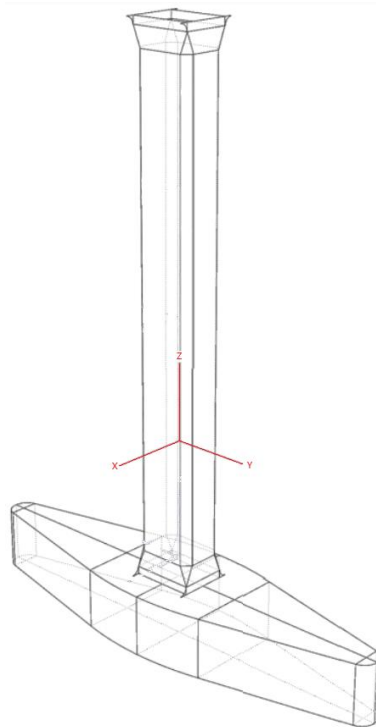
Figure 6-6: Local coordinate system columns (and tower) [21]

Figure 6-7: Local coordinate system stay cables [21]
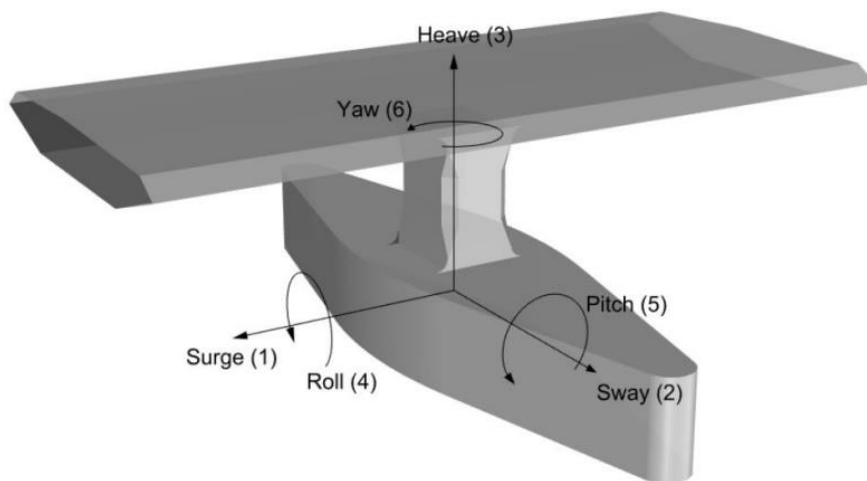
Figure 6-8: Local coordinate system pontoons [21]

Orcaflex has its own built-in units. The system is in SI unit and follows the following in this thesis:

- Length in m
- Force in kN
- Mass in ton or kg
- Density in kg/m^3
- Time in s

6.2   Description of the bridge

The preferred design of NPRA is the K12 bridge design. An end-anchored floating bridge with a cable-stayed part in the south end as shown in Figure 1-2. The rest of the bridge consist of 38 floating pontoons. Three of the pontoons will have 4 mooring lines attached to each end. The bridge is 5439 meter long and is curved from the south end to the north.

The structure of the bridge may be broken down into three distinct sections: the low bridge, the high bridge, and the cable-stayed bridge. The bridge begins in the south with the cable-stayed bridge, continues to the "high" bridge for ships to pass beneath, and then gradually decreases in height as it travels to the north end of the span. The low bridge section begins at the axis 9-41, while the high bridge section begins at the axis 3-8, and the cable-stayed bridge begins at the axis 1-3. The tower section is 780 meters long and is made up of 72 cables that are connected from the "side" and "main" of the tower. The important statistics for the end-anchored bridge are presented in Table 4 1.

Table 6-1: Key figures

Bridge length between abutments	5530 m
Arch length cable-stayed bridge	780 m
Arch length of floating bridge part	4750 m

The material properties used is shown in the table below.

Table 6-2: Material properties [23]

Material	E [MPa]	G [MPa]	ρ [kN/m^3]
Structural steel	210000	80770	77
Concrete	29760	12400	26
Stay cables	195000	-	77·1.2=92.4

6.2.1 Bridge Girder

The bridge girder is modelled as line object. The bridge girders have difference properties for different sections. For the south end cable-stayed bridge, the bridge girder is made of concrete, this also implies for the north end of the bridge. While the remaining of the girders are made of steel. A illustration from [5] is shown below in Figure 6-9.

A typical cross-section is shown in Figure 6-9. The variation will be mainly the thickness of the stiffing plates as well as the south end and north-end side which is made from concrete. The properties for all girders are shown in Table 6-3, and the stiffness properties are calculated out of these properties.
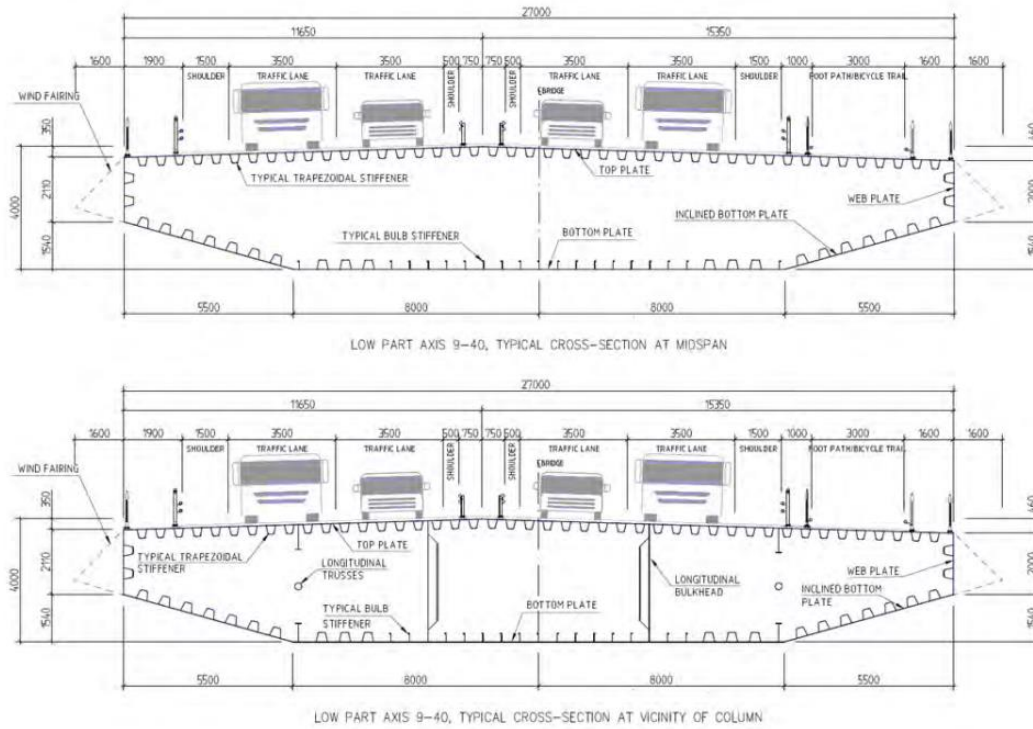
Figure 6-9: Geometric shape of steel bridge girder at midspan and in vicinity of column [5]

The bridge is separated into parts with different types of bridge properties. There are multiple types of cross-sections as shown in Figure 6-10. In Orcaflex the lines are defined with multiple segments, illustrating the different properties of the bridge girder. The girder cross-section properties employed in Orcaflex are shown in Table 6-3.
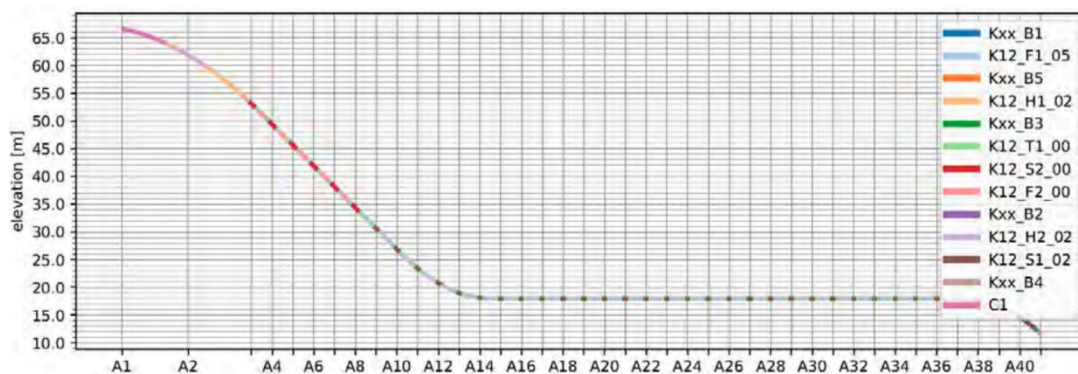
Figure 6-10: Sectional property definition [21]

Table 6-3: Key sectional properties for bridge girder [21]

	M	Iy	Iz	J	Ax	Ly	Lz	VCGt
	[ton/m]	[m^4]	[m^4]	[m^4]	[m^2]	[m]	[m]	[m]
K12_S1_02	19	3.668	110.4	11.349	1.779	27	4	1.989
K12_S2_00	19	3.785	121.83	12.01	1.8829	27	4	2.041
K12_T1_00	19	3.311	98.583	10.105	1.521	27	4	1.878
K12_F2_00	19	2.781	89.597	9.4228	1.331	27	4	1.763
K12_F1_05	19	2.569	84.698	8.6111	1.2699	27	4	1.682
K12_H1_02	19	2.534	89.531	6.629	1.297	27	3.5	1.463
K12_H2_02	19	3.64	123.34	9.663	1.797	27	3.5	1.633
C1	79.1	40.5	2138	135.4	27.951	29	3.5	1.463
Kxx_B1	19	5.32	170	18.2	2.09	27	4	1.989
Kxx_B2	20.52	5.95	226	20	2.28	27	4	1.989
Kxx_B3	25.16	7.7	314	24.3	2.86	27	4	1.989
Kxx_B4	29	9.74	423	28.5	3.34	27	4	1.989
Kxx_B5	30.12	10.06	461	29.7	3.48	27	4	1.989

The values for the second moment of inertia are obtained from [21]. Simple hand-calculation using (Eq 6-1) and (Eq 6-2) were done to acquire the bending stiffness, torsional stiffness, and axial stiffness for the steel girders. Using the material properties given in Table 6-2.

Axial stiffness - $\frac{E \cdot A}{L}$ *(Eq 6-1)*

Bending stiffness - $\frac{E \cdot I}{L}$ *(Eq 6-2)*

Torsional stiffness - $\frac{G \cdot J}{L}$ *(Eq 6-3)*

6.2.2 Tower

This model consists of only one cable-stayed bridge. The A shaped tower shown in Figure 6-11 is made from concrete. The tower is 220 meter high, and the tower is fixed to the ground. The tower has different properties depending on the elevation and section.

The tower was modelled as line objects in Orcaflex, see Figure 6-11. Reasonable constraints are added as implied in [21] to obtain a rigid tower. For simplification, the tower properties are divided into two sections in Orcaflex, Tower legs and Tower crown. The properties in Table 6-4 are obtained from [23] where Tower legs are recovered from Table 3-13 Section 8, while the tower crown properties are required from Table 3-18 Section 1.

Table 6-4: Tower properties [23]

		Tower legs	Tower crown
Weight	ton/m	91.66	41.84
Area	m^2	34.58	15.79
Torsional inertia	m^4	582.32	170.43
Inertia around weak axis	m^4	302.14	81.72
Inertia around strong axis	m^4	34.58	15.79
Axial stiffness, EA	kN	1.03E+09	4.70E+08
Weak axis bending stiffness, EIY	kNm^2	9.00E+09	2.44E+09
Strong axis bending stiffness, EIZ	kNm^2	1.03E+09	4.70E+08
Torsion stiffness, GIX	kNm^2	7.23E+09	2.12E+09
Gyration radius	m	4.94	4.04
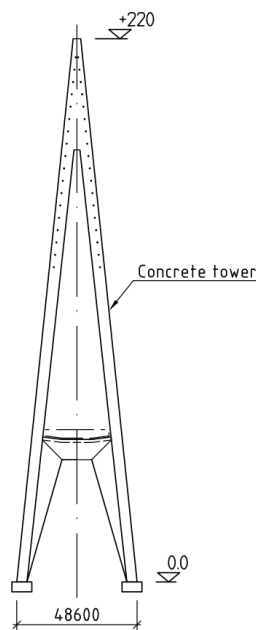
Figure 6-11: Tower shape [22]
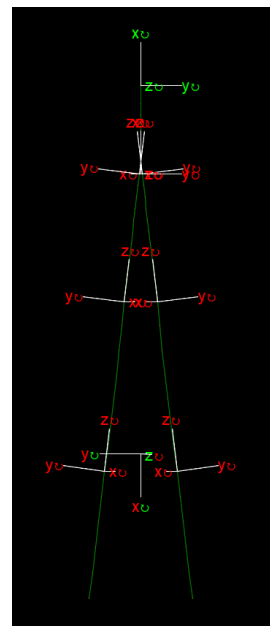
Figure 6-12: Orcaflex model of tower with constraints

6.2.3 Tension Cables

Parallel multi-strand cables serve as the stays. The stays closest to the tower have 31 strands, while the longest have 67. Strand-by-strand tensioning is used to build the stays. Individually PE-sheathed strands are contained in HDPE-pipes. At either end of the cables are anchorages that fit into steel tubes incorporated into the main construction. The wire has a tensile strength of 1860 MPa, and the overall weight is around 1000 tons. [24]
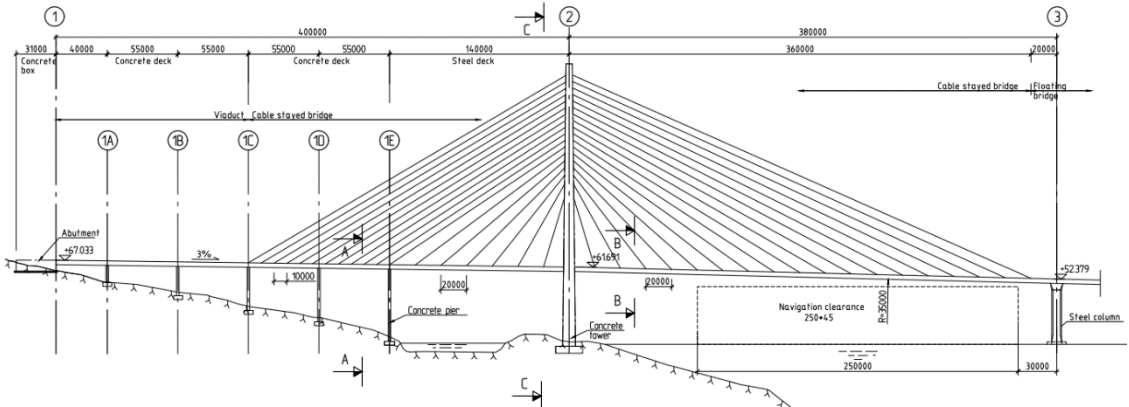
Figure 6-13: Side view stay-cabled tower [22]
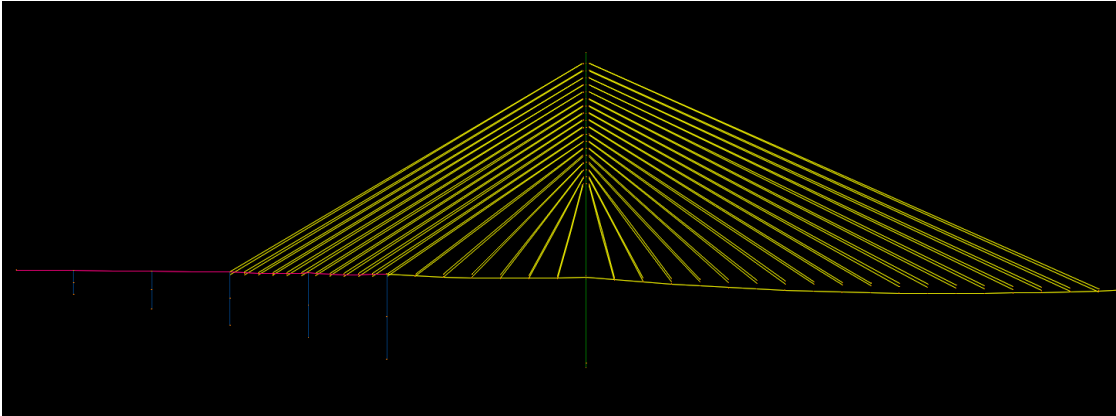
Figure 6-14: Orcaflex model of stay-cabled model
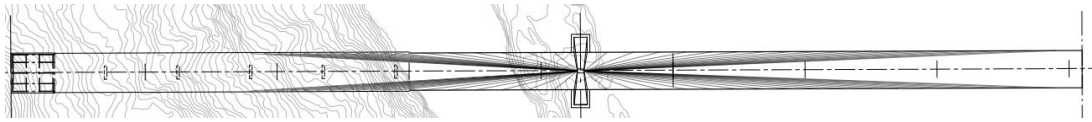
Figure 6-15: Top view of stay-cabled tower [22]
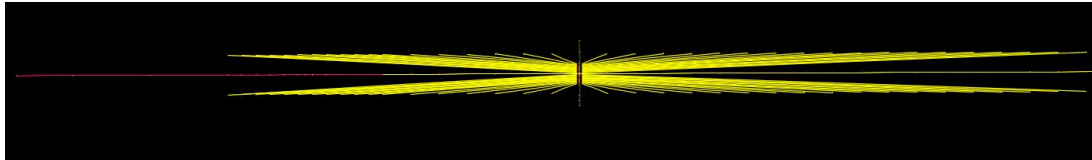
Figure 6-16: Top view of stay-cabled tower in Orcaflex

The stay-cables has 36 different properties, depending on which side of the tower it is connected. From the towers perspective the cables and connected with 5-meter space, while the connection in the bridge girder depends in spacing, varying from 10 to 20 meters. See Figure 6-13 for an illustration.

The bridge deck is supported by stay-cables that run parallel to the tower top and bridge girder. Due to nodes only at the deck center, the cables are linked at an off-center distance. All the cables are arranged in pairs, resulting in one cable on each side of the bridge girder with the same cross-sectional area.

The cables will serve as tensile members and are arranged in strand bunts. As a result, when constructing cables, EA is the most crucial component to consider. The stay-cables properties are acquired from [23] and is shown in Table A. 1. Some key properties like the yield strength, weight, and breaking load are obtained from the main report done by NPRA [22] and are given in Table A. 2.

The properties from Table A. 1 were used in Orcaflex. The tower cables were modelled as line objects with no torsional rotation applied, and at one end connected to the tower and at the other end connected to the bridge girder. As mentioned earlier, the connections are linked at an off-center distance to get a more precise modelling of the tower part. The numbering of the tension-cables can be seen in Figure 6-17 bellow and the pre-tension for each cable can are given in Figure 6-18: and Figure 6-19:. The hand-calculations were done by [21].
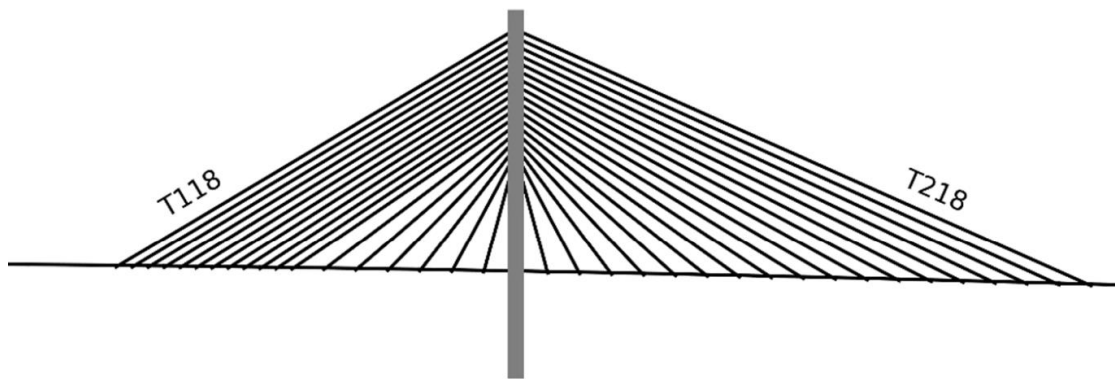
Figure 6-17: Stay calbe identification numbering [23]

Back span stay-cables

	101	102	103	104	105	106	107	108	109	110	111	112	113	114	115	116	117	118
Hand Calc.	2.03	2.21	2.43	2.68	2.92	3.16	3.39	3.66	3.93	4.17	4.40	4.61	4.80	5.00	5.19	5.37	5.54	5.69
Orcaflex	2.47	2.28	2.49	2.66	2.75	2.74	3.60	3.64	3.86	4.06	4.29	4.52	4.52	4.89	5.24	5.45	5.34	5.42
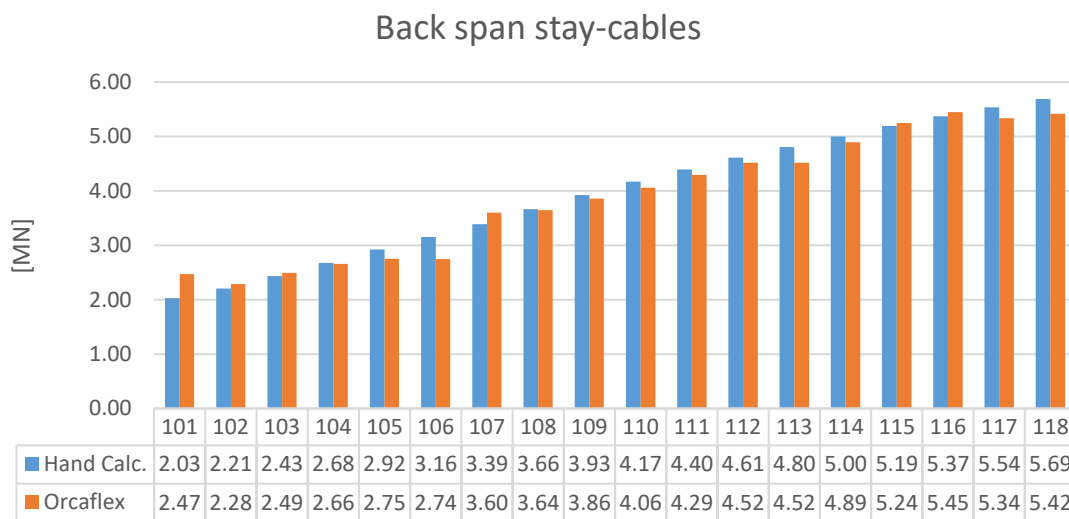
Figure 6-18: Pre-tension cables main span

Front span stay-cables

	201	202	203	204	205	206	207	208	209	210	211	212	213	214	215	216	217	218
Hand Calc.	2.05	2.24	2.47	2.72	2.97	3.20	3.43	3.65	3.85	4.05	4.24	4.42	4.58	4.75	4.92	5.07	5.22	5.36
Orcaflex	2.44	2.44	2.36	2.69	2.93	3.14	3.38	3.45	3.65	3.94	4.11	4.27	4.37	4.53	4.85	5.00	5.04	5.11
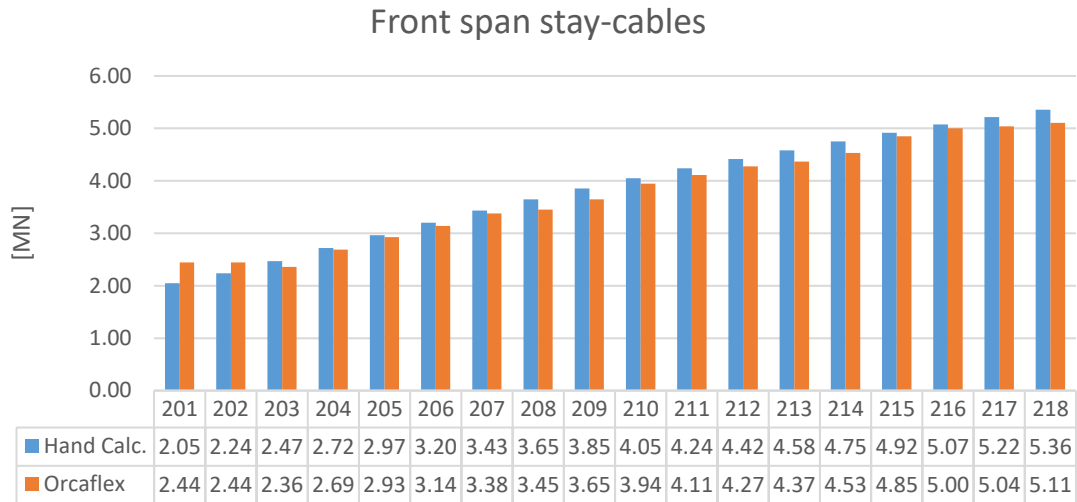
Figure 6-19: Pre-tension cables front span

6.2.4 Pontoons

The pontoons are made of steel and have two types of geometry depending on the location of the pontoons. Figure 6-20 and Figure 6-21 shows the two different pontoon types, conventional and moored. The pontoon's width, length and diameter are the same for the two types, only the height differs. The bridge has 38 pontoons where 3 of the pontoons have supports for mooring lines. These pontoons are in axis 13, 20 and 27. It is worth mentioning that the weight of the pontoons in Table 6-5 is higher than what was calculated by [24] this is to leave a margin for weight increase without effecting the global dynamic response [21].
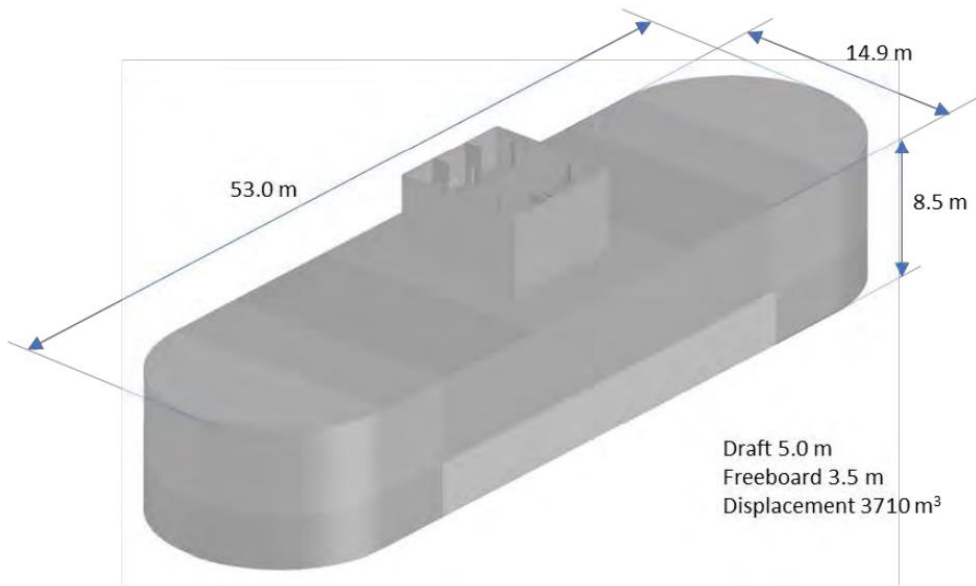
Figure 6-20: The geometric shape of pontoon without mooring lines [24]
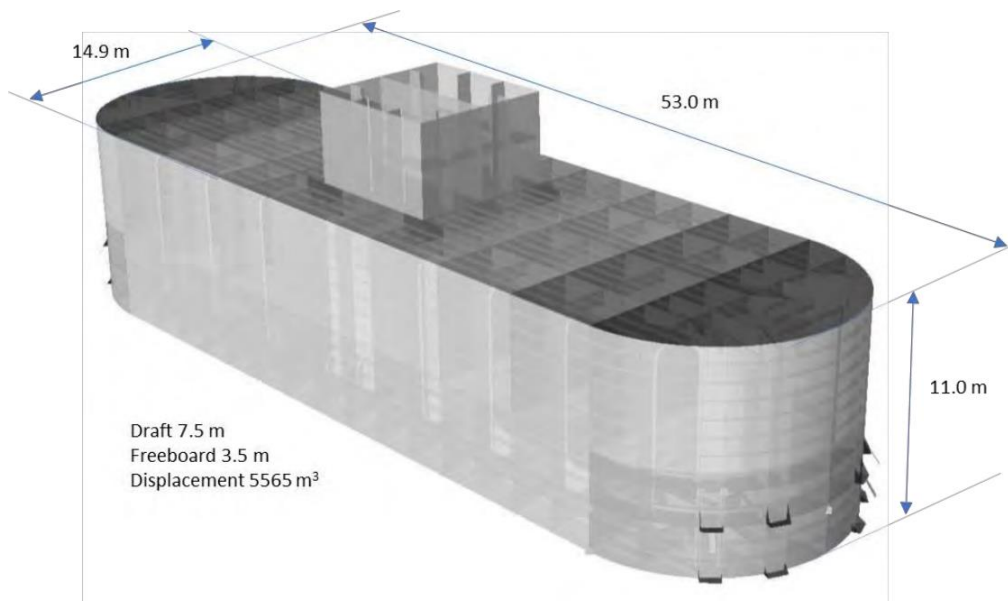
Figure 6-21: The geometric shape of pontoon with mooring lines [24]

The pontoons are modelled as vessel in Orcaflex with the properties found in Table 6-5. In principle the pontoons stiffness, added mass and damping vary, but for simplicity the pontoons hydrostatic properties are divided into two parts, conversional or moored. The

hydrostatic stiffness is acquired from Table 6-5 while the added mass and damping was given by PHD-student Zihao Wang as an output file imported from Orcawave.

Table 6-5: Circtangle properties [21]

Pontoon type	Moored	Conventional
Length [m]	53	53
Width [m]	14.9	14.9
Draft [m]	7.5	5.0
Mass [ton]	1540	985
Displaced volume [m^3]	5566	3710
C33 [kN/m]	7459	7459
C44 [kNm/rad]	1,56 E6	1,56 E6
$I_{xx}[ton \, m^2]$	415 E3	252 E3
$I_{yy}[ton \, m^2]$	63,8 E3	33,1 E3
$I_{zz}[ton \, m^2]$	430 E3	252 E3
Center of gravity [m]	-2.0	-0.75
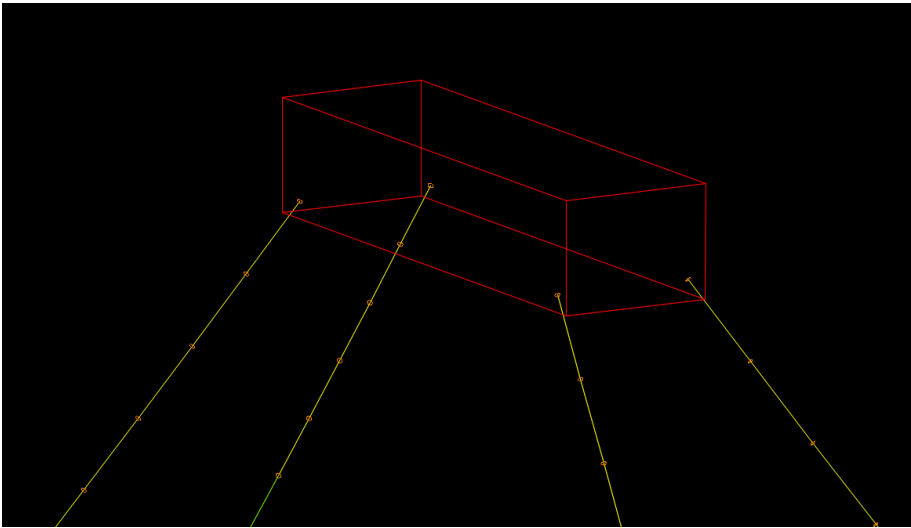
Figure 6-22: Pontoon w/mooring lines model in Orcaflex

6.2.5 Columns

The columns in the model vary both in size and material. For the south end part, the columns are made from concrete and are fixed to the ground. While the columns from axis 3-40 are made from steel and is connected to the pontoons at one end, and at the other end connected to the bridge girder. The steel columns also vary in size depending on ``high`` bridge and ``low`` bridge part. See Figure 6-23 and Figure 6-24 for and illustration of the high-bridge columns and the low-bridge columns.

The main dimensions of the columns along axis 3-8 are 7.6m x 7.6m in the middle, 9.6m x 9.6 m towards the bridge girder, and 8m x 8m near the pontoon, as shown in figure 1-4. The columns range in height from 45.566 to 26.855 meters. [24]

The columns at axis 9-40 are 5.2m x 6m in the middle, 7.2m x 8 m towards the bridge girder, and 8m x 8 m towards the pontoon, as shown in figure 1.5. The columns range in height from 23.105 to 10.500 meters. [24]
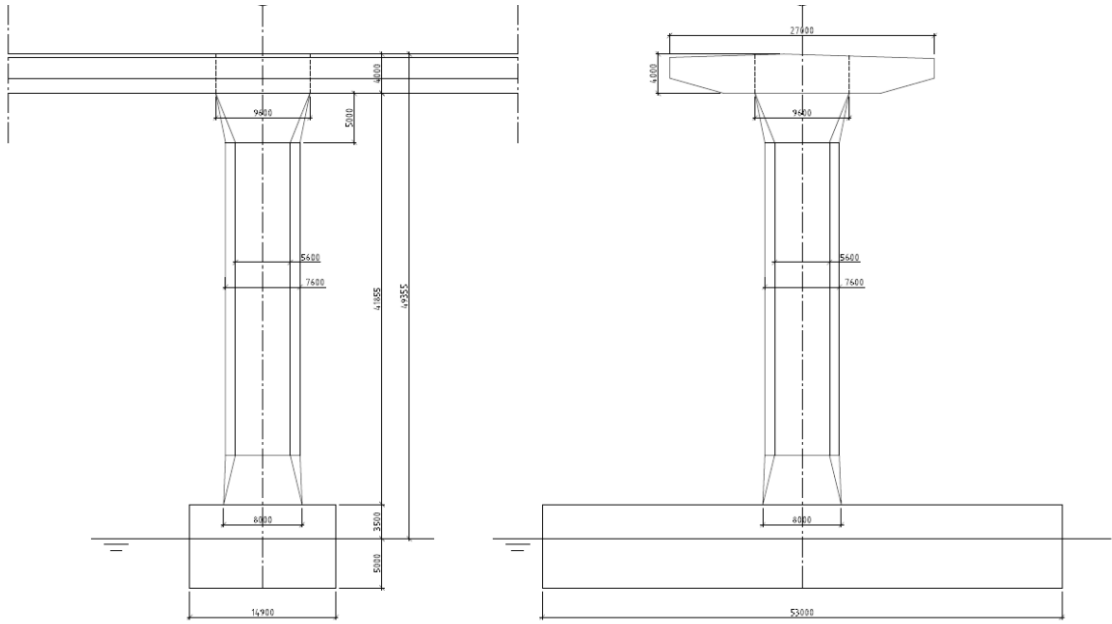
Figure 6-23: The geometric shape of column for high floating bridge part [24]
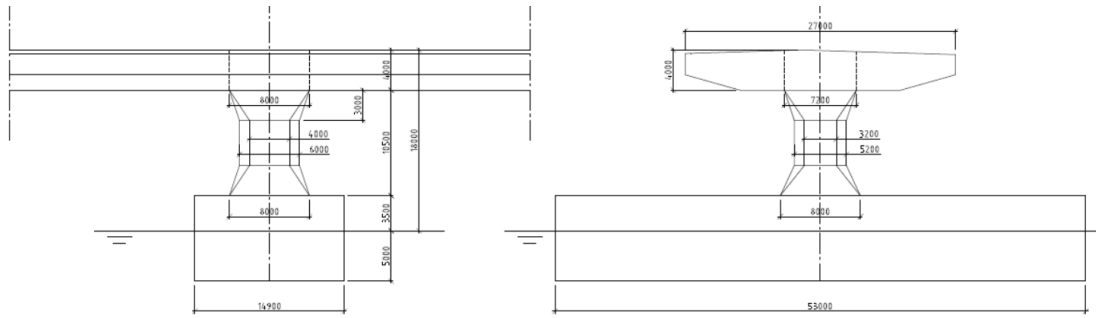
Figure 6-24: The geometric shape of column for low floating bridge part [24]

The columns are modelled as one line object, where one end is connected to the bridge girder and the other end connected to the pontoons. The properties for the columns are presented in Table 6-6 and Table 6-7.
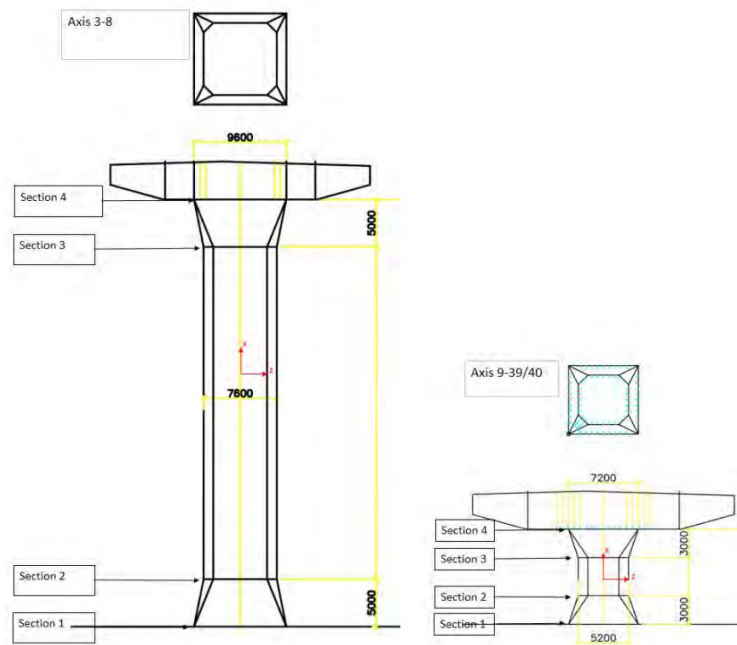
Figure 6-25: Column axis 3-8 (left) and axis 9- (right) [25]

Table 6-6: Steel column properties [25]

Section name	A_x [m^2]	A_y [m^2]	A_y [m^2]	I_x [m^4]	I_y [m^4]	I_z [m^4]
L1	1.280	0.640	0.640	20.170	13.650	13.650
L2	1.122	0.608	0.608	17.280	10.120	10.120
L3	1.122	0.608	0.608	17.280	10.120	10.120
L4	1.536	0.768	0.768	34.950	23.590	23.590
S1	1.280	0.640	0.640	20.170	13.650	13.650
S2	0.802	0.480	0.416	6.804	3.398	4.164
S3	0.802	0.480	0.416	6.804	3.398	4.164
S4	1.216	0.640	0.576	17.190	10.780	12.630

Table 6-7: Calculated steel column properties

Section name	Axial Stiffness EA [KN]	Bending stiffness [KNm^2] x	Bending stiffness [KNm^2] y	Torsional [KNm^2]
L1	2.69E+08	2.867E+09	2.867E+09	1.629E+09
L2	2.36E+08	2.125E+09	2.125E+09	1.396E+09
L3	2.36E+08	2.125E+09	2.125E+09	1.396E+09
L4	3.23E+08	4.954E+09	4.954E+09	2.823E+09
S1	2.69E+08	2.867E+09	2.867E+09	1.629E+09
S2	1.68E+08	8.744E+08	7.136E+08	5.496E+08
S3	1.68E+08	8.744E+08	7.136E+08	5.496E+08
S4	2.55E+08	2.652E+09	2.264E+09	1.388E+09

Where (Eq 6-4), (Eq 6-5) and (Eq 6-6 is used to determine the stiffness of material.

$$\text{Axial stiffness} - \frac{E \cdot A}{L} \qquad \textbf{(Eq 6-4)}$$

$$\text{Bending stiffness} - \frac{E \cdot I}{L} \qquad \textbf{(Eq 6-5)}$$

$$\text{Torsional stiffness} - \frac{G \cdot J}{L} \qquad \textbf{(Eq 6-6)}$$

6.2.6 Mooring Lines

Three of the 38 pontoons are each linked to one of the four side mooring lines. The 11th pontoon is at arch position 2030 meters, the 18th pontoon is at 2905 meters, and the 25th pontoon is at 3780 meters. The side mooring lines improve the bridge's load collecting ability

while also adding rigidity and viscous damping. When the mooring lines are properly pretensioned, the horizontal stiffness is effective.

Line wizard in Orcaflex was used to achieve the same pretension values provided by NPRA [21]. Line wizard configurates multiple lines to achieve a desired tension by adjusting the length of the mooring lines. Table 6-8 shows the pretension reached in this model, compared to the desired one from the NPRA report.

Table 6-8: Mooring line pretension

Line number	Pretension(MN)	
	Main report	Acquired in this model
1	1.98	1.97
2	2.00	1.99
3	2.08	2.09
4	1.93	1.94
5	2.59	2.58
6	2.28	2.28
7	2.54	2.55
8	2.63	2.64
9	2.17	2.16
10	1.69	1.69
11	2.09	2.10
12	2.04	2.05
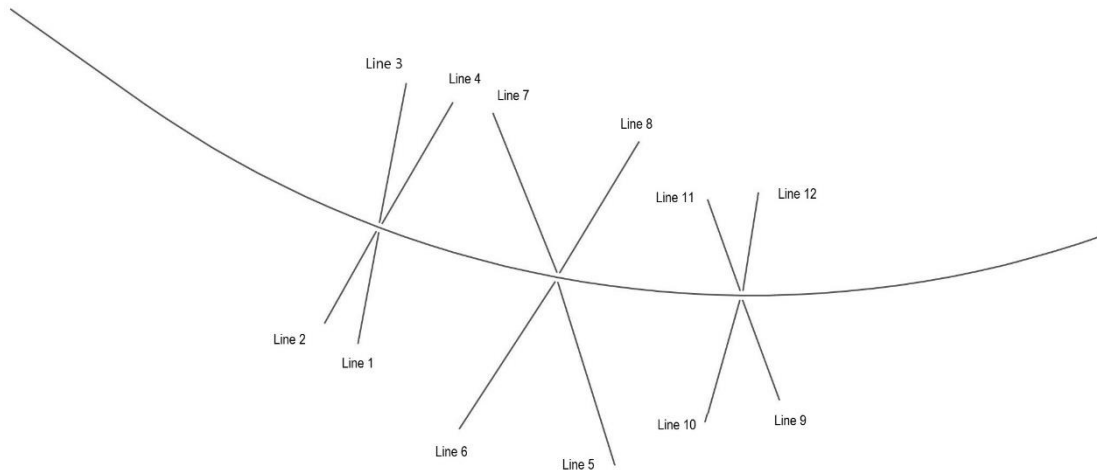
Figure 6-26: Numbering of mooring lines

The mooring lines consist of three segments, where the top and bottom segment is the same length for all mooring lines, while the middle segment varies in length. Table 6-9 shows the different lengths and diameter for each mooring lines.

Table 6-9: Mooring segment dimensions [26]

	Segment	Diameter [m]	Length [m]
1	Top chain	0.147	50
2	Steel wire	0.124	varies
3	Bottom chain	0.147	100

The first segment is the top chain connected to the pontoon, the second segment is the middle segment, while the third and last segment is the bottom chain anchored to the seabed.

Mooring lines are modelled using line objects with structural properties listed in Table 6-10.

Table 6-10: Mooring segment properties [26]

Segment	Elastic modulus (EA)	Breaking load	Cd,n	Cd,l
Top chain	1.73E6 kN	19 089 kN	2.4	1.15
Steel wire	1.45E6 kN	15 073 kN	1.2	0.10
Bottom chain	1.73E6 kN	19 089 kN	2.4	1.15

6.3 Modelling of earthquake

Orcaflex does not have a direct seismic ground motion function. However, constraints can have a time history data. Therefor the seismic ground motion in Orcaflex is attached as constraint and fixed to its corresponding position at the seabed. The seismic ground motion is applied at every element anchored, fixed to the seabed or to the mainland. Table 6-11 shows the different elements and location starting from the south-end side of the bridge.

Table 6-11: Constraint location

Constraint number	Connection	X-direction [m]	Y-direction [m]	Z-direction [m]
11	South end girder	-2581	1267.8	66.7
12	Concrete column #1	-2548.3	1244.7	49.5
13	Concrete column #2	-2503.5	1212.9	39.7
14	Concrete column #3	-2458.6	1181.1	28.2
15	Concrete column #4	-2413.7	1149.3	19.5
16	Concrete column #5	-2368.8	1117.6	4.3
21	Tower leg #1	-2267.8	1017.9	0
22	Tower leg #2	-2241.2	1055.5	0
31	Mooring line #1	-941.3	-312.4	-18
32	Mooring line #2	-1098.3	-216.4	-18
33	Mooring line #3	-714.3	915.6	-18
34	Mooring line #4	-494.3	825.6	-15
41	Mooring line #5	270.7	-886.4	-15
42	Mooring line #6	-462.3	-716.4	-15
43	Mooring line #7	-303.3	774.6	-15
44	Mooring line #8	385.7	640.6	-18
51	Mooring line #9	1048.7	-578.4	-14
52	Mooring line #10	700.7	-683.4	-10
53	Mooring line #11	710.7	365.6	-15
54	Mooring line #12	949.7	398.6	-14
61	North end girder	2587.3	199.8	11.6

Dr. Kaiming Bi created the artificial ground motions that were applied to the constraints. The behavior of various simulation instances on the bridge will be evaluated and studied.

This dynamic analysis uses a time step of 0.005 seconds and an earthquake length of 20 seconds. The simulation takes 50 seconds in total, leaving 30 seconds after the earthquake to observe the response.

6.4 Modelling of tsunami

The earthquake induced tsunami is applied as Load force in Orcaflex. Where the load is force time history acquired in Section 5.2. The load is applied at the center of the pontoon at the east side. Figure 6-27 illustrates the location of the applied force on the pontoons.
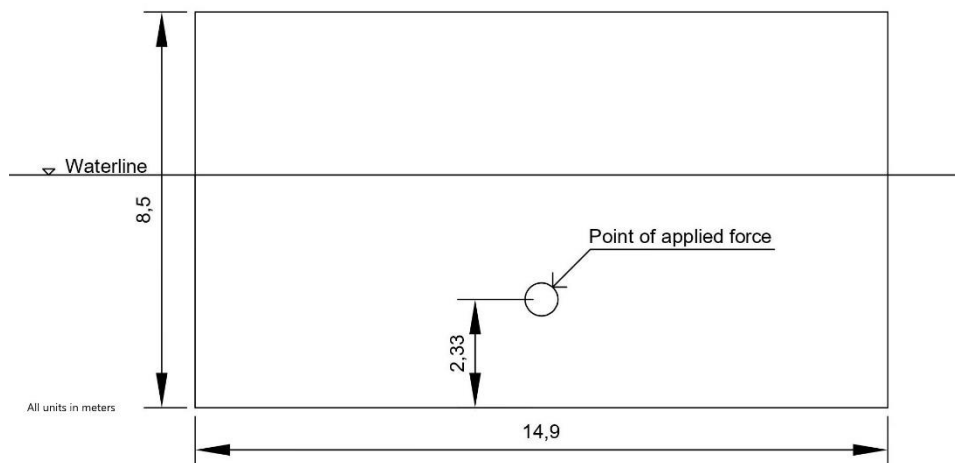
Figure 6-27: Location of applied tsunami force on pontoons without mooring lines

To capture the tsunami force, a dynamic analysis with a time step of 0.01 seconds and a time force history of 400 seconds. The whole simulation takes 1000 seconds, where the earthquake motion is applied at 10 seconds. The tsunami time force history is then applied at 400 seconds, this is to capture the motion of the earthquake before applying the tsunami force. Figure 6-28 illustrates an example of input for both the earthquake and the tsunami load.
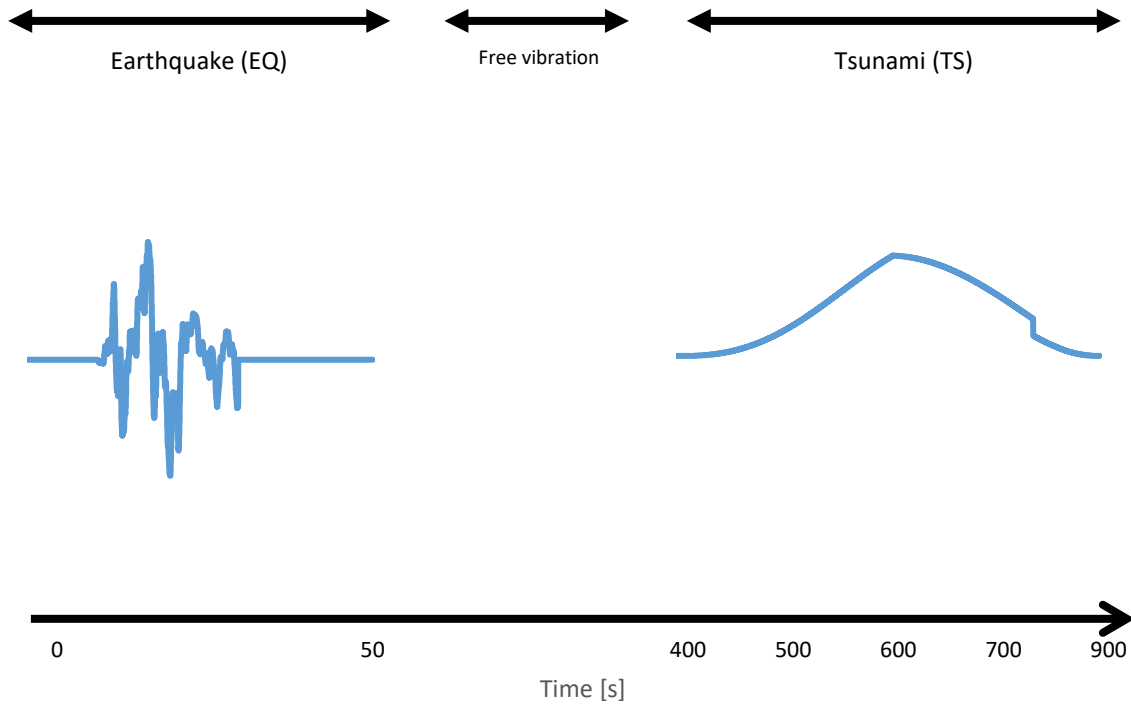
Figure 6-28: Sequential earthquake and tsunami time-history

Chapter 7: Analysis results

7.1 Introduction

The analysis in this study is investigated under 3-dimensional earthquake excitations. Orcaflex was utilized to mimic and evaluate the response. As mentioned in section 5.1.1, Dr. Kaiming Bi created the input earthquake data used in this thesis, which span a wide variety of frequencies. The seismic input needed to simulate the bridge is discussed in section 6.3.

Note that the simulation will only consider seismic motion and seismic-induced tsunami. Wind and Wave is not part of the simulation.

7.1.1 Allowable motion

Bridges must be designed to provide comfort and safety to the bridge users. According to NPRA's handbook, N400 [14] section 3.5-2, the maximum allowable displacement of the bridge deck should be limited to $L/350$ for traffic load alone, where L is the length of the bridge span.

Section 3.5-4 in N400 refers to section A2.4.3.2 in [27] that stats that the comfort criteria should not exceed the following acceleration m/s^2 of any part of the bridge deck;

- 0.7 for vertical oscillations
- 0.2 for horizontal oscillations
- 0.4 for unusually large crowds

Table 7-1 summarizes the acceptable motions for the bridge deck.

Table 7-1: Summarized acceptable motion for bridge deck

Motion	Maximum response
Vertical displacement	$L/350$
Vertical acceleration	$0.7 \, m/s^2$
Horizontal Acceleration	$0.2 \, m/s^2$

7.1.2 Allowable forces/stresses

7.1.2.1 Bridge girder Axial stress

The yielding stress for steel bridge girder is 420MPa. That mean maximum allowable stress occurring on the bridge girder is $f_y/\gamma_m = 382\ MPa$.

Using (Eq 7-1, we can obtain maximum allowable axial force depending on the cross-section of the bridge girder.

$$\sigma = \frac{F}{A} \qquad \text{(Eq 7-1)}$$

$$F = \sigma \cdot A \qquad \text{(Eq 7-2)}$$

For simplicity, one cross-section will be used to obtain maximum allowable axial force. 1.33 m^2. Solving (Eq 7-2 we obtain a force of 508 MN.

7.1.2.2 Bridge girder Moment resistance

According to [28] the cross section of the bridge girder is class 4, meaning buckling will occur before the attainment of yield stress in one or more parts of the cross-section. The $W_{strong,eff}$ and $W_{weak,eff}$ for the bridge girder type F1_0 corresponds to 5.406 m^3 and 1.620 m^3 respectively. Bridge girder F1_0 was selected due to have the smallest values of W_{eff}, resulting in a conversative bending resistance.

For simplicity we will check for bending resistance for yielding in compression flange while tension flange in fracture. The equation is as following according to Eq. (6.15) of [29]

$$M_{c,rd} = \frac{W_{eff,min} \cdot f_y}{\gamma_{M0}} \qquad \text{(Eq 7-3)}$$

Where:

f_y – Yield strength of material = 420 MPa for steel S420

γ_{M0} - Partial factor for material 1,05 (NA 2008)

Solving equation (Eq 7-3 we obtain $M_{strong,rd} = 2270\ MNm$ and $M_{weak,rd} = 680 MNm$. NPRA states that $M_{strong,rd}$ for the bridge girders is between 2000 MNm and 3000 MNm. For simplicity this thesis will use the values of $M_{strong,rd} = 2300 MNm$ and $M_{weak,rd} = 650 MNm$ for every bridge girder.

According to [30] a strong axis moment load of 3300MNm for the concrete box girder can easily be resisted. Therefore, the same moment resistance for steel bridges will apply for the concrete bridge girder.

7.1.2.3   Stay-Cables

According to [30] the breaking strength varies from 8.6 MN to 18.7 MN depending on the number om strands. Table 7-2 summarized the breaking strength of each cable.

Table 7-2: Breaking strength of stay-cables

Side pan	118	117	116	115	114	113	112	111	110	109	108	107	106	105	104	103	102	101
Breaking strength [MN]	17,0	17,0	17,0	17,0	17,0	17,0	15,3	15,3	15,3	15,3	12,0	12,0	12,0	10,3	10,3	8,6	8,6	8,6
Main span	201	202	203	204	205	206	207	208	209	210	211	212	213	214	215	216	217	219
Breaking strength [MN]	8,6	8,6	8,6	10,3	12,0	12,0	15,3	15,3	15,3	15,3	17,0	17,0	18,7	18,7	18,7	18,7	18,7	18,7

7.1.2.4   Mooring lines
According to [26] the breaking strength for the mooring lines is 19MN, 15MN and 19MN for the top chain, steel wire and bottom chain respectably. Sense every mooring line contains Top chain, steel wire and bottom chain, the breaking strength will be chosen to be 19MN throughout the mooring lines.

7.2 Mode shapes

The mode forms shown in this section indicate the first 5 modes of each motion; horizontal, vertical, and torsional, which determine the floating structure's response. Comparison of the mode frequency against the consultant's report can be seen in Table 7-3.

Table 7-3: Mode period and frequency's

Mode	Period (s)	Frequency (Hz)	Consultant's period (s)
1	51.9997	0.0192	56.3
2	41.1001	0.0243	43.2
3	30.1450	0.0332	31.0
4	21.3554	0.0468	21.4
5	21.0814	0.0474	17.1
6	17.7095	0.0565	13.4
7	14.0233	0.0713	12.7
8	12.9878	0.0770	10.3
9	11.8937	0.0841	9.48
10	11.5639	0.0865	8.36
11	11.4274	0.0875	8.36
12	11.2035	0.0893	7.39
13	11.0671	0.0904	6.89
14	10.8020	0.0926	6.89
15	10.5485	0.0948	6.88

Mode 1, T=51.9

Longitudinal displacement — Horizontal displacement — Vertical displacment — Rotation about bridge axis — Rotation about transverse axis — Rotation about vertical axis
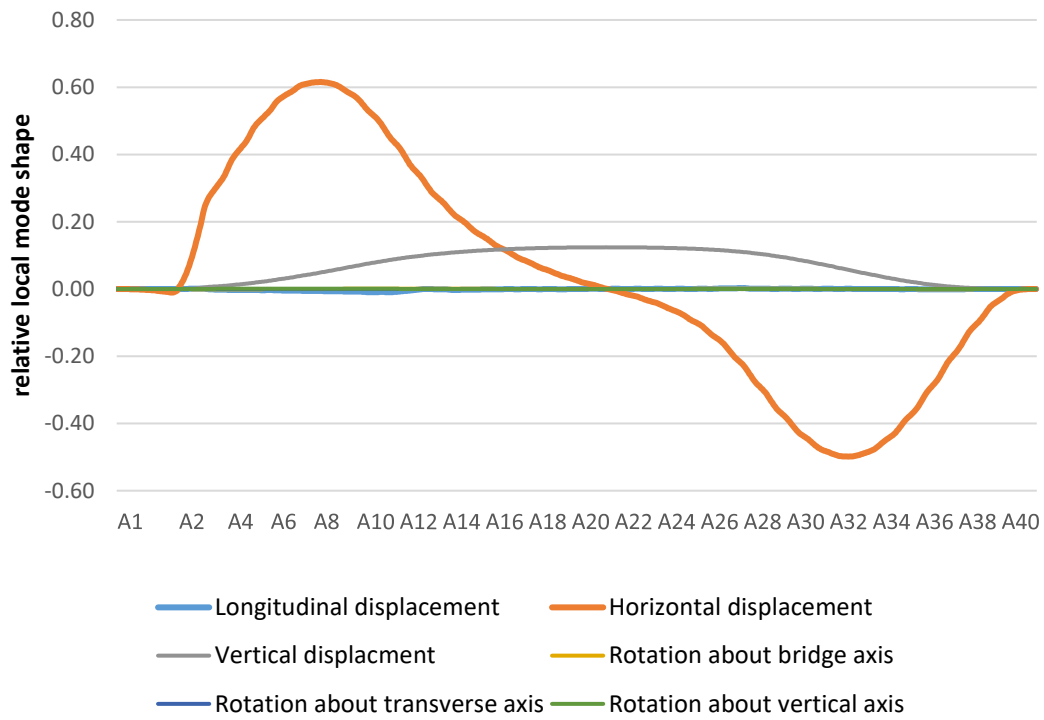
Mode 2, T=41.1
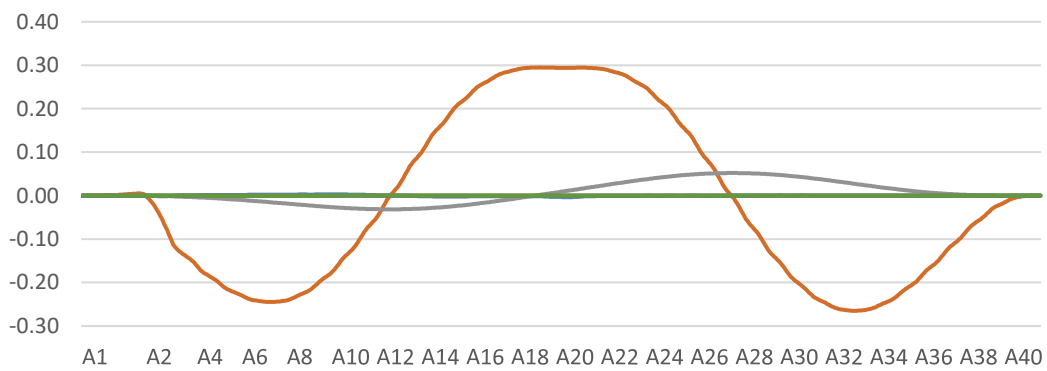
Mode 3, T=30.14
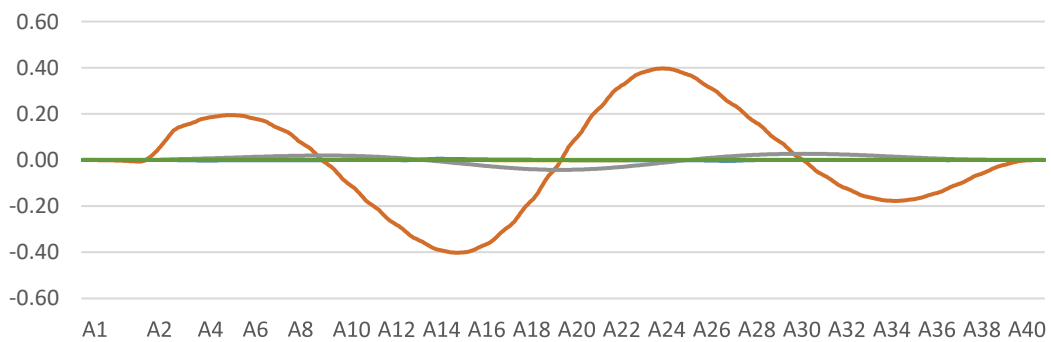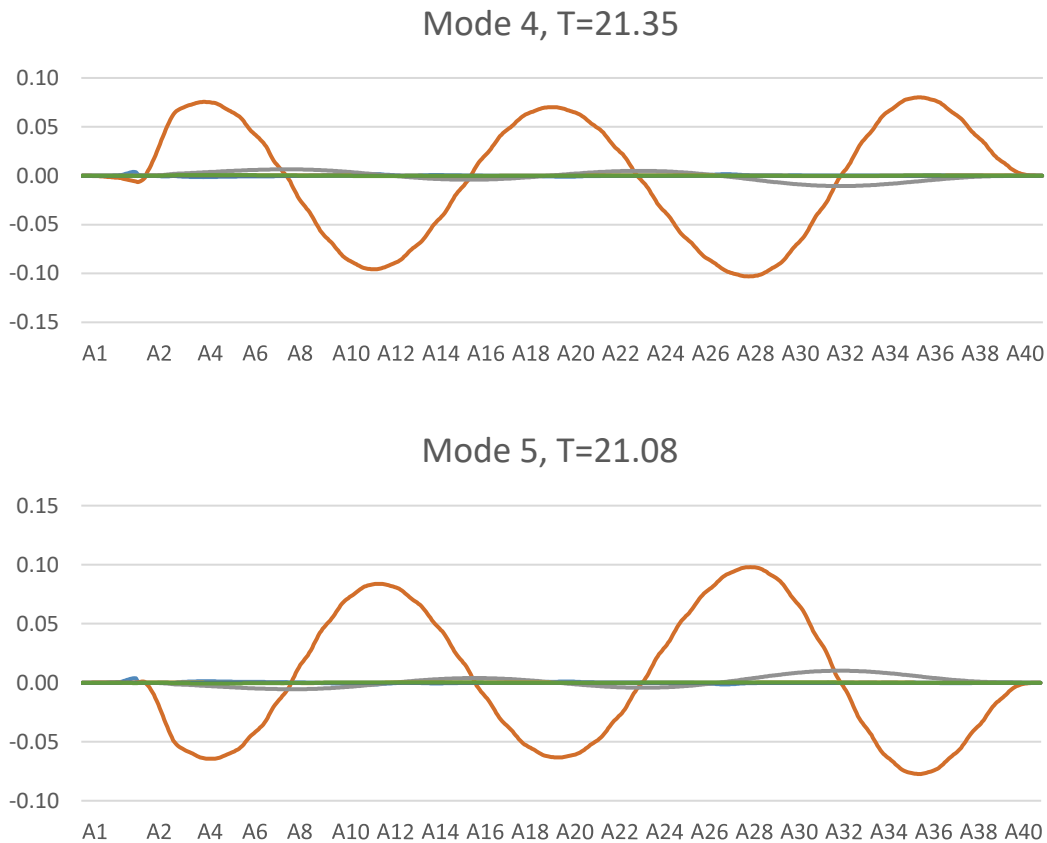
Figure 7-1: First five (5) mode shapes

7.3 Forces acting on bridge

This section presents the results of the numerical analysis of the global forces acting on the bridge girder. These forces include the axial forces, the strong axis bending moment, the weak axis bending moment and the torsional moment. This thesis does. In order to provide the most accurate representation possible of the global force response, peak values are plotted along the length of the bridge. It is imperative that the capacity of the bridge girder be evaluated since it must not exceed its capacity.

As mentioned in section 7.1.2.2 above, the bending moment capacity of the bridge girder along the strong axis is 2500 MNm, whereas the capacity of the girder along the weak axis is 600 MNm.

7.3.1 Forces acting on bridge girder

The axial force increases a lot in the sound side of the bridge due to the seismic motion otherwise the increase of axial force due to seismic motion increases proportionally tough out the bridge length.
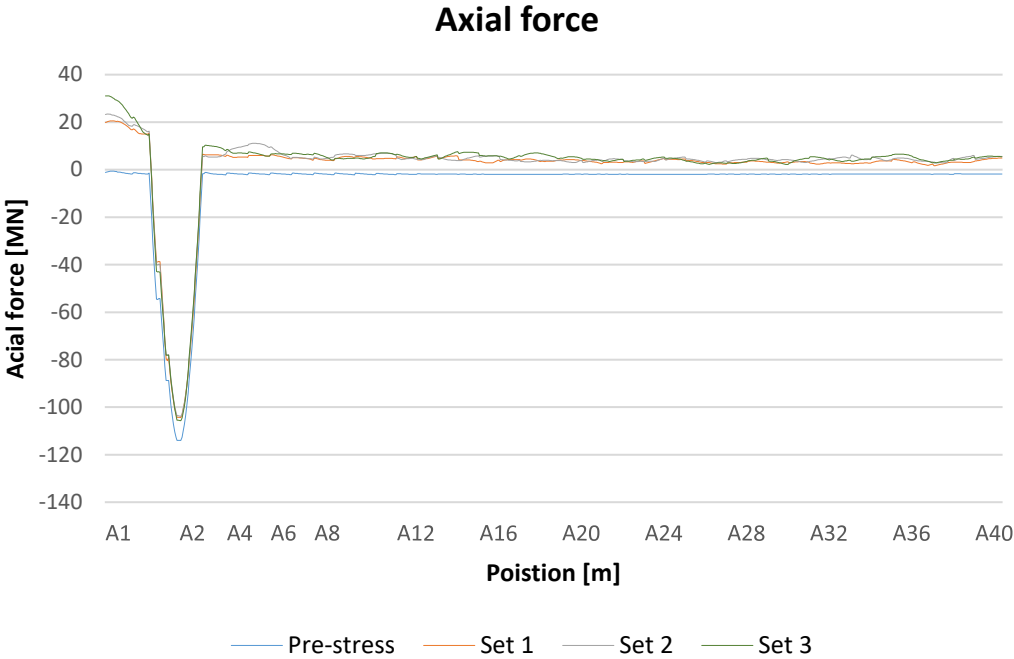
Axial force

Figure 7-2: Axial force

The axial force increases with 2588%, from 1.15MN to 30.9MN, which is an extremely high increase percentage. For the rest of the bridge girder the seismic motion increases with around 500% of its initial value. The highest tension force is 30.9 MN, occurring at the south end of the bridge and 114 MN in compression near the tower. That results in a stress of 85MPa which is a utilization ratio of 0.28.
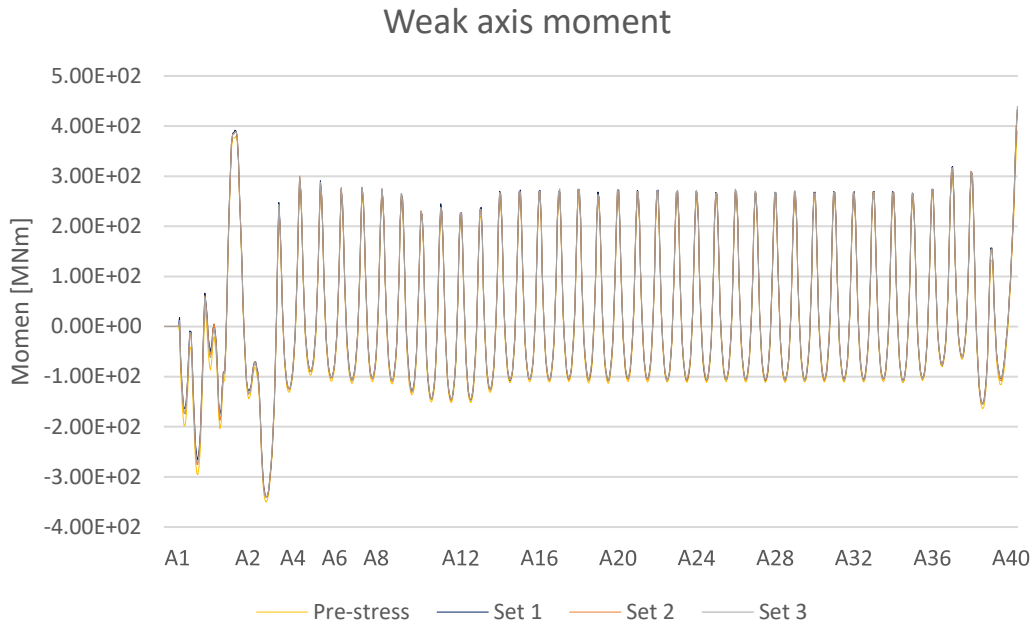
Figure 7-3: Weak axis bending moment

Figure 7-3 illustrates the weak axis bending moment. As seen in the figure, the seismic ground motion does have a big effect on the bridge girder. The weak axis bending moment has an increase of 12.5 % at the highest point due to seismic ground motion. This happens at north end of the bridge, with a bending moment of 439.63 MNm, which is 64.6% of its capacity utilization of 680MNm.
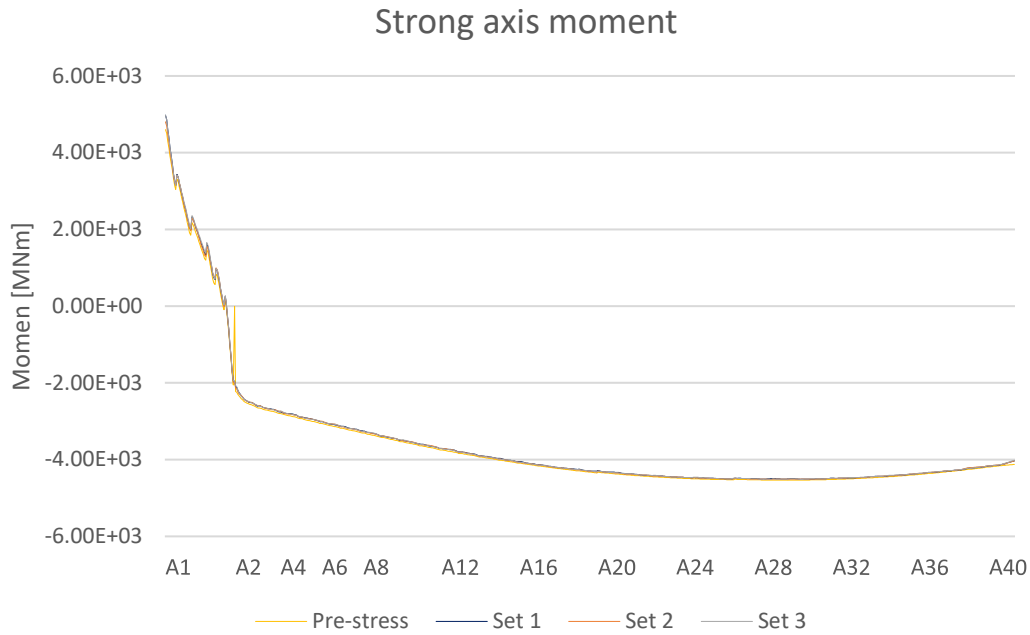
Strong axis moment

Figure 7-4: Strong axis bending moment

For the strong axis bending moment, the capacity is 2200MN. However, we can clearly see in Figure 7-4 that the bending moment exceeds its limit by far, going as far as 4979.3 MNm. This happens at the south end of the bridge, nevertheless the pre-stress at the south end part is 4600 MNm, which means the seismic motion increases the strong axis bending moment by only 7%.

It is worth mention that the strong axis bending moment for the bridge girder doesn't not correspond well with the pre-stress strong axis bending moment NPRA generated. Therefore, the response of the strong axis bending moment will be neglecting.
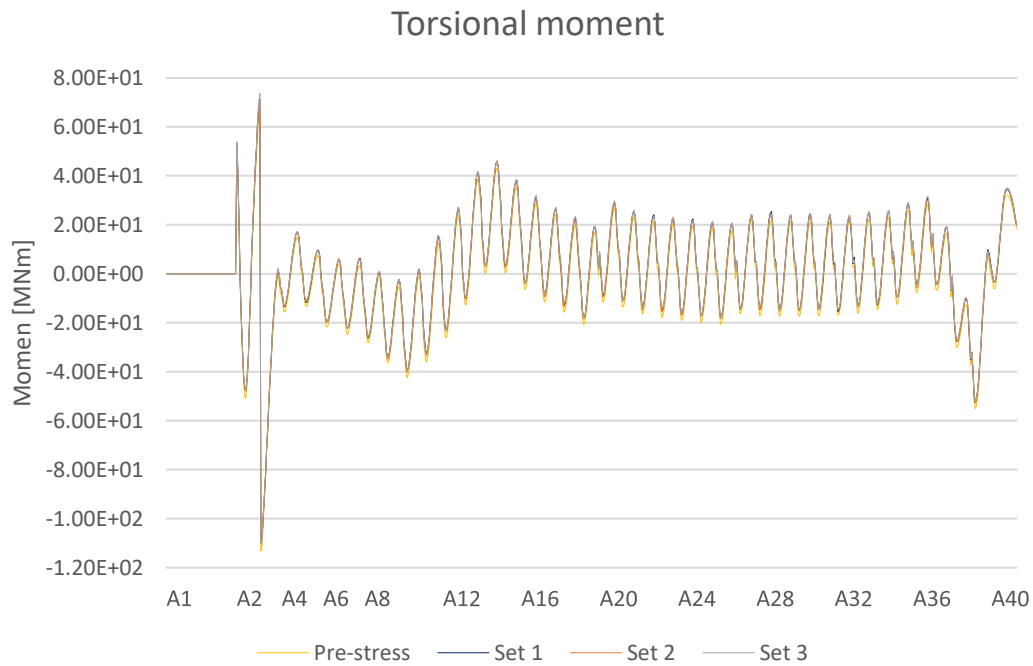
Figure 7-5: Torsional moment

The torsional moment shown in Figure 7-5 shows a maximum moment occurring at the main span of the tower bridge. The torsional moment due to seismic motion reaches a value of 73.6MNm, which is an increase of 10.4% compared to the pre-stress torsional moment of 66.7MNm

7.3.2   Forces on mooring lines

The mooring lines is subjected to increase in axial force and therefore needs to be investigated closer. Figure 7-6 illustrates the axial force on the mooring lines for each ground motion set.
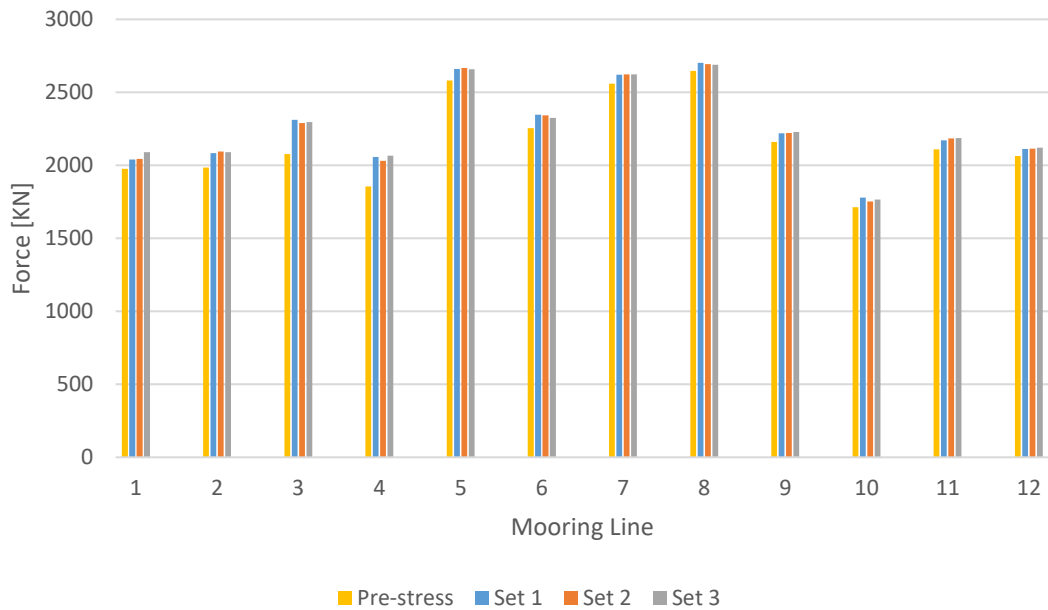
Figure 7-6: Mooring line axial force due to seismic motion

The mooring line slightly increases due to seismic motion. The highest increase happens in mooring line 3 with an increase of 235 KN. However, considering that the breaking strength of the mooring lines is 19 000KN and the highest axial loading acquired is 2312.34 KN. It is reasonable to assume that the seismic motion has almost no impact on the mooring lines.

7.3.3 Response of Stay-cables

The stay-cables must be examined more closely because bridge deck vibrations will produce forces in the bridge, which may cause the cables to yield. As discussed in section 7.1.2.3 the breaking load for the cables is between 8.6 MN to 18.7 MN
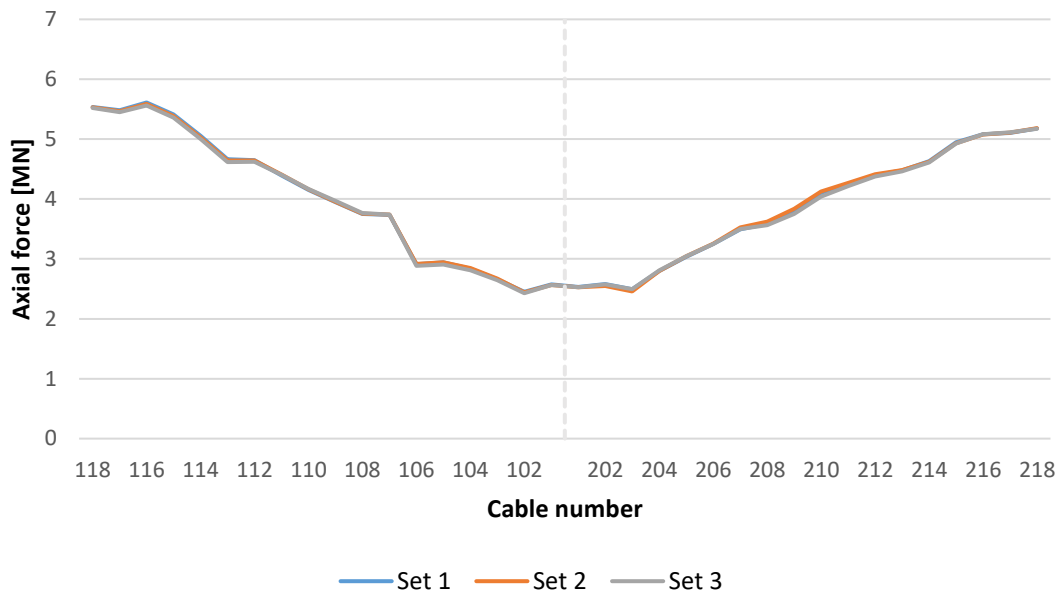
Figure 7-7: Comparison of maximum axial force due to seismic motion

Taking a closer look at Figure 7-7 we can see that the stay cables doesn't even exceed 6MN for the long cables and stays bellow 3MN for the short cables that is way below the breaking load of the stay-cables. Table 7-4: summarized the axial force in four of the cable stays.

Table 7-4: Axial force in four cables when subjected to ground motion

Cable id		Max force [MN]	Breaking load [MN]	Utilization [%]
Longest cable	118	5.65	17	33.2
Shortest cable	101	2.6	8.6	30.2
Shortest cable	201	2.55	8.6	29.6
Longest cable	218	5.31	18.7	28.4

As we can see the utilization around 30% of the breaking load. This is considered not high enough to be a problem especially when considering that the axial force in the cables only increases around 0.1 MN due to seismic motion.

Figure 7-7 illustrate the axial force time history of the cables for three cables, longest cable in the side span, shortest cable in the side span and the longest cable in the main span. For a better understanding of the influence of the seismic motion, the pre-stress forces are eliminated in Figure 7-9 As we can see, the axial force increases slightly due to seismic motion, around 0.1 MN.
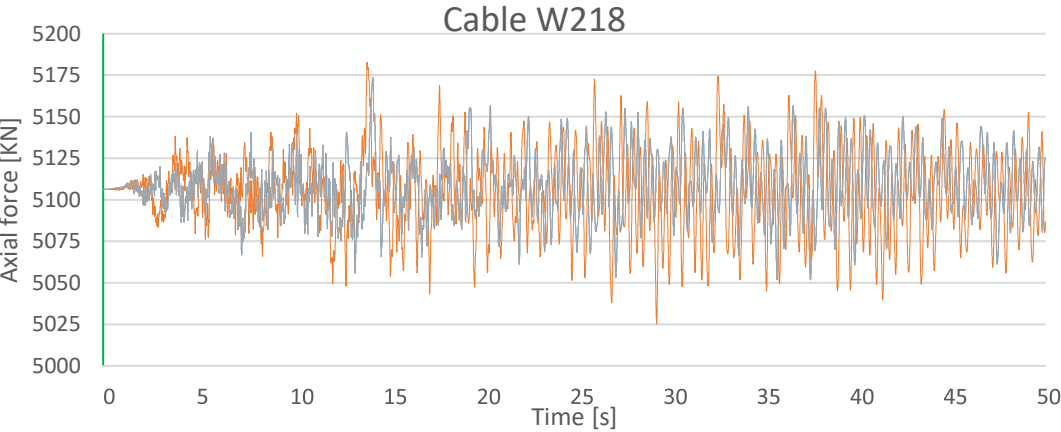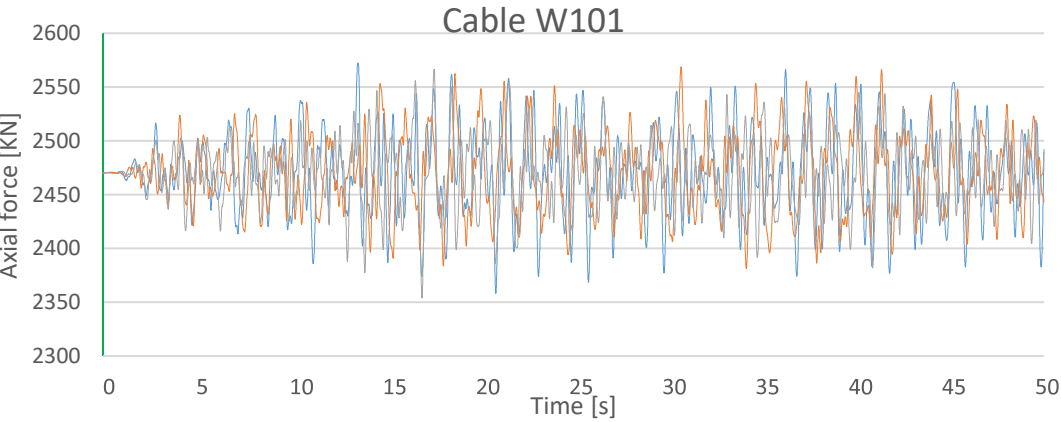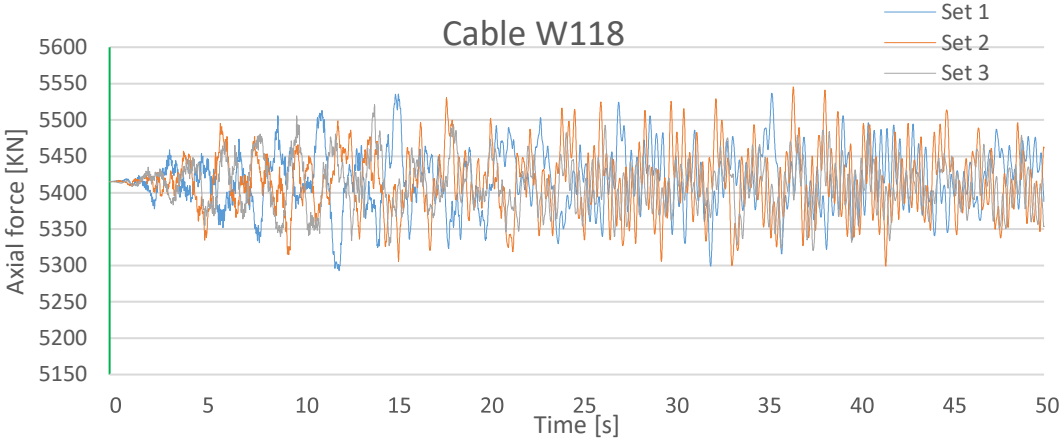
Figure 7-8: Cables Axial force due to seismic motion
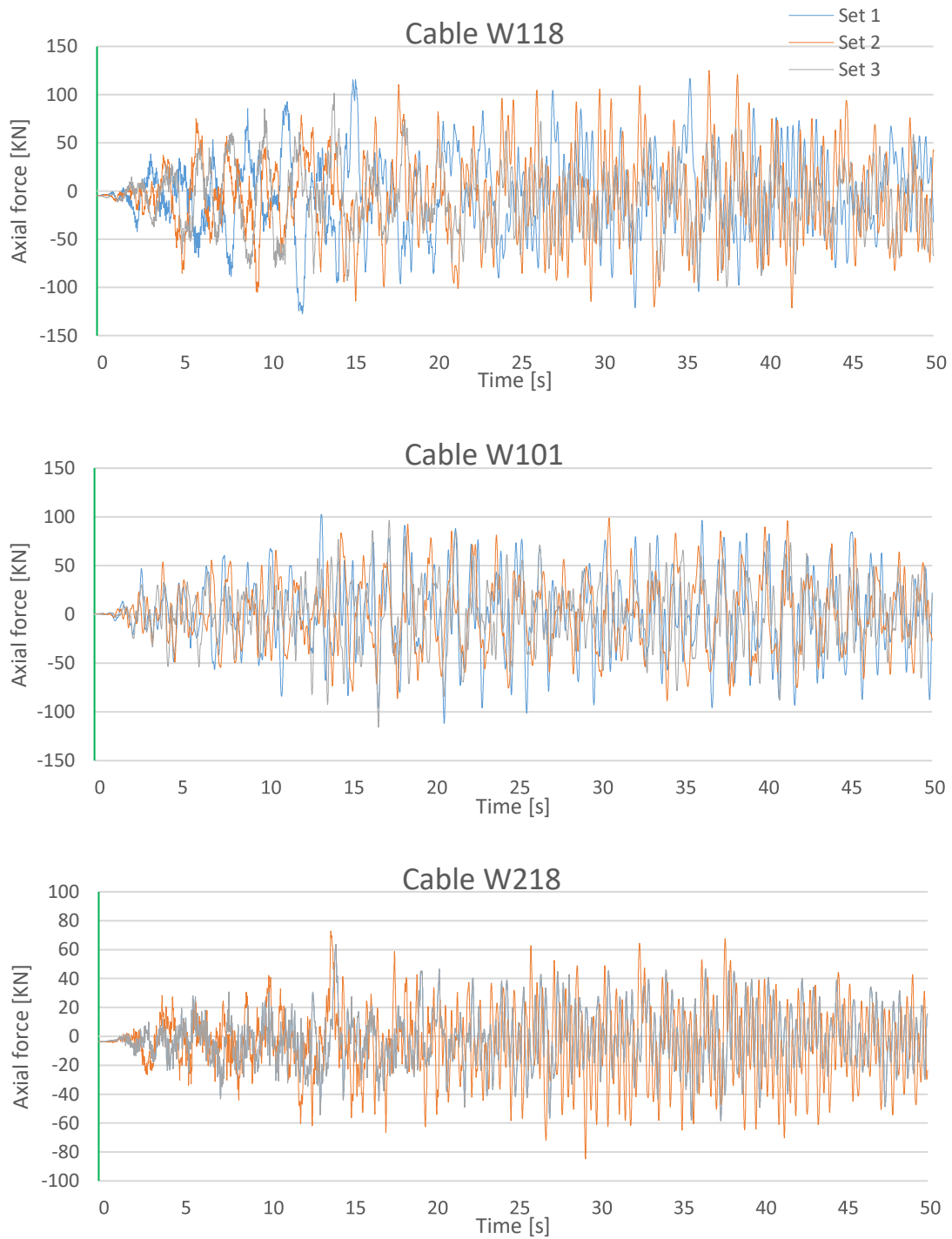
Figure 7-9: Cables Axial force due to only seismic motion

7.4 Motions acting on bridge girder

The motions of the bridge need to be researched to guarantee the safety of the traffic. In the following subsection, we will investigate the accelerations and displacements experienced by the bridge girder. It is necessary to locate the points of maximum displacement along the bridge to guarantee the structural integrity.

The nodal accelerations will be examined from three different places, as marked in red circles in Figure 7-10: the cable-stayed component (a), the high-bridge (b), and the low bridge (c). This is done to represent the variations in acceleration time histories between places. As discussed in section 7.1.1, a maximum vertical acceleration of $0.7 \ m/s^2$ and a horizontal acceleration of $0.2 \ m/s^2$ must not be exceeded to ensure safe traffic on the bridge. The same applies for vertical displacement where the maximum allowed displacement is $L/350$.
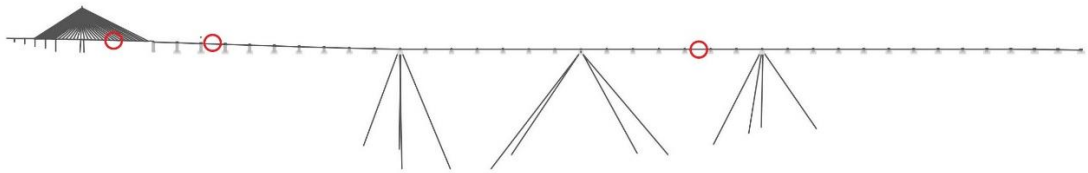
Figure 7-10: Locations that will be compared

7.4.1 Acceleration due to seismic motion
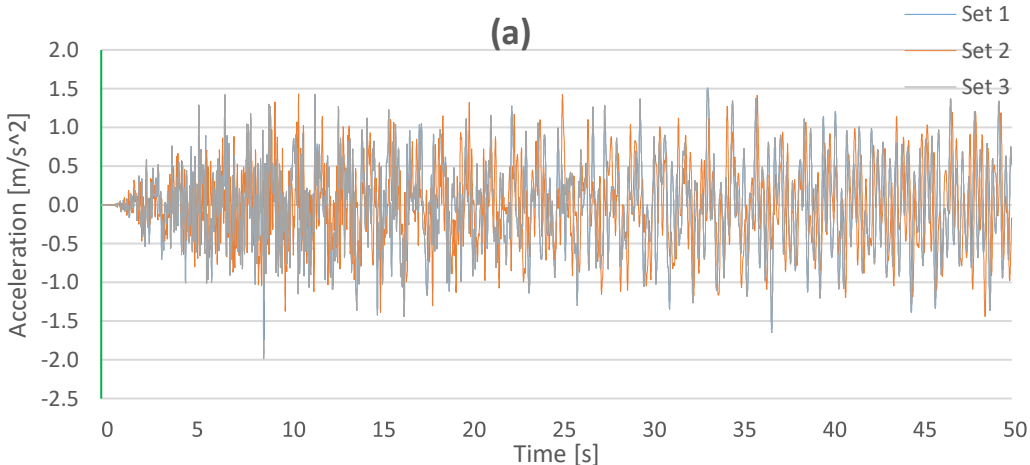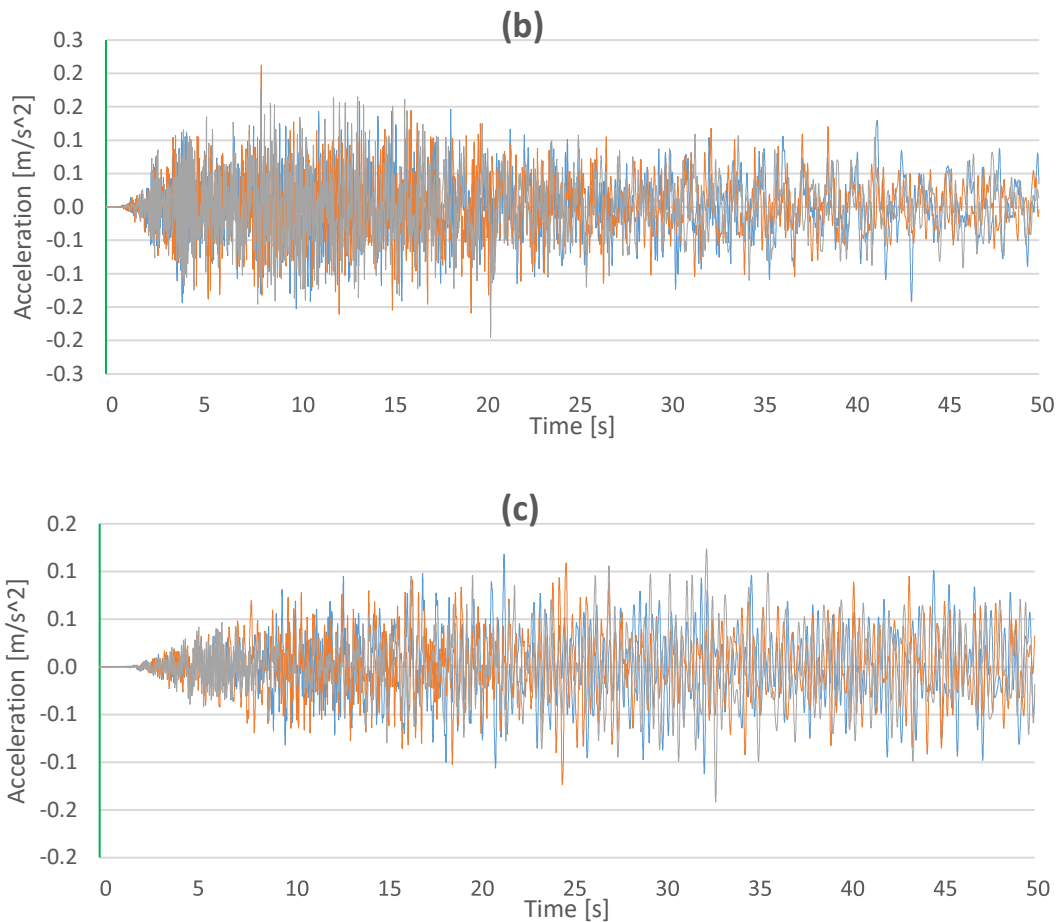
Figure 7-11: Vertical (z-direction) accelerations

As illustrated in Figure 7-11 **(a)**, the vertical acceleration (z-direction) for the bridge part exceeds the maximum allowable motion of $0.7\ m/s^2$. The maximum response value reaches up to $1.9\ m/s^2$ (~0.19g). This is due to the large span of the continuous bridge girder (320m) causing more motion on the bridge girder.

However, the vertical acceleration for the ``high`` bridge part and ``low`` bridge part shown in Figure 7-11 **(b) and (c)** respectively demonstrates a maximum response up to $0.22\ m/s^2$ and $0.15\ m/s^2$, which is significantly less than the maximum allowable motion of $0.7\ m/s^2$.

Additionally, viewing Figure 7-11 we can notice that at the beginning of the figure, we have high period (frequency), and it decelerate towards the end. If the simulation time was longer, we would have noticed a deceleration in period and acceleration.
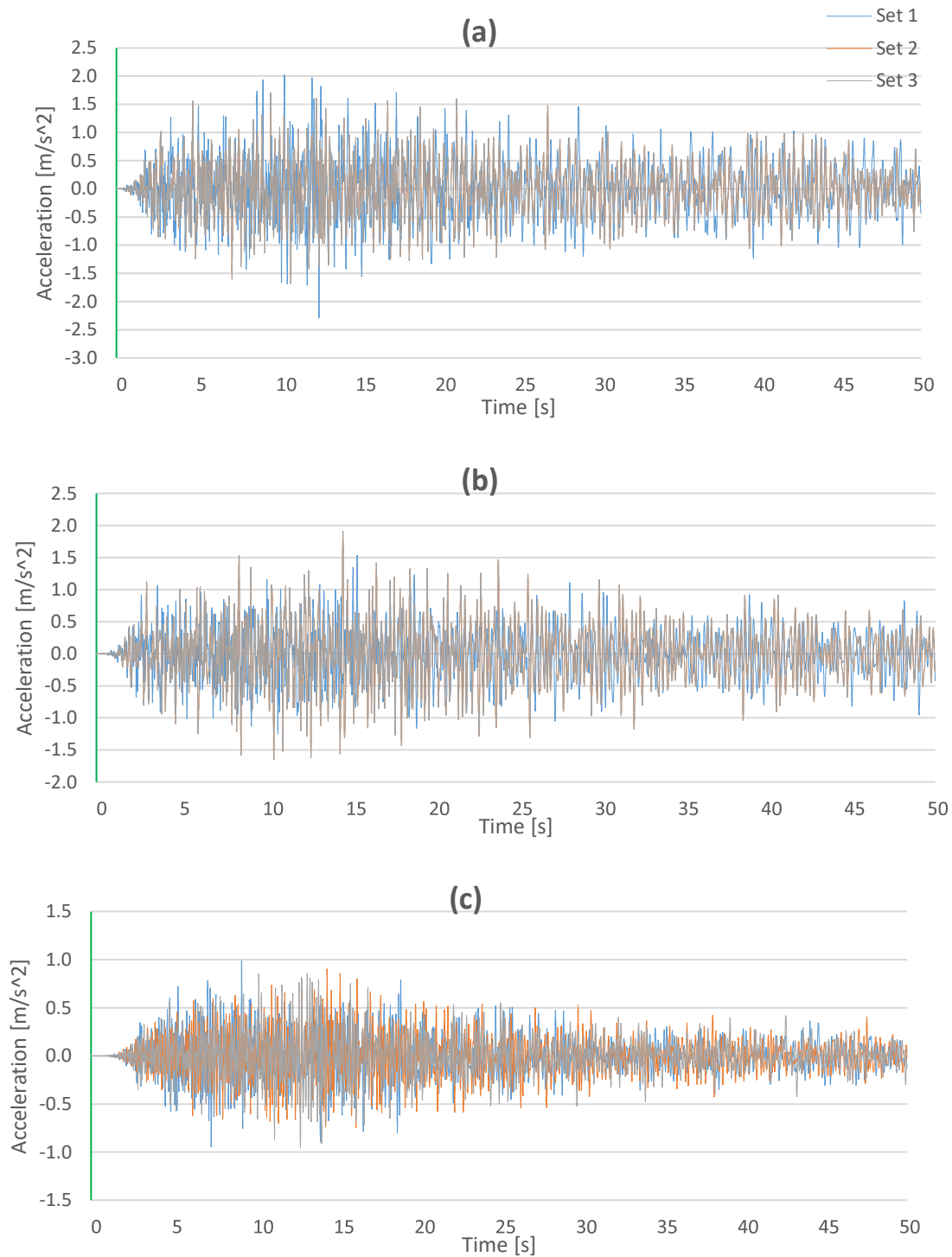
Figure 7-12: horizontal (y-direction) acceleration

The horizontal (y-direction) acceleration for all points exceeds the maximum allowable motion for horizontal motion of $0.2 \, m/s^2$. The maximum response for point (a), (b) and (c) are $2.3 \, m/s^2$, $1.9 \, m/s^2$ and $1.0 \, m/s^2$ respectively is far to high.
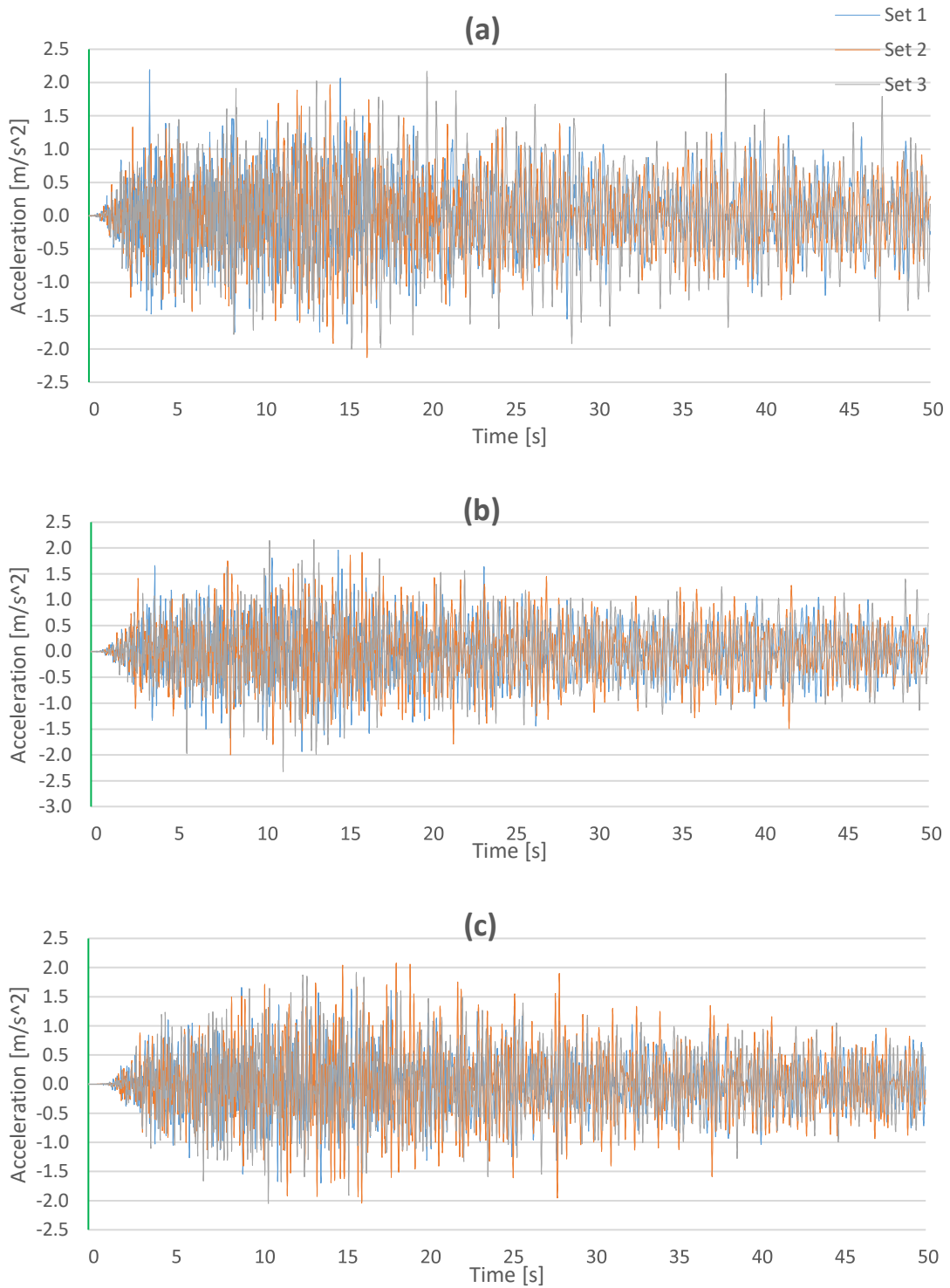
Figure 7-13: horizontal (x-direction) acceleration

The same applies for the acceleration in the x-direction. As mentioned earlier, the maximum

allowable acceleration is $0.2\ m/s^2$, which we can clearly see in Figure 7-13 exceeds that limit

by far. Acquiring an acceleration of $2.19\ m/s^2$, $2.3\ m/s^2$ and $2.05\ m/s^2$ for point (a), (b) and (c) respectably.

Figure 7-14 to Figure 7-16 summarized the peak acceleration for each set along the bridge. It is worth to mention that the peak acceleration along the bridge line does not happen simultaneously.
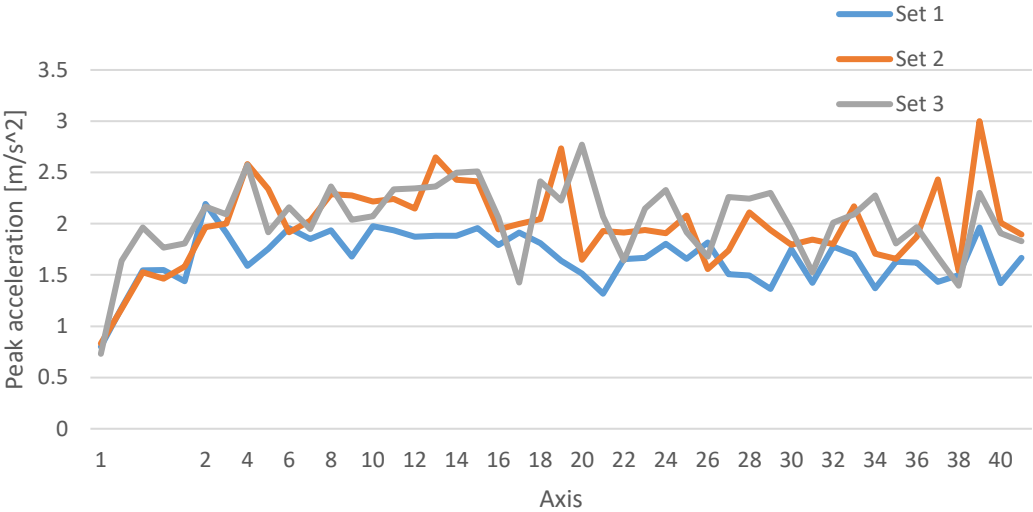
Figure 7-14: Peak longitudinal accelration along the whole bridge
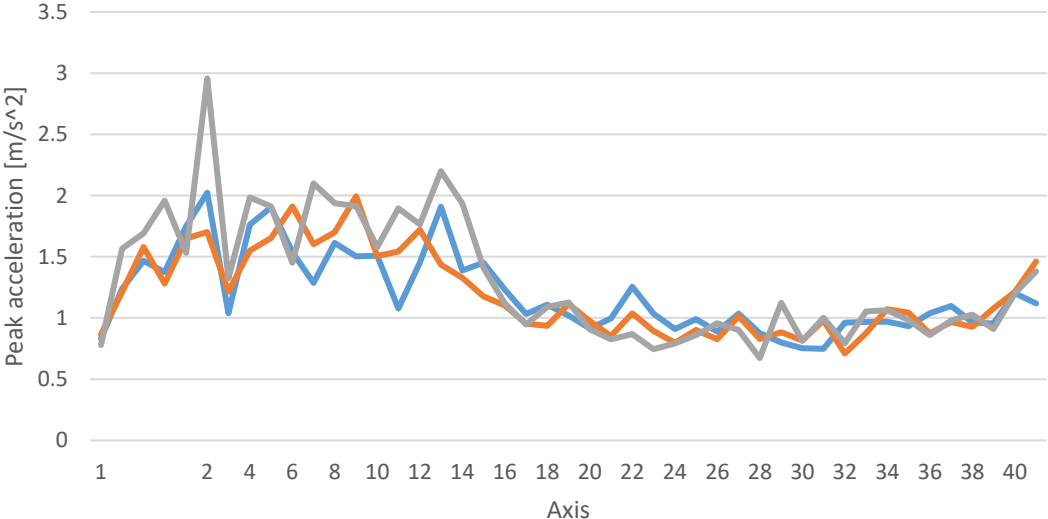
Figure 7-15:Peak horizontal accelration along the whole bridge
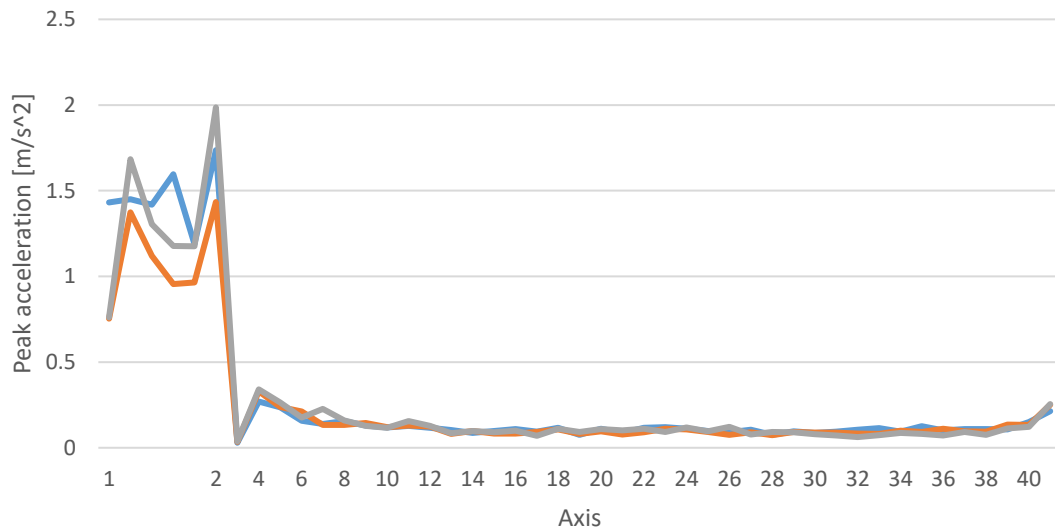
Figure 7-16: Peak Vertical accelration along the whole bridge

7.4.2 Displacement due to seismic motion

The displacement in the Longitudinal, horizontal, and vertical displacement is shown in Figure 7-17 to Figure 7-19. Although the accelerations at the cable-stayed section are higher than in the previous subchapter 7.4.1, the displacements are minimal. In both horizontal and vertical directions, the bridge's floating section exhibits an elastic reaction. In comparison to the cable-stayed reaction, the vertical direction produces a minor or non-existent response in the floating section. The bridge deck's overall maximum displacement for the tower part, ``high`` bridge and ``low`` bridge is summarized in Table 7-5 bellow.

Table 7-5: Displacement along the bridge due to seismic motion

	Maximum displacement [mm]		
	Longitudinal	Transverse	Vertical
Tower	49.15	21.88	11.44
``High`` bridge	27.51	24.26	13.30
``Low`` bridge	28.50	22.02	15.36
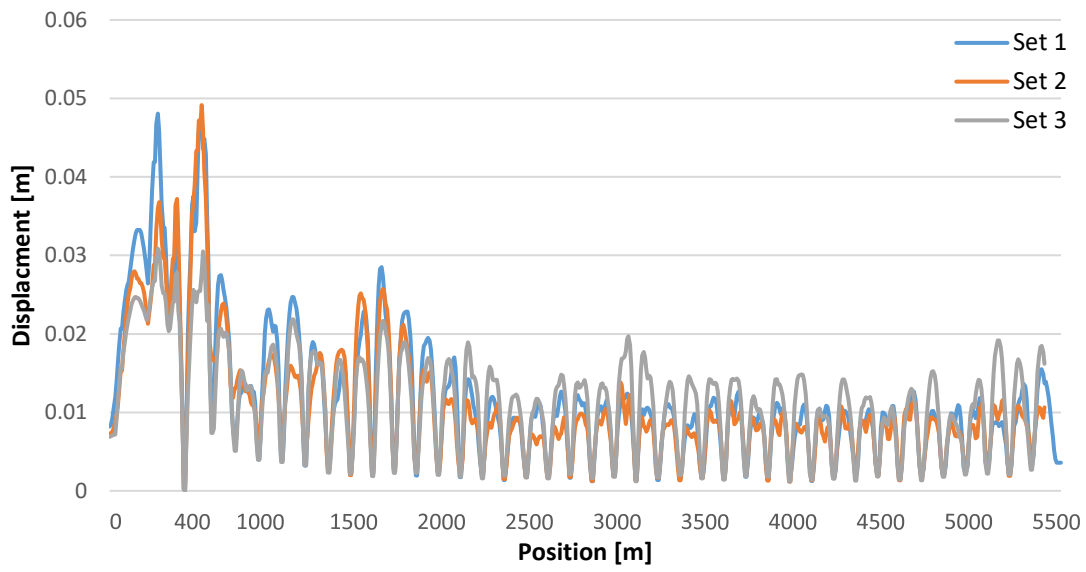
Figure 7-17: Longitudinal displacment due to seismic motion
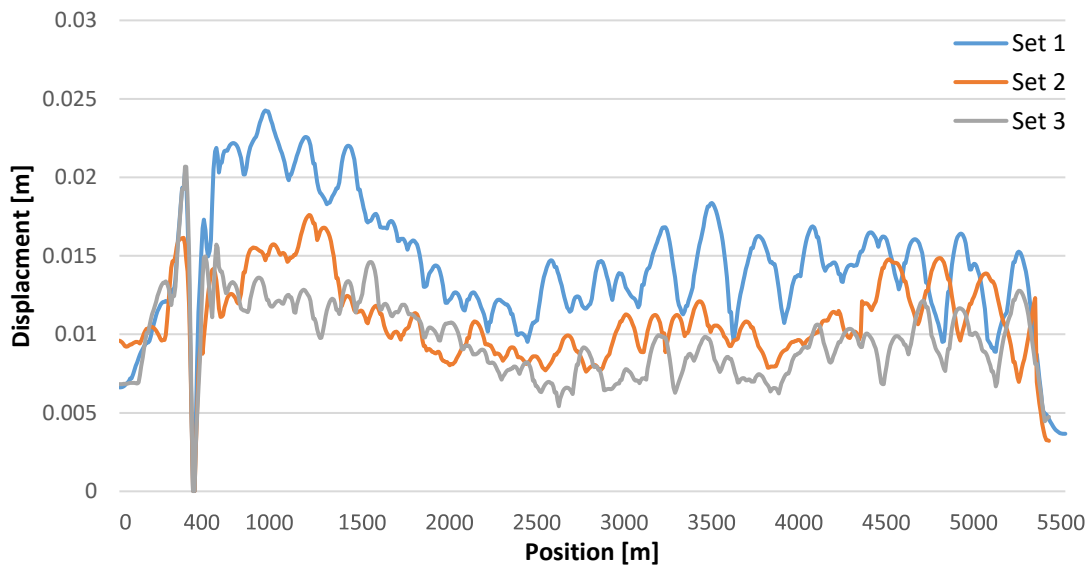
Figure 7-18: Transverse displacment due to seismic motion
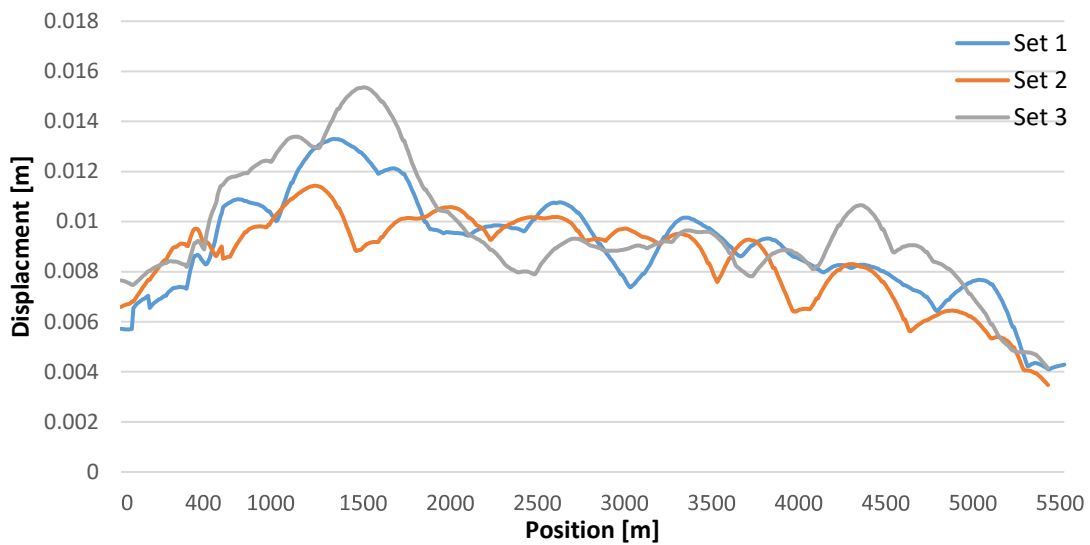
Figure 7-19: Vertical displacment due to seismic motion

The overall displacements for the ground motions made for PGA 0.08g are quite small, as seen in the figures above. As mentioned in 7.1.1, the vertical displacement criteria are $L/350$. The highest vertical displacement occurs at the ``high`` bridge part where the standard bridge girder length is 125 meters. Meaning that a displacement of 0.015 meters is far below the vertical displacement criteria of 0.357 meters. Therefor structural damage due to displacement is unlikely to occur in the event of a 0.08g seismic action.

Kindly note that the reason for 0 displacement at around 400m in Figure 7-17 and Figure 7-18 is due to the bridge girder modelled to a constrain that is fixed.

7.4.3   Displacement due to seismic motion and tsunami

The overall peak vertical displacement along the bridge length is shown in Figure 7-20. As mentioned before, the displacements don't occur simultaneous.
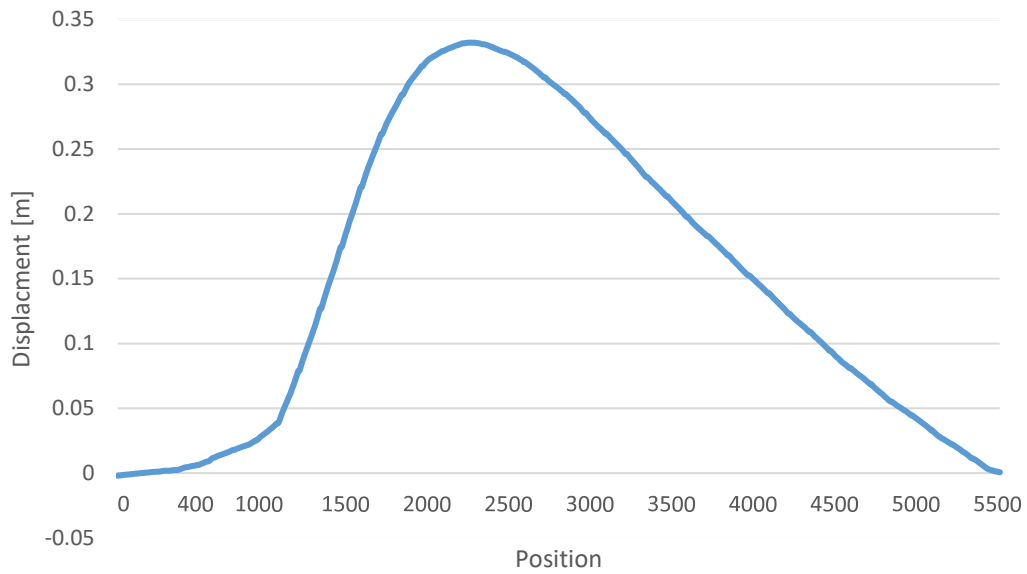
Figure 7-20: Peak vertical displacment along the bridge girder due to seismic motion and tsunami loading

The highest peak displacement happens on the ``low`` bridge part and has a value of 0.334 meters. Figure 7-21 illustrates the time history for the bridge girder with the highest peak displacement.
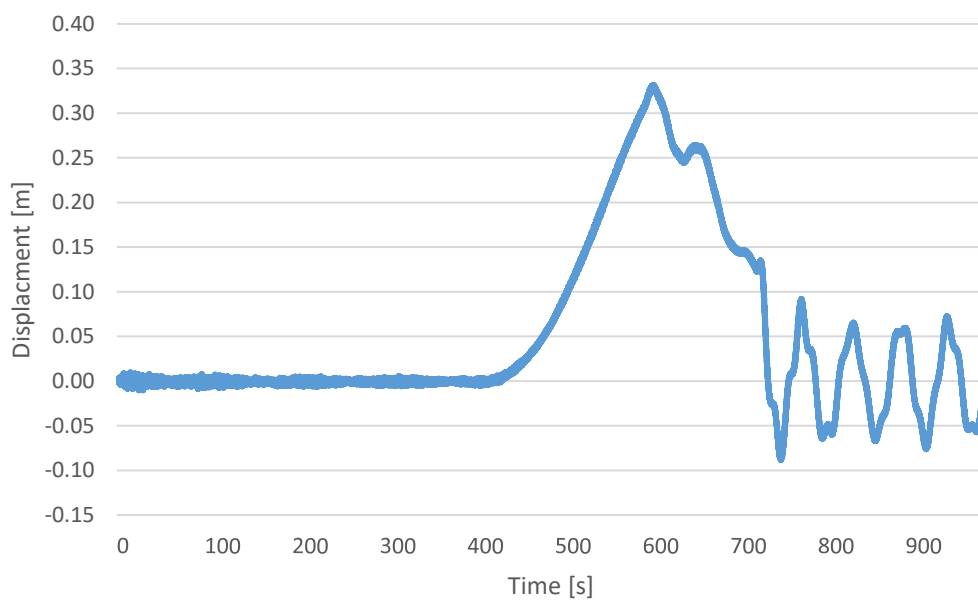
Figure 7-21: Vertical displacment due to seismic motion and tsunami

The displacement in the vertical direction for the ``low`` bridge is shown in Figure 7-21. The tsunami hits the pontoons after 400 seconds. The displacement follows the force time figure in the beginning, where the displacement, as seen in the figure bellow drastically increases. This is expected due to the sudden force applied on the pontoon. 200 seconds after the tsunami hits, the displacement starts to decrease, again this is because the force time history starts too decent. The maximum displacement is 0.334 meters.

7.5   Sensitivity study

A sensitive study is performed to examine if the displacement will drastically increase. The previous section was results due to seismic motion of PGA=$0.83\ m/s^2$, around 0.08g. To model the scenarios of 0.4g and 0.8g, the sensitivity study will scale the displacement input for Set 1 up to 5 and 10 times its original size.

7.5.1   Forces acting on bridge girder

The axial load, the strong axis moment, the weak axis moment, and torsional moment are all displayed throughout the length of the bridge for each of the three different possible scenarios. These responses are useful in assessing the behavior of bridge when subjected to extreme scenarios.
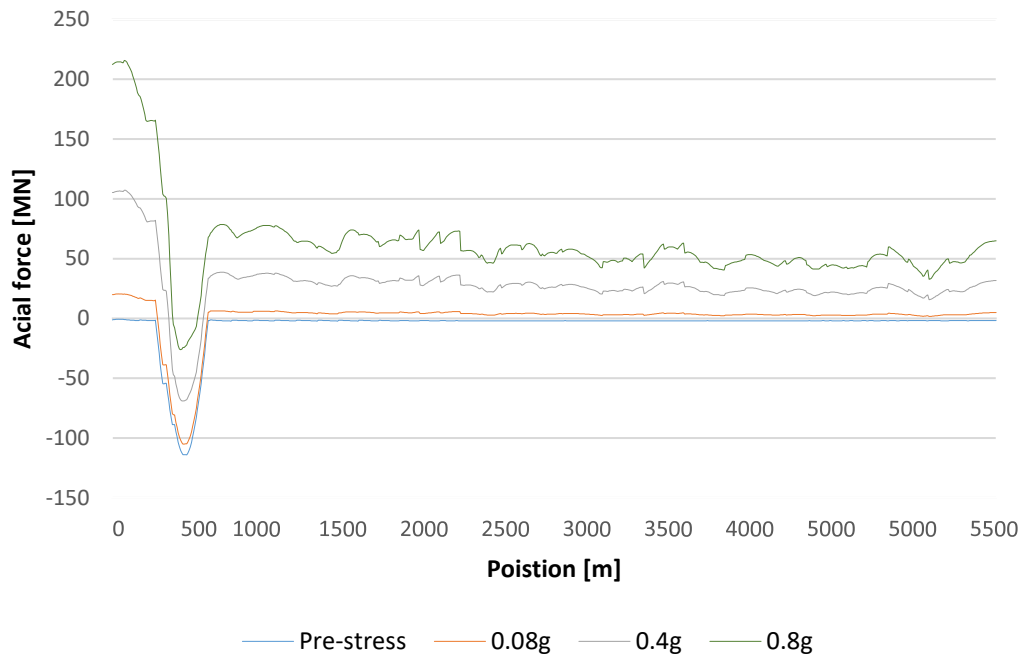
Figure 7-22: Axial force for 0.08g, 0.4g and 0.8g

The axial force is shown in Figure 7-22. As seen in the previous ground motions of set 1 to set 3, the bridge responds the same way. However, for these scenarios, we notice an even high increase at the south end side. While the rest of the bridge length increases proportional just as we noticed in section 7.3.2.

By examining the axial response, the bridge girder near the tower is in compression for 0.08g, however, when increasing the ground motion the bridge girder increases in value, getting close to been in tension.

The south end side increases from near 19 MN for 0.08g ground motion, to 105MN for 0.4g and 212MN for the 0.8g seismic motion. Illustrating a proportional increase for each scenario. Sense the south end side is concrete girder, assuming the same resistance as steel girders, it is safe to say that the concrete girder won't exceed its capacity. . However, the steel girders increase up to 78 MN in tension. That is equal to 58Mpa, which is far below the yielding stress of 382.
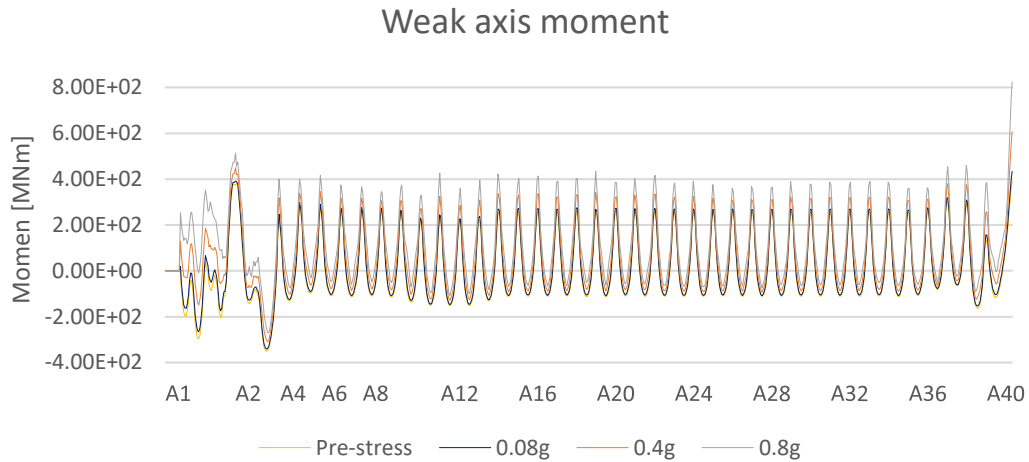
Figure 7-23: Weak axis bending moment for 0.08g, 0.4g and 0.8g

The weak axis bending moment increases almost linearly with the increase of seismic ground motion. At the south end side of the bridge, the weak axis bending moment is 606 MNm and 823 MNm for 0.4g and 0.8g ground motion respectably. Which is an increase in moment of 1.38 and 1.87. For 0.4g the bending moment is slightly below the allowable moment of 680MNm, while 0.8g is far higher than the allowable bending moment.
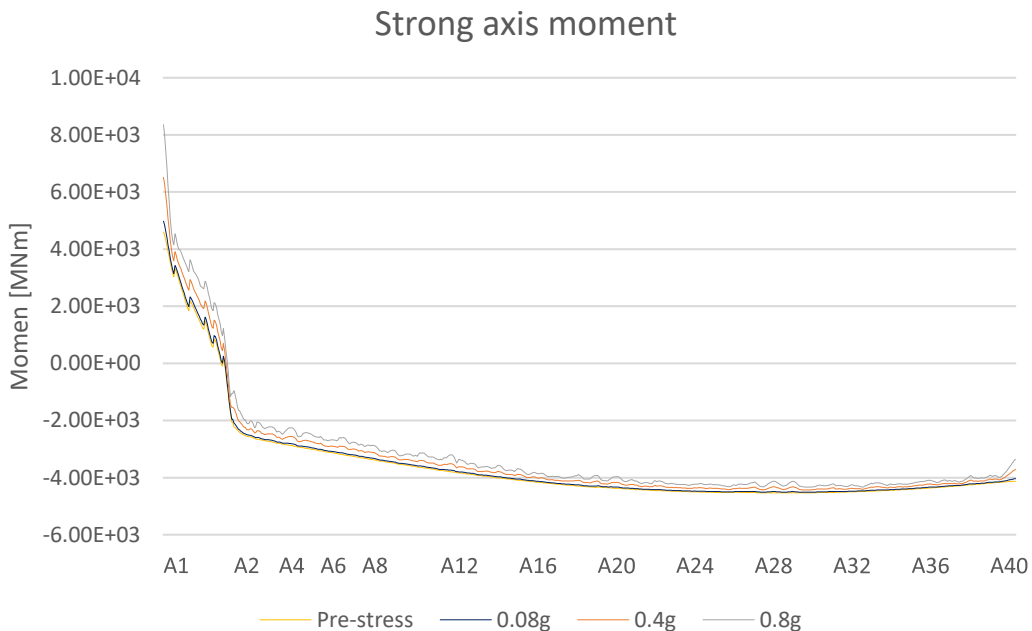
Figure 7-24: Strong axis bending moment for 0.08g, 0.4g and 0.8g

Just as mentioned in section 7.3.1, the strong axis bending moment results will be neglected due to incorrect bending moment graph.
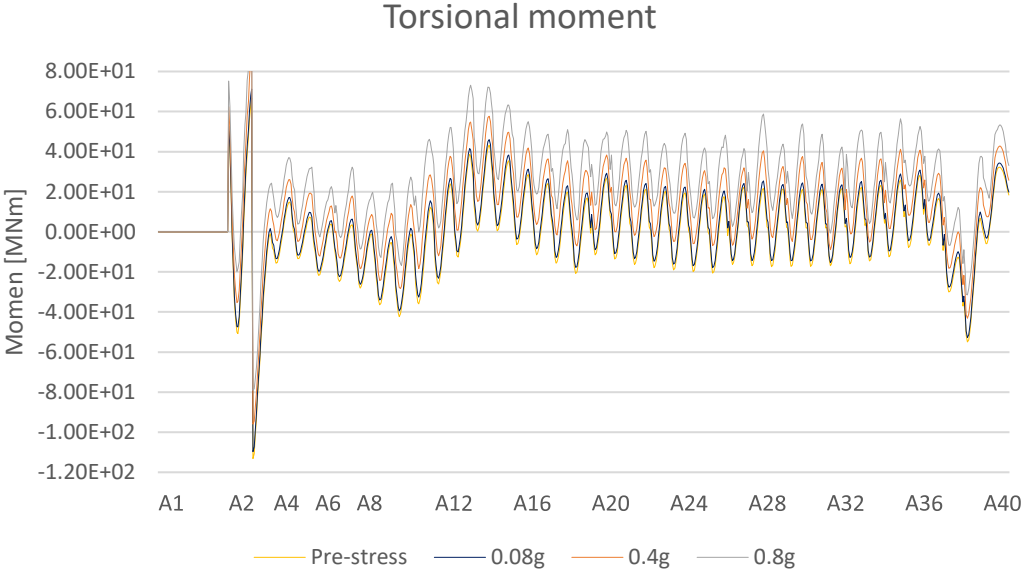
Figure 7-25: Torsional moment for 0.08g, 0.4g and 0.8g

The torsional moment seen in Figure 7-25 increases nearly linearly as well. Where the highest torsional moment occurs to the right side of the tower (Main side). For 0.4g the torsional moment is 90 MNm while for the 0.8g the output is 115MNm.

7.5.2 Forces on mooring lines

The response on the mooring lines due to seismic motion of 0.4g and 0.8 needs to be investigated. Still, the breaking strength of the mooring lines is 19 MN, and as discussed in section 7.3.2, the seismic motions has almost no impact on the mooring lines. Nevertheless Figure 7-26 illustrates the axial loading on the mooring lines due to exaggerated ground motion of 0.4g and 0.8g
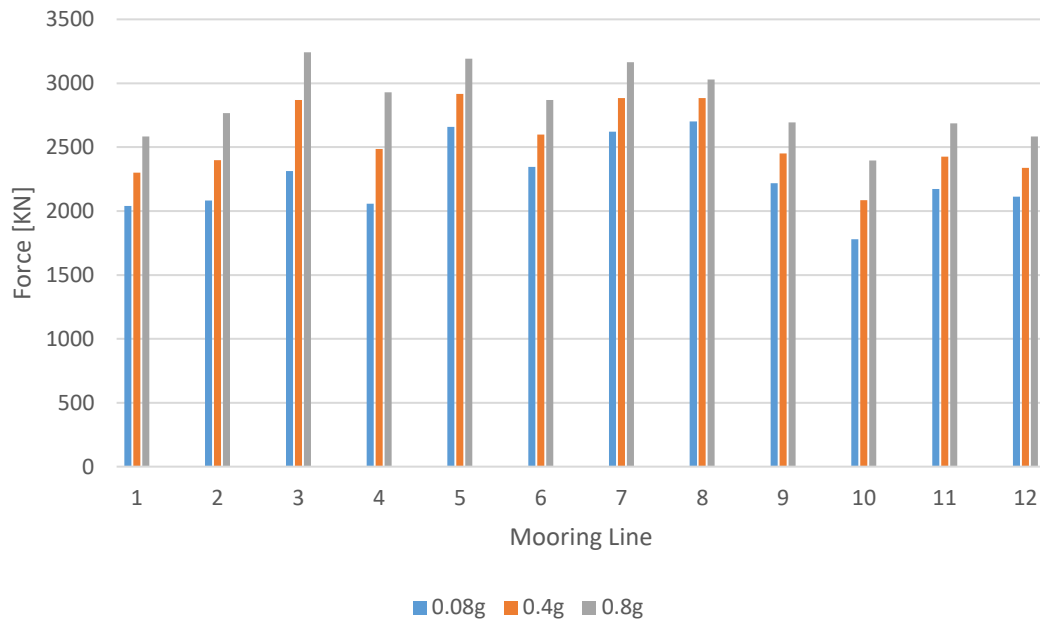
Figure 7-26: Axial loading on mooring lines due to sesmic motion of 0.4g and 0.8g

The mooring lines still doesn't come close to its breaking strength of 19 000KN. The highest acquired axial force occurs in Mooring Line 3 with a value of 3241 KN. Which corresponds to 17% of its utilization capacity. The highest value for 0.4g is 2917.4 KN and it occurs in Mooring Line 5.

7.5.3 Response of Stay-cables

Because the seismic input for ground motions consists of random vibrations, the reaction of the bridge will respond in a manner that is analogous to this behavior. Because of this, the forces will be increased to their maximum amounts, but this will depend on the load scenario. Figure 7-27 presents a comparison of the west side stay-cables when they were subjected to seismic motions of 0.8g (The original motion), 0.4g, and 0.08g respectively.
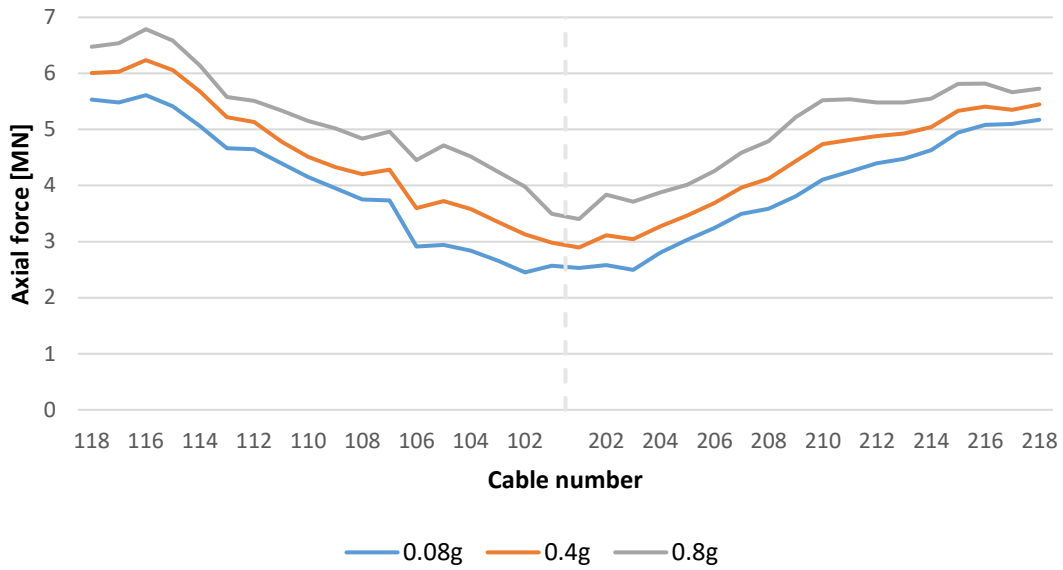
Figure 7-27: Axial force for each cable for 0.08g, 0.4g and 0.8g seismic motion

As can be seen in Figure 7-27, the scaled ground motion produces the expected outcome of a greater axial force. The following table provides an overview of the four distinct cables, with two from each side of the tower (Side span and main span).

Table 7-6: Axial force in four cables subjected to 0.4g and 0.8g ground motion

Cable id		Max force [MN]		Breaking load [MN]	Utilization [%]	
-		0.4g	0.8g	-		
Longest cable	118	6.01	6.47	17	35.4	38.1
Shortest cable	101	2.98	3.49	8.6	34.7	40.6
Shortest cable	201	2.90	3.40	8.6	33.7	39.5
Longest cable	218	5.44	5.73	18.7	29	30.6

Even a seismic motion of 0.8g is sufficient enough not to cause the stay-cables to break.

7.5.4 Acceleration motions on bridge girder

The vertical acceleration for three points along the bridge length is shown in Figure 7-28. The acceleration depends on the location as previously shown in section 7.4.1. However, for the increased seismic motion the acceleration exceeds the allowable motion for vertical acceleration of $0.7\ m/s^2$. Acceleration for the bridge part is $9.86\ m/s^2$ and $19.89\ m/s^2$ for seismic motion of 0.4g and 0.8g respectably. This is far beyond the safety limit. To lower the high acceleration, significant measures must be taken. The same applies for the ``high`` bridge part and ``low`` bridge part. In both scenarios the acceleration is beyond the safety limit. The ``high`` bridge part has an acceleration of $0.77\ m/s^2$ and $1.59\ m/s^2$, while the ``low`` bridge part has $0.54\ m/s^2$ and $1.04\ m/s^2$ for seismic motion of 0.4g and 0.8g. Only the ``low`` bridge part for seismic ground motion of 0.4g is below the safety limit of $0.7\ m/s^2$.
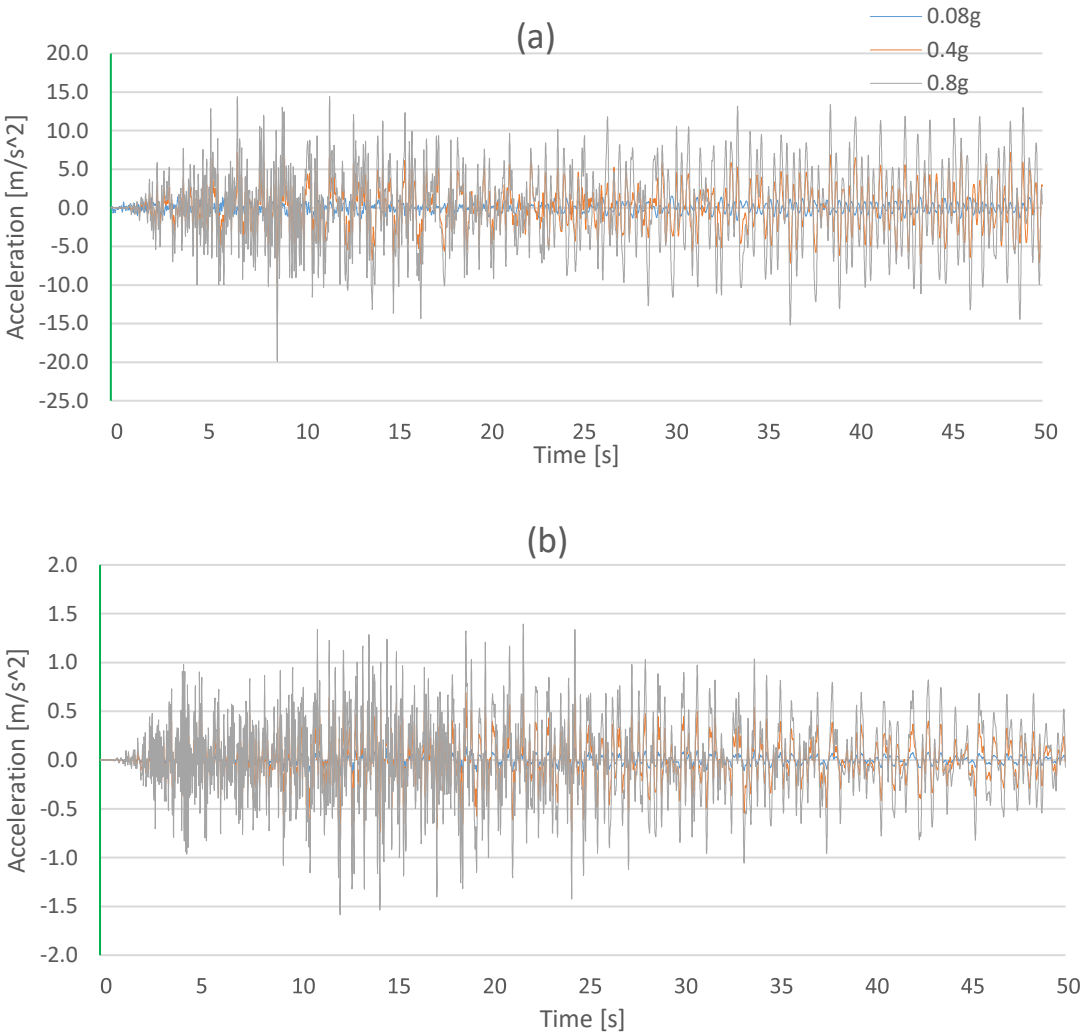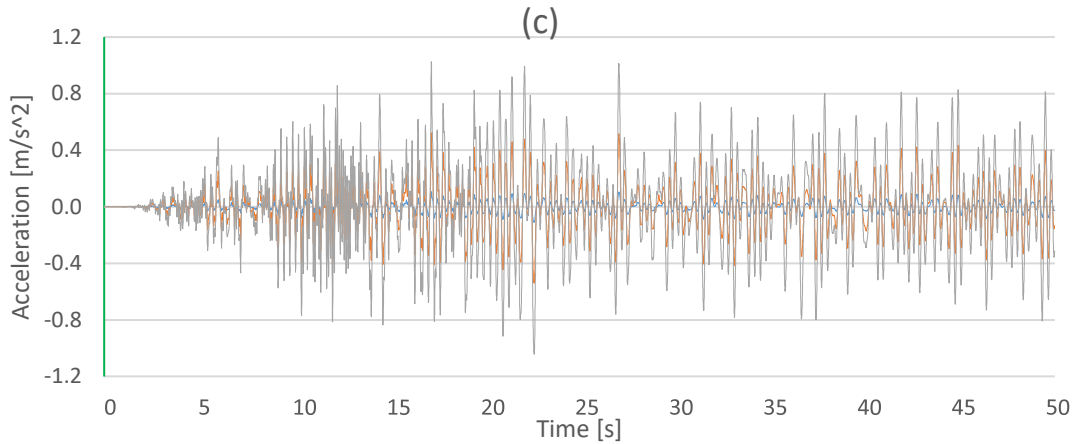
Figure 7-28: Vertical acceleration for Cable-stayed part (a), ``high`` bridge (b) and ``low`` bridge (c)

7.5.5   Displacement motions on bridge girder

Like in previous section 7.5.5, the peak displacement for three parts will be investigated closer.

Table 7-7 summarized the peak displacement for the three seismic scenarios of 0.08g, 0.4g and 0.8g. The displacement increases almost linearly from 0.08g to 0.8g. As seen in the longitudinal displacement for the tower part, the displacement for 0.08g is 49.5 mm while for 0.8g its 461.43 mm.

Peak displacement along the whole bridge length for the longitudinal, Transverse and vertical direction is shown in Figure 7-29, Figure 7-30 and Figure 7-31 respectively.

Table 7-7: Peak displacment in bridge girders for all seismic scenarios

	Maximum displacement [mm]								
	Longitudinal			Transverse			Vertical		
Scenario	**0.08g**	**0.4g**	**0.8g**	**0.08g**	**0.4g**	**0.8g**	**0.08g**	**0.4g**	**0.8g**
Tower	49.15	229.24	461.43	21.88	94.35	189.18	11.44	51.21	100.37
``High`` bridge	27.51	87.60	178.83	24.26	95.49	193.58	13.30	53.88	105.80
``Low`` bridge	28.50	66.94	134.90	22.02	77.01	156.80	15.36	60.06	117.98
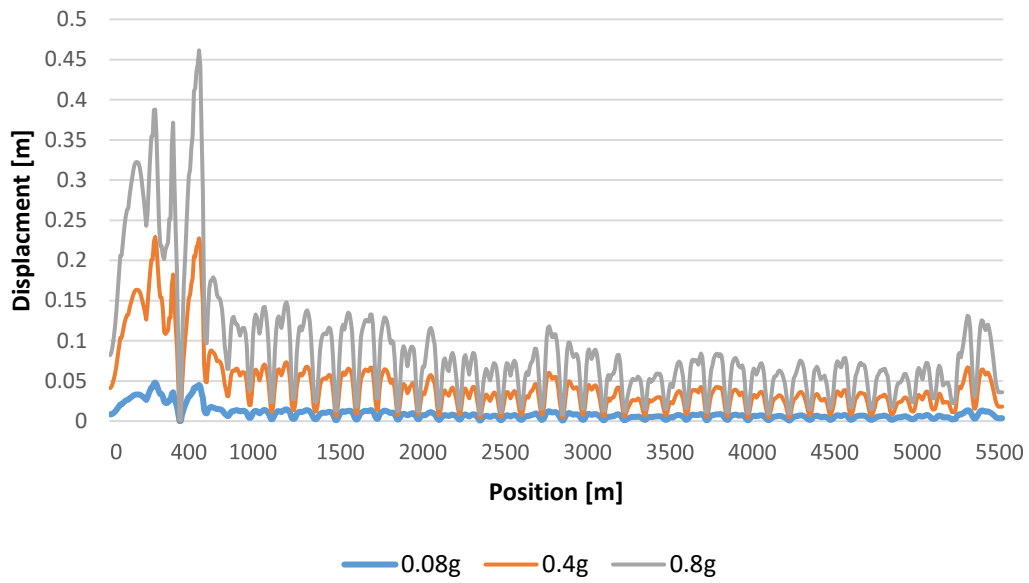
Figure 7-29: Longitudinal displacment due to increased seismic motion
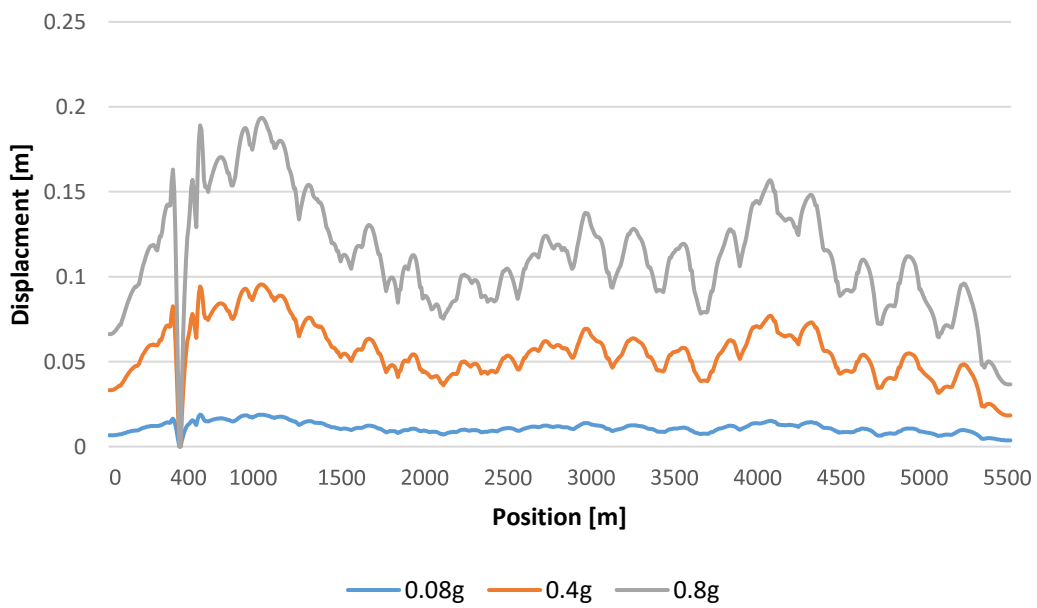
Figure 7-30: Transverse displacment due to increased seismic motion
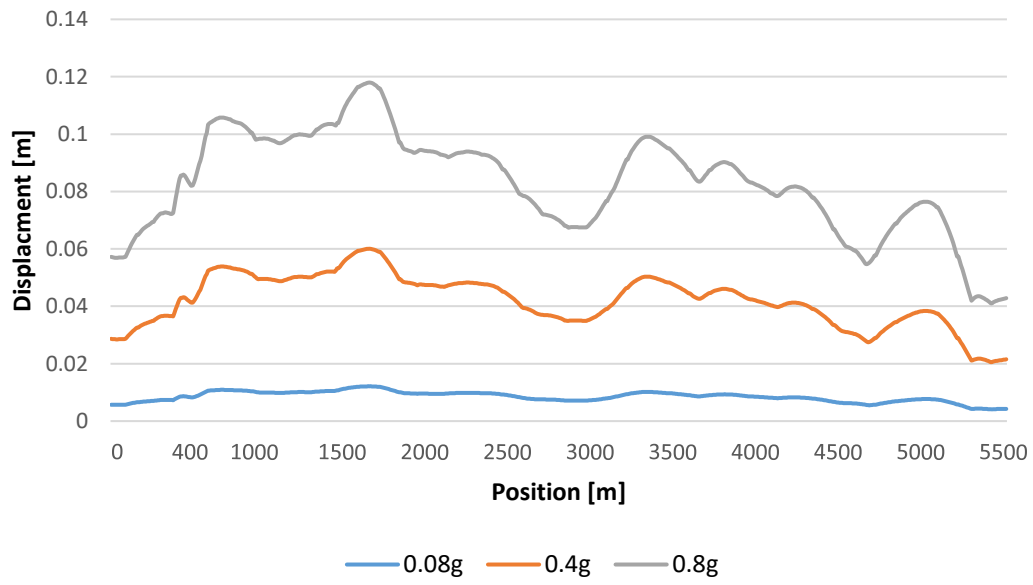
Figure 7-31: Vertical displacment due to increased seismic motion

Chapter 8: Discussion

8.1 Seismic ground motion of 0.08g

Different seismic loading scenarios on the bridge have been simulated. In three different load cases, the responses of stay-cables and the bridge girder, as well as the motions of the bridge girder, are studied. For the situation with PGA = 0.08g, Table 8-1 shows the values for the maximum or critical responses and motions. According to the findings, the forces in the stay-cables are small when compared to the capacity in all circumstances. The cables are regarded safe if the force is in tension and not exceeding the breaking load.

The forces and moments occurring in the bridge girder is deemed acceptable. But just as mentioned earlier, due to incorrect strong axis bending moment, the moment will be neglected in this discussion. Other then that, the weak axis bending moment is sufficient even when been controversial with the bending resistance.

The vertical displacement along the bridge girder is below the displacement criteria required by the Eurocode. Whilst the longitudinal and transverse displacement is minimal, Eurocode does not have any requirements.

It should be noted that the allowable vertical acceleration is the criteria for comfort. For this reason, failing the criteria does not necessary mean that the structure will be damaged.

Table 8-1: Maximum bridge motion and forces for seismic load 0.08g

	Value	Capacity/Criteria	Utilization
Axial force (Stay-cable)	5.65 MN	9.4MN	OK
Axial force (Bridge girder)	30.9 MN	508MN	OK
Axial force (Mooring Lines)	2312.34KN	19 000KN	OK
Strong axis bending moment	4979.3 MNm	2200 MNm	Neglected
Weak axis bending moment	439.63 MNm	680 MNm	OK
Vertical acceleration	$1.9 \, m/s^2$	$< 0.7 \, m/s^2$	Not OK
Horizontal (y dir) acceleration	$2.3 \, m/s^2$	$< 0.2 \, m/s^2$	Not OK
Horizontal (x dir) acceleration	$2.19 \, m/s^2$	$< 0.2 \, m/s^2$	Not OK
Longitudinal displacement	0.049 m	-	-
Transverse displacement	0.024 m	-	-
Vertical displacement*	0.015 m	$L/350$	OK
Vertical displacement**	0.334m	$L/350$	OK

*Highest vertical displacement occurs at ``low`` bridge, where the bridge girder is 125 m long

** Highest vertical displacement due to seismic motion and tsunami occurs at ``low`` bridge. The corresponding girder is 125 m long

8.2   Seismic ground motion of 0.4g and 0.8g

The outcomes of both scenarios (0.4g and 0.8g) are presented in Table 8-2. A near linear increase can be noticed in the responses when compared to the original ground motion of 0.08g.

The forces that are present in the cables for 0.4g and 0.8g give values and variations in tension that are acceptable. As stated earlier, the strong axis bending moment is neglected. The weak axis bending moment exceeds the bending resistance. However, a closer look on the bending moment would be needed due to the bending moment barley exceeding the bending resistance used in this thesis. Note that the bending resistance was generalized along the bridge girder, and the resistance is regarded as conservative, meaning that a structural collapse or damage might not occur for seismic ground motion of 0.4g and 0.8g even though the bending moment exceeds the bending resistance chosen in thesis.

Table 8-2: Maximum bridge motion and forces for seismic load 0.4g and 0.8g

	Values (0.4g)	Values (0.8g)	Capacity/ Criteria	Utilization	
				0.4g	0.8g
Axial force (Stay-cable)	6.01 MN	6.47 MN	Tension / 9.4 MN	OK	OK
Axial force (Bridge girder)	107 MN	215 MN	508MN	OK	OK
Axial force (Mooring lines)	2917.4KN	3241KN	19 000KN	OK	OK
Strong axis bending moment	6500 MNm	8356 MNm	2200 MNm	Neglected	Neglected
Weak axis bending moment	606 MNm	823 MNm	680 MNm	OK	Not OK
Vertical acceleration	$9.86\ m/s^2$	$19.89\ m/s^2$	$< 0.7\ m/s^2$	Not Ok	Not OK
Longitudinal displacement	0.23m	0.461m	-	-	-
Transverse displacement	0.096m	0.193m	-	-	-
Vertical displacement*	0.06m	0.117m	$L/350$	OK	OK

*Highest vertical displacement for 0.4g occurs at the ``low`` part of the bridge, where the bridge girder is 125 m long

*Highest vertical displacement for 0.8g occurs at the ``low`` part of the bridge, where the bridge girder is 125 m long

Chapter 9: Conclusion

The purpose of this study is to investigate the impact that earthquakes have on floating bridges. This study analyses the effect that seismic vibrations and seismic induced tsunami have on a curved floating bridge that is end anchored. The findings of a time-domain analysis of a floating bridge can be obtained by the utilization of the software Orcaflex. To calculate artificial ground motion that takes into account spatial fluctuations, Dr. Kaiming Bi makes use of Eurocode 8, and then obtains the findings (3 different cases with 3 ground motions). This numerical study produced a wide range of possible outcomes, and from those outcomes, the following conclusions can be drawn:

It is reasonable to assume that the K12 floating bridge would remain intact for a seismic ground vibration of 0.08g. The cables in the tower remains far below the breaking strength. The displacements that occur on the bridge, in all direction are considered minimal. Even though Eurocode does not have any requirements for longitudinal and transverse displacement, the vertical displacement remains below the allowable displacement. Even when considering a tsunami load striking the pontoons, the displacement in the vertical direction does not exceed the Eurocode requirements.

It is found that the bridge girder forces, and moments does not subject the bridge to failure or collapse. However, it is observed that the seismic ground motion of 0.08g generates a vertical acceleration below the comfort limit of bridges for the floating bridge part. This is not true for the tower part of the bridge where the vertical acceleration exceeds the comfort limit. Meanwhile, the horizontal direction acceleration is higher than what's acceptable throughout the whole bridge. A modification on the long span bridge girder close to the tower would be needed to keep the vertical acceleration down.

The responses for a ground motion of 0.4g are deemed inadequate. The vertical and horizontal acceleration is far above the comfort limit. The axial forces in the cables and the bridge girder and the vertical displacement along the bridge is considered to be acceptable. While the rest of the responses fails the requirements / limits discussed in section 7.1.1 and section 7.1.2, except for the weak axis bending moment stat is slightly below the moment resistance.

The same applies for ground motion of 0.8g where the responses are rather high. But just as mentioned for ground motion 0.4g, the axial force in the cables and bridge girders are found

to be sufficient. It is true for the vertical displacement as well. While the motion of the bridge girders and cables are excessively high.

The response outcome from ground motion 0.4g and 0.8 required modifications to the bridges current design.

The chances of an earthquake of a magnitude of 0.4g or 0.8g occurring in Norway are extremely slim. As a result, the Bjørnafjorden bridge's design does not need to account for the large ground vibrations that occur in this area. However, even if it's a slim chance of occurring, additional research on the bridge's reflexes and motions in the event of an earthquake and extreme wind events is required to ensure that the structure can be entirely relied upon.

Chapter 10: Future developments and studies

This thesis focused more on the time-domain analysis of the bridge when subjected to seismic motion and seismic-induced tsunami. A closer look on the local stresses would be interesting to investigate. Even though the forces and moments doesn't exceed the requirements for ground motion 0.08g, the local stresses might differ.

The seismic and tsunami load is the only external load that has been considered in this simulation. Traffic and other external loads such as wind and wave loads need also to be considered. Other thesis and journals have investigated wave, wind, and current, and they are vital to include in the bridge.

Even though this simulation had tsunami load, a more accurate dynamic study of tsunami wave loads would be necessary to conduct a more accurate dynamic simulation. This thesis used a simplified version of an onshore RC building subjected to tsunami. A more in-depth design of offshore tsunami loads would achieve a better understand of the behavior of the bridge.

Bibliography

1. *Utviklingsstrategi for ferjefri og utbetra E39*. 2016, Statens Vegvesen.
2. Chen, W.F. and L. Duan, *Bridge engineering handbook*. 2000, Boca Raton, Fla: CRC Press.
3. Eiichi Watanabe, T.U., *Analysis and Design of Floating Bridges.* 2003.
4. Watanabe, E., *Floating Bridges: Past and Present.* Structural Engineering International, 2003. **13**(2): p. 128-132.
5. *SBJ-33-C5-AMC-90-RE-100 Preferred solution, K12 - main report_Part1* 2019, Statens vegvesen.
6. *Ferjefri E39*. 2022 [cited 2022 04].
7. Mirzapour, J., et al., *Vibration of submerged floating tunnels due to moving loads.* Applied Mathematical Modelling - APPL MATH MODEL, 2011. **35**: p. 5413-5425.
8. Shearer, P.M., *Introduction to Seismology*. 3 ed. 2019, Cambridge: Cambridge University Press.
9. Thitimakorn, T. and N. Anderson, *A 2-D MASW SHEAR-WAVE VELOCITY PROFILE ALONG A TEST SEGMENT OF INTERSTATE I-70, ST. LOUIS, MISSOURI.* 2005.
10. Li, D., et al., *Tsunami - A Growing Disaster*, in *Tsunami*, M. Mokhtari, Editor. 2020, InTech.
11. Standard, E., *NS-EN 1998-1:2004+NA:2008*. 2021.
12. Standard, N., *NS-EN 1998-2:2005+A1:2009+A2:2011+NA:2014*. 2014.
13. American Society of Civil Engineers., *Minimum design loads and associated criteria for buildings and other structures*. 2017, Reston, Virginia: American Society of Civil Engineers. volumes.
14. *N400 Bruprosjektering*. 2022.
15. Petrone, C., et al., *Fragility functions for a reinforced concrete structure subjected to earthquake and tsunami in sequence.* Engineering Structures, 2020. **205**: p. 110120.
16. Petrone, C., T. Rossetto, and K. Goda, *Fragility assessment of a RC structure under tsunami actions via nonlinear static and dynamic analyses.* Engineering Structures, 2017. **136**: p. 36-53.
17. J, C. and H.G. M, *A time integration algorithm for structural dynamics with improved numerical dissipation: The generalized-α method*. 1993.
18. Orinca. *Orcaflex webhelp*. 2022.
19. Rao, S.S., *Mechanical vibrations*. Sixth edition. ed. 2017, Hoboken: Pearson. xxvii, 1118 pages.
20. vegvesen, S., *SBJ-33-C5-OON-22-RE-022-0 Marine geotecnical design_sladdet* 2019.
21. vegvesen, S., *SBJ-33-C5-AMC-90-RE-106_0 Appendix F - Global Analyses - Modelling and assumptions* 2019.

22. *SBJ-33-C5-AMC-90-RE-101_1 Appendix A - Drawings binder_Part1* 2019, Statens vegvesen

23. Vegdirektoratet, S.v., *SBJ-32-C5-DNV-62-RE-023-0-Independent Analyses of AMC Floating Bridge BJF 2019* 2019.

24. *SBJ-33-C5-AMC-22-RE-111_0 Appendix K - Design of floating bridge part_Part1* 2019, Statens vegvesen.

25. vegvesen, S., *SBJ-33-C5-AMC-22-RE-111_0 Appendix K - Design of floating bridge part_Part2* 2019.

26. vegvesen, S., *SBJ-33-C5-AMC-26-RE-113 Appendix M - Mooring system* 2019.

27. *Eurokode : grunnlag for prosjektering av konstruksjoner = Eurocode : basis of structural design*, in *Eurocode basis of structural design*. 2016, Standard Norge: Lysaker.

28. vegvesen, S., *SBJ-33-C5-AMC-22-RE-111_0 Appendix K - Design of floating bridge part_Part4* 2019.

29. *Eurokode 3: Prosjektering av stålkonstruksjoner = Eurocode 3: Design of steel structures. Part 1-1: General rules and rules for buildings : Del 1-1 : Allmenne regler og regler for bygninger*. Norsk standard. Vol. NS-EN 1993-1-1:2005+NA:2008. 2008, Lysaker: Standard Norge.

30. vegvesen, S., *SBJ-33-C5-AMC-22-RE-112_0 Appendix L - Design of cable stayed bridge and abutments_Part1*. 2019.

Appendix A: Stay-cables properties

Table A. 1: Cable properties from independent report [23]

Cable pair number	Mass	Axial stiffness [kN]	Stretched length [m]	Unstreched length [m]	Cross section area
	[ton/m]	[kN]	[m]	[m]	[mm^2]
T118	0.0234	2.02E+06	288.917	288.137	34636
T117	0.0225	2.02E+06	277.813	277.066	34636
T116	0.0216	2.02E+06	266.713	265.979	34636
T115	0.0201	1.96E+06	255.618	254.917	34636
T114	0.0181	1.84E+06	244.531	243.863	34636
T113	0.0164	1.76E+06	233.459	232.827	28353
T112	0.0157	1.76E+06	222.392	221.792	28353
T111	0.0141	1.67E+06	211.336	210.766	28353
T110	0.0127	1.58E+06	200.288	199.752	25447
T109	0.0113	1.49E+06	189.250	188.740	25447
T108	0.0100	1.40E+06	178.226	177.751	25447
T107	0.0092	1.37E+06	167.216	166.768	25447
T106	0.0071	1.20E+06	148.226	147.882	17671
T105	0.0058	1.11E+06	129.720	129.402	17671
T104	0.0045	9.95E+05	111.936	111.646	17671
T103	0.0034	8.78E+05	95.278	95.028	15394
T102	0.0026	8.19E+05	80.448	80.254	15394
T101	0.0021	7.61E+05	68.636	68.461	15394
T201	0.0021	7.61E+05	69.307	69.127	15394
T202	0.0027	8.19E+05	81.675	81.460	15394
T203	0.0034	8.78E+05	96.943	96.697	15394
T204	0.0045	9.95E+05	113.950	113.648	17671
T205	0.0059	1.11E+06	132.029	131.680	21382
T206	0.0073	1.20E+06	150.795	150.394	21382
T207	0.0094	1.37E+06	170.023	169.595	25447
T208	0.0107	1.40E+06	189.573	189.090	25447
T209	0.0125	1.49E+06	209.355	208.822	25447
T210	0.0145	1.58E+06	229.311	228.709	25447
T211	0.0167	1.67E+06	249.399	248.746	25447
T212	0.0190	1.76E+06	269.590	268.886	28353
T213	0.0204	1.76E+06	289.864	289.083	28353
T214	0.0230	1.84E+06	310.206	309.383	28353
T215	0.0260	1.96E+06	330.610	329.723	34636
T216	0.0284	2.02E+06	351.059	350.110	34636
T217	0.0301	2.02E+06	371.547	370.531	34636
T218	0.0318	2.02E+06	392.051	390.968	34636

Table A. 2: Cable properties from main drawing [22]

Cable no		101	102	103	104	105	106	107	108	109	110	111	112	113	114	115	116	117	118
Length	m	69	81	97	114	132	150	170	181	192	203	214	225	236	247	258	270	281	292
No of strands		31	31	31	37	37	43	43	43	55	55	55	55	61	61	61	61	61	61
Breaking load	MN	8,6	8,6	8,6	10,3	10,3	12,0	12,0	12,0	15,3	15,3	15,3	15,3	17,0	17,0	17,0	17,0	17,0	17,0
Linear weight	kg/m	36,50	36,50	36,50	43,57	43,57	50,63	50,63	50,63	64,76	64,76	64,76	64,76	71,83	71,83	71,83	71,83	71,83	71,83
Total weight*	T	2,5	3,0	3,5	5,0	5,8	7,6	8,6	9,2	12,4	13,1	13,9	14,6	17,0	17,7	18,5	19,4	20,2	21,0
HDPE tube	mm	160	160	160	180	180	200	200	200	200	200	200	200	225	225	225	225	225	225
Anchor tube deck	mm	244	244	244	273	273	323	323	323	323	323	323	323	355	355	355	355	355	355
Anchor tube tower	mm	323	323	323	355	355	406	406	406	419	419	419	419	419	419	419	419	419	419
Permanent load	MN	2,0	2,2	2,5	2,7	3,0	3,1	3,3	3,5	3,6	3,8	4,0	4,2	4,1	4,5	4,6	4,8	4,9	5,0
Traffic load	MN	1,0	1,1	1,2	1,3	1,4	1,5	1,6	1,7	1,8	1,9	2,0	2,0	1,9	1,8	1,7	1,5	1,4	1,3
Wave load	MN	0,1	0,1	0,1	0,2	0,2	0,3	0,3	0,3	0,4	0,5	0,6	0,7	0,7	0,8	0,8	0,8	0,9	0,9
Wind load	MN	0,3	0,3	0,3	0,3	0,3	0,3	0,3	0,4	0,4	0,4	0,4	0,4	0,4	0,4	0,4	0,4	0,4	0,4
Temperature load	MN	0,0	0,0	0,0	0,0	0,0	0,0	0,0	0,0	0,0	0,1	0,1	0,1	0,1	0,2	0,2	0,3	0,4	0,4
Tide load	MN	0,0	0,0	0,0	0,0	0,0	0,0	0,0	0,1	0,1	0,1	0,2	0,2	0,2	0,2	0,2	0,3	0,3	0,3
ULS1	MN	3,9	4,3	4,8	5,2	5,7	6,0	6,4	6,9	7,2	7,7	8,2	8,6	8,3	8,9	8,9	9,2	9,3	9,4
ULS2	MN	4,0	4,4	4,9	5,3	5,8	6,2	6,5	7,1	7,4	7,9	8,4	8,7	8,5	9,0	8,9	9,0	9,2	9,2
ULS3	MN	3,0	3,3	3,6	4,0	4,4	4,7	4,9	5,5	5,8	6,3	6,9	7,3	7,2	8,0	8,1	8,6	9,1	9,2
Max ULS	MN	4,0	4,4	4,9	5,3	5,8	6,2	6,5	7,1	7,4	7,9	8,4	8,7	8,5	9,0	8,9	9,2	9,3	9,4
Breaking load (design)	MN	4,8	4,8	4,8	5,7	5,7	6,7	6,7	6,7	8,5	8,5	8,5	8,5	9,5	9,5	9,5	9,5	9,5	9,5

Cable no		201	202	203	204	205	206	207	208	209	210	211	212	213	214	215	216	217	218
Length	m	69	81	97	114	132	150	170	189	209	229	249	269	289	309	329	350	370	390
No of strands		31	31	31	37	43	43	55	55	55	55	61	61	67	67	67	67	67	67
Breaking load	MN	8,6	8,6	8,6	10,3	12,0	12,0	15,3	15,3	15,3	15,3	17,0	17,0	18,7	18,7	18,7	18,7	18,7	18,7
Linear weight	kg/m	36,50	36,50	36,50	43,57	50,63	50,63	64,76	64,76	64,76	64,76	71,83	71,83	78,89	78,89	78,89	78,89	78,89	78,89
Total weight*	T	2,5	3,0	3,5	5,0	6,7	7,6	11,0	12,2	13,5	14,8	17,9	19,3	22,8	24,4	26,0	27,6	29,2	30,8
HDPE tube	mm	160	160	160	180	200	200	200	200	200	200	225	225	250	250	250	250	250	250
Anchor tube deck	mm	244	244	244	273	323	323	323	323	323	323	355	355	406	406	406	406	406	406
Anchor tube tower	mm	323	323	323	355	406	406	419	419	419	419	419	419	508	508	508	508	508	508
Permanent load	MN	2,0	2,2	2,5	2,7	3,0	3,2	3,4	3,6	3,8	4,1	4,4	4,7	4,9	5,2	5,2	5,2	5,2	5,2
Traffic load	MN	0,5	0,9	1,1	1,3	1,5	1,6	1,7	1,8	1,8	1,9	1,8	1,8	1,8	1,7	1,7	1,6	1,5	1,3
Wave load	MN	0,0	0,0	0,0	0,1	0,2	0,3	0,4	0,4	0,4	0,5	0,6	0,7	0,8	1,0	1,1	1,2	1,1	1,0
Wind load	MN	0,2	0,3	0,3	0,4	0,4	0,5	0,5	0,6	0,6	0,6	0,6	0,6	0,6	0,6	0,6	0,6	0,6	0,6
Temperature load	MN	0,0	0,0	0,0	0,0	0,0	0,0	0,0	0,1	0,1	0,1	0,2	0,2	0,3	0,3	0,3	0,3	0,4	0,4
Tide load	MN	0,0	0,0	0,0	0,0	0,0	0,0	0,0	0,1	0,1	0,1	0,1	0,1	0,1	0,2	0,3	0,4	0,6	0,8
ULS1	MN	3,3	4,0	4,6	5,2	5,9	6,4	6,8	7,4	7,7	8,3	8,7	9,2	9,6	10,1	10,2	10,3	10,3	10,2
ULS2	MN	3,2	4,1	4,7	5,3	6,0	6,6	7,0	7,6	7,8	8,4	8,8	9,2	9,6	10,0	10,1	10,2	10,2	10,0
ULS3	MN	2,7	3,1	3,5	4,0	4,6	5,1	5,5	6,2	6,5	7,0	7,7	8,2	8,8	9,6	9,9	10,2	10,6	10,7
Max ULS	MN	3,3	4,1	4,7	5,3	6,0	6,6	7,0	7,6	7,8	8,4	8,8	9,2	9,6	10,1	10,2	10,3	10,6	10,7
Breaking load (design)	MN	4,8	4,8	4,8	5,7	6,7	6,7	8,5	8,5	8,5	8,5	9,5	9,5	10,4	10,4	10,4	10,4	10,4	10,4

Appendix B: Ground motion generation

Dr. Kaiming Bi created the ground motions utilized to analyze the bridge against seismic excitations. According to the code's response spectrum, the motions generated are displacement and acceleration time histories.

The ground motion acceleration for all directions is shown in Figure B- 1 to Figure B- 6. The ground motion displacement for all directions is shown in Figure B- 7 to Figure B- 12.
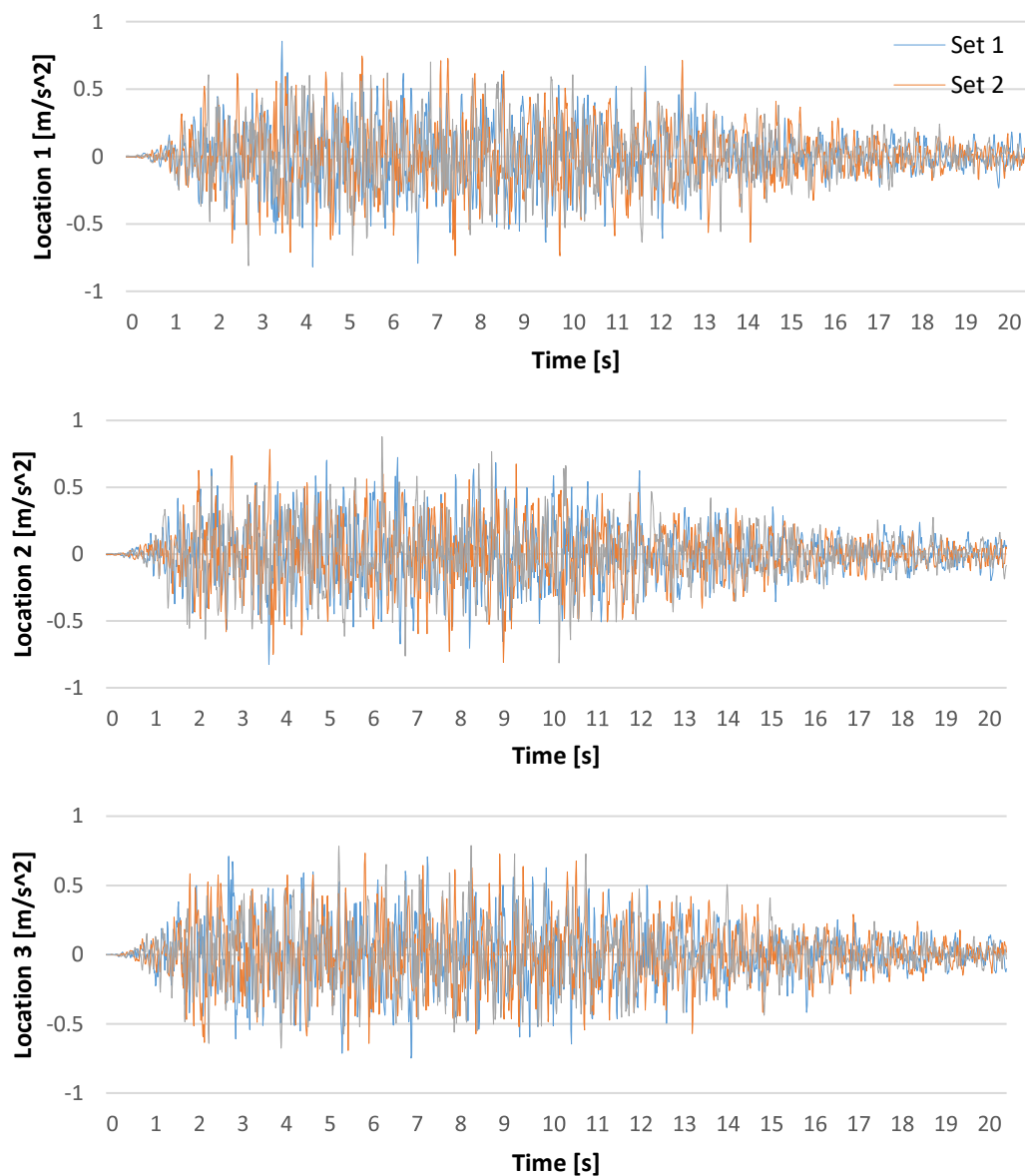
X-direction ground motion acceleration

Figure B- 1: Generated ground motion in x-direction: Acceleration; Location 1-3
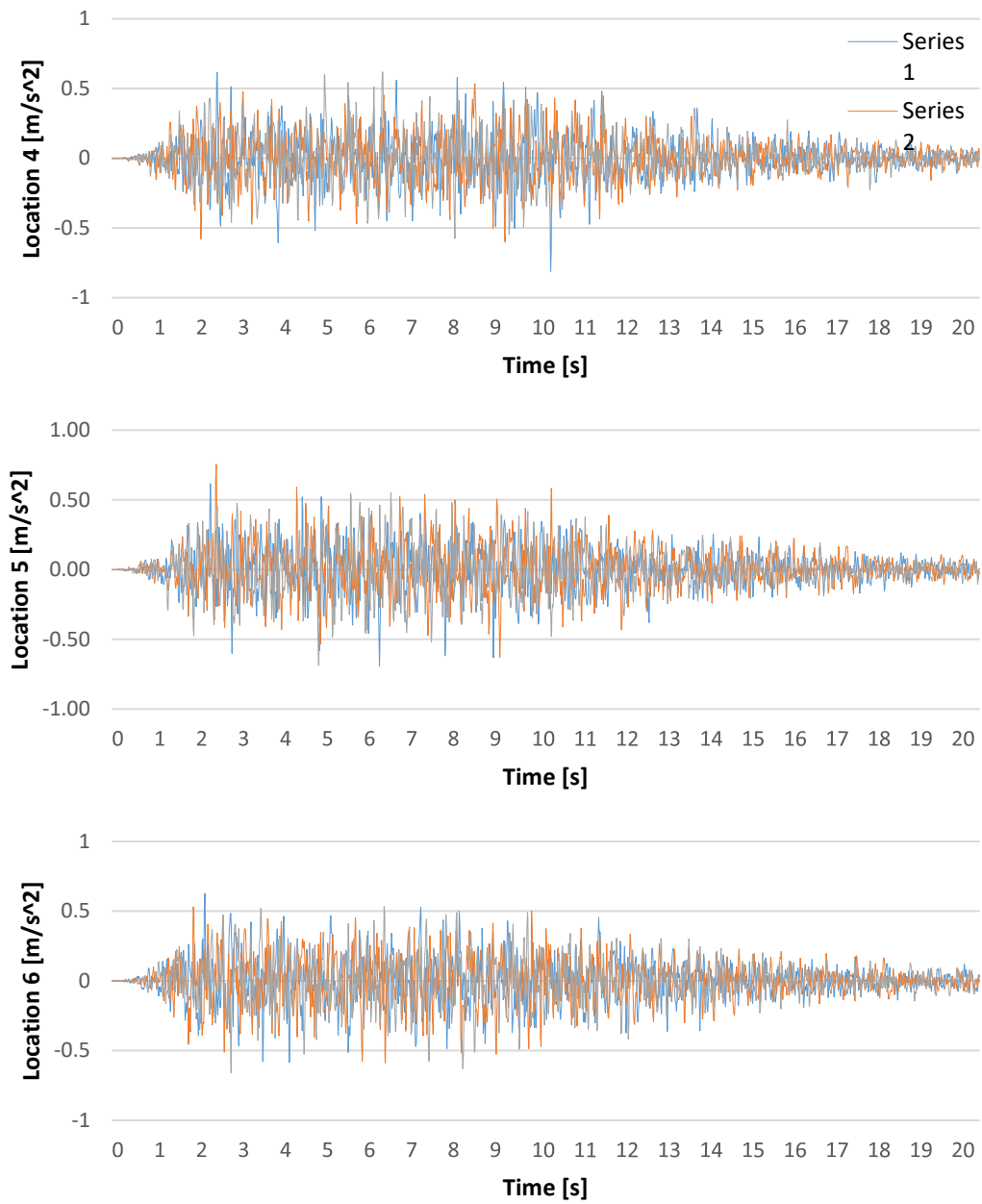
Figure B- 2: Generated ground motion in x-direction: Acceleration; Location 4-6

Y-direction ground motion acceleration
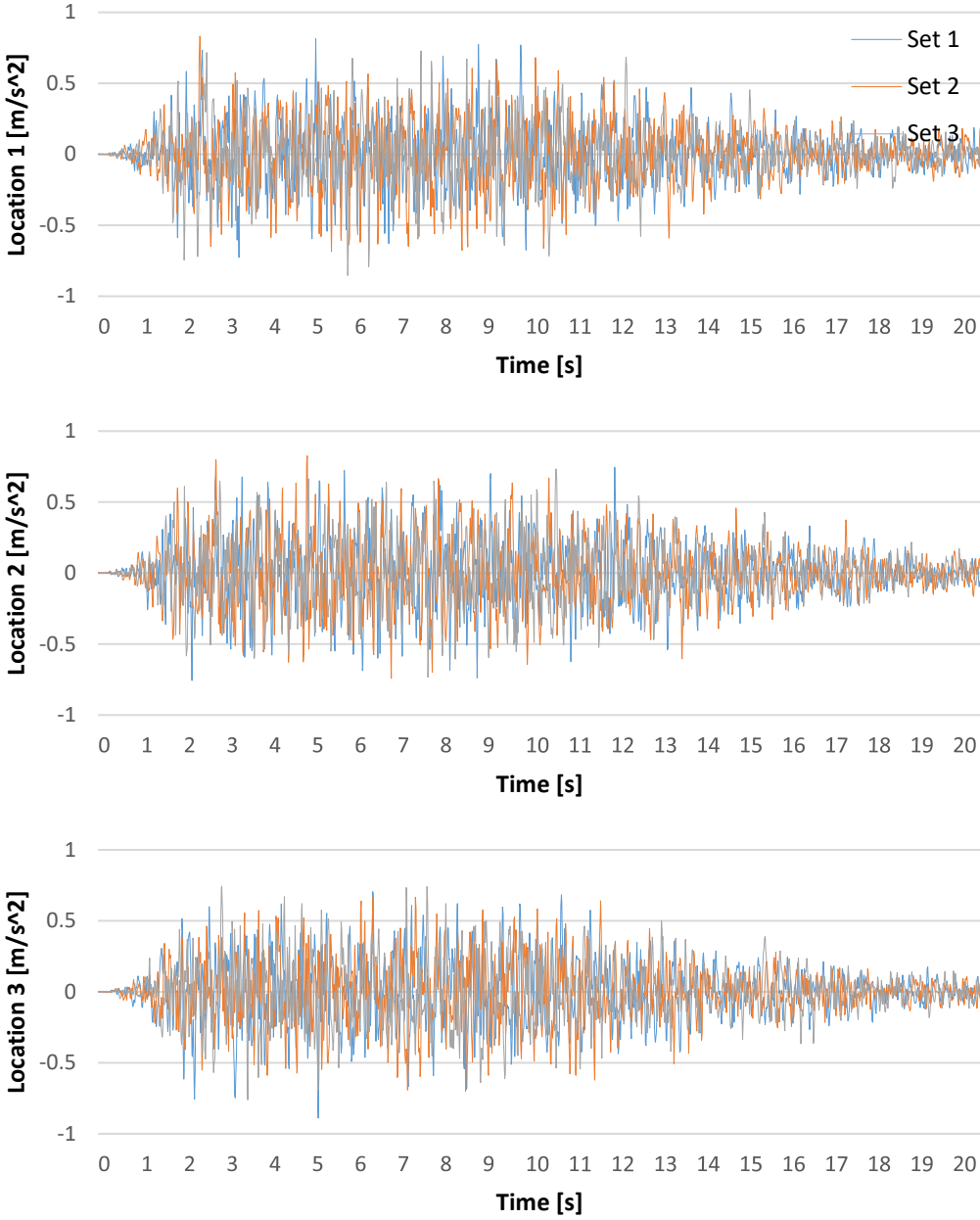
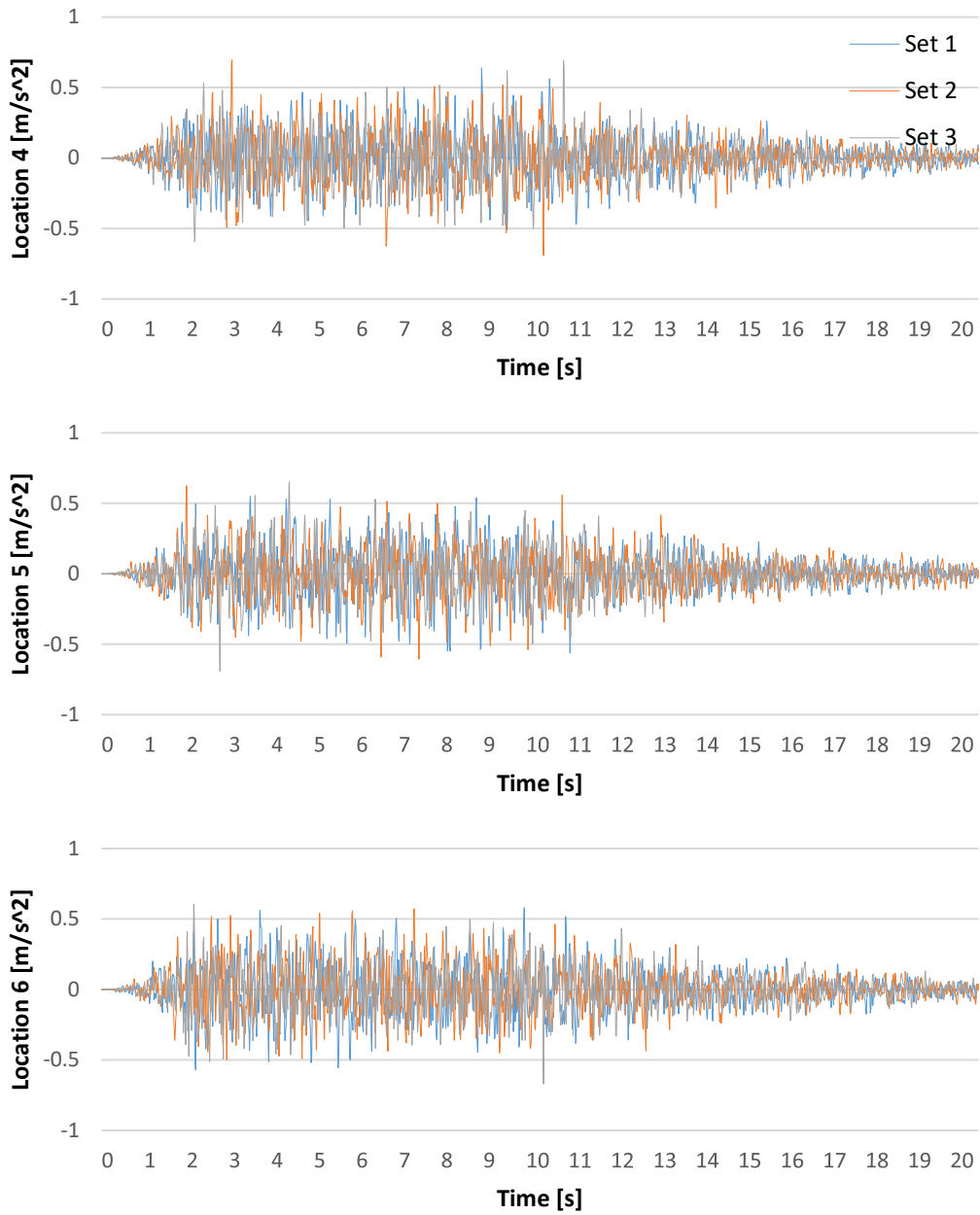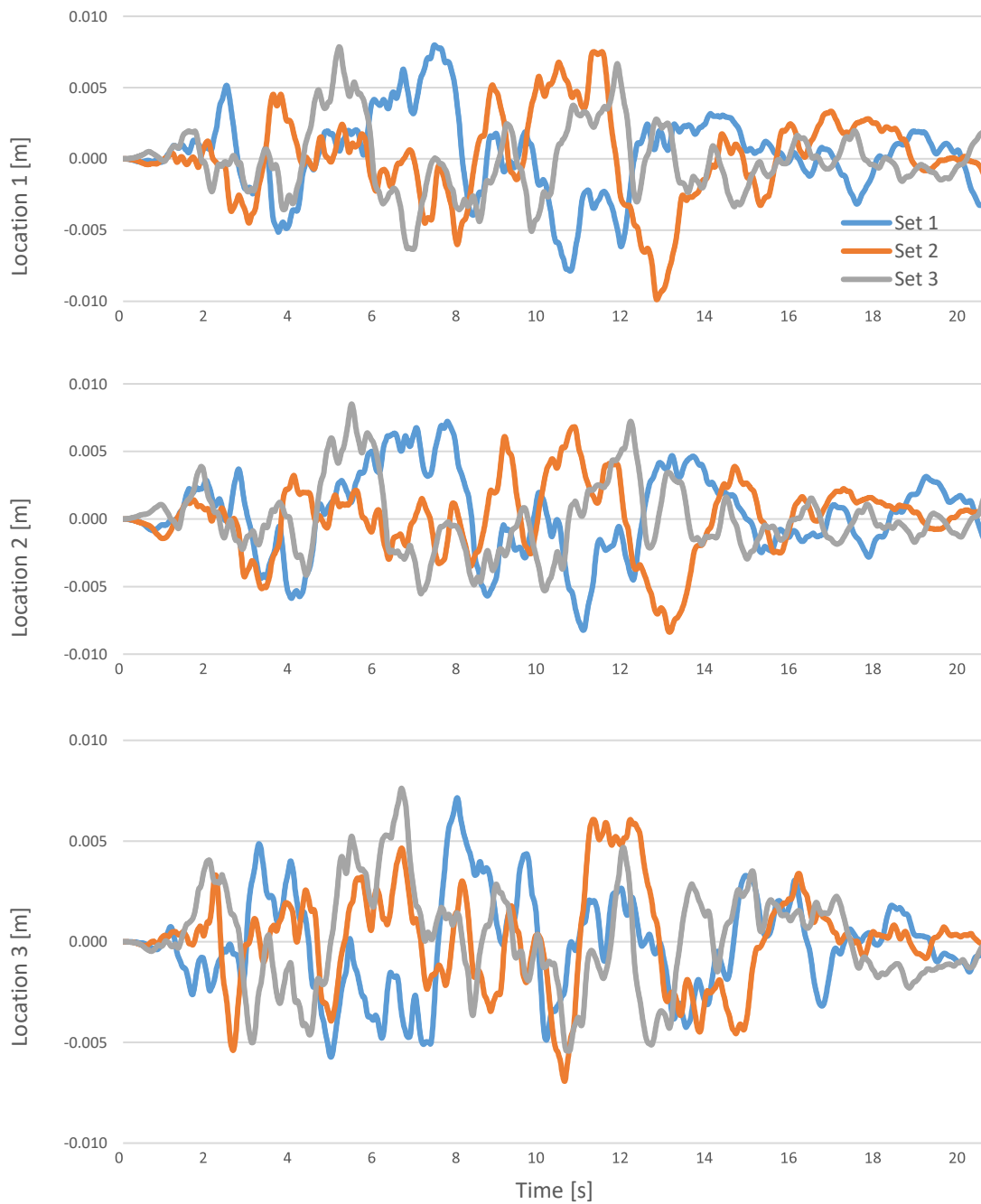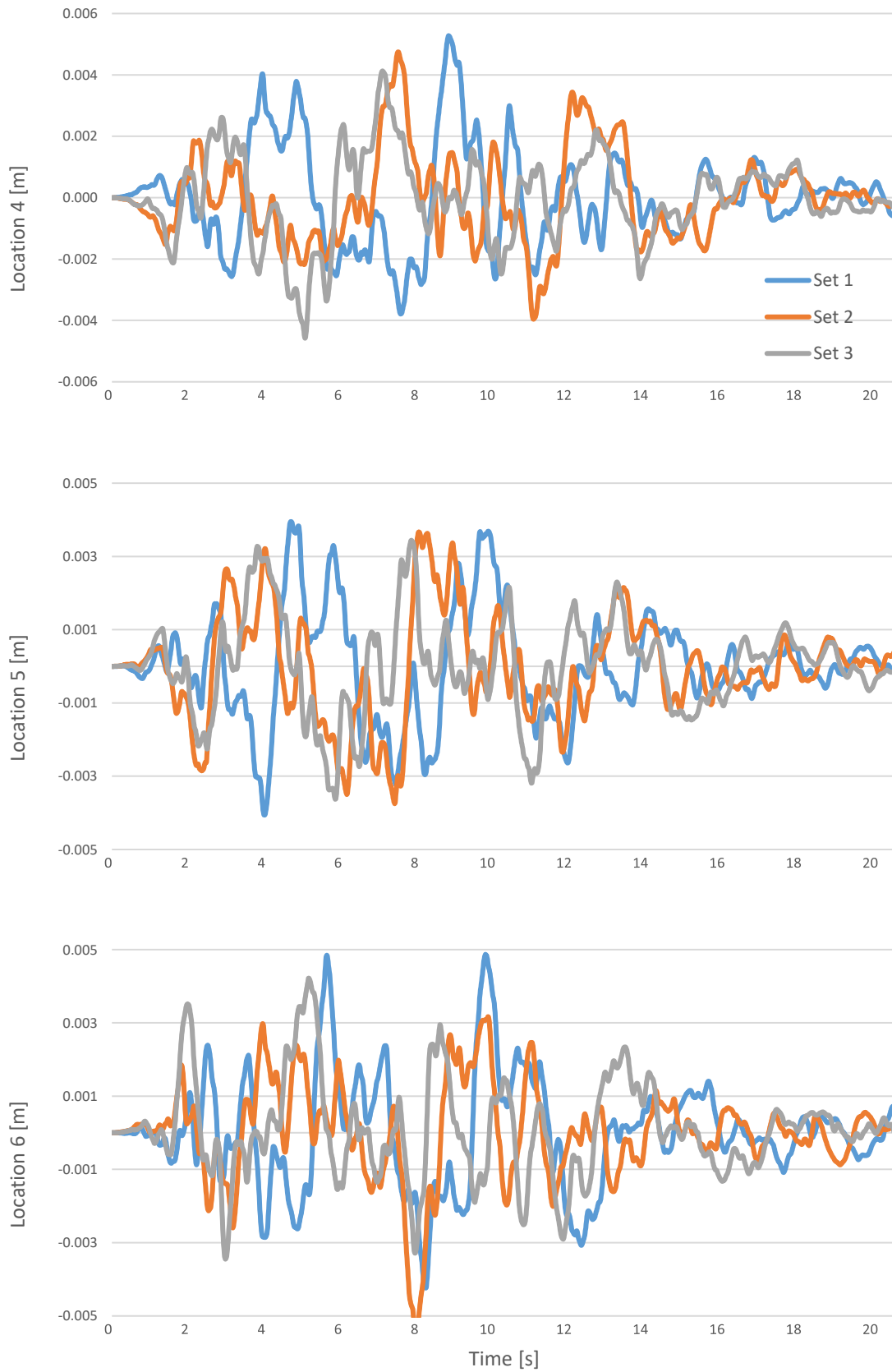**Figure B- 3: Generated ground motion in y-direction: Acceleration; Location 1-3**
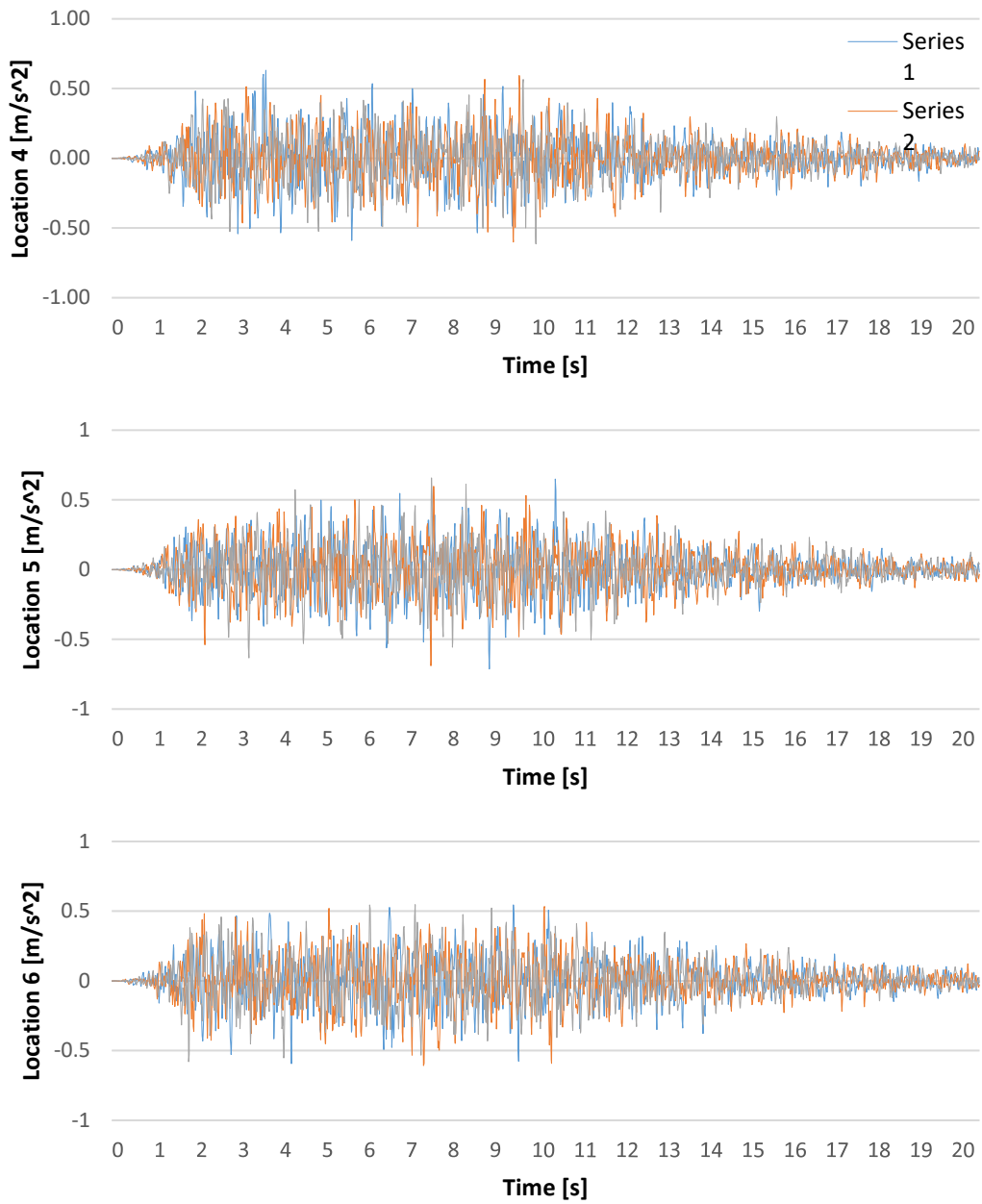
Figure B- 4: Generated ground motion in y-direction: Acceleration; Location 4-6

Z-direction ground motion acceleration
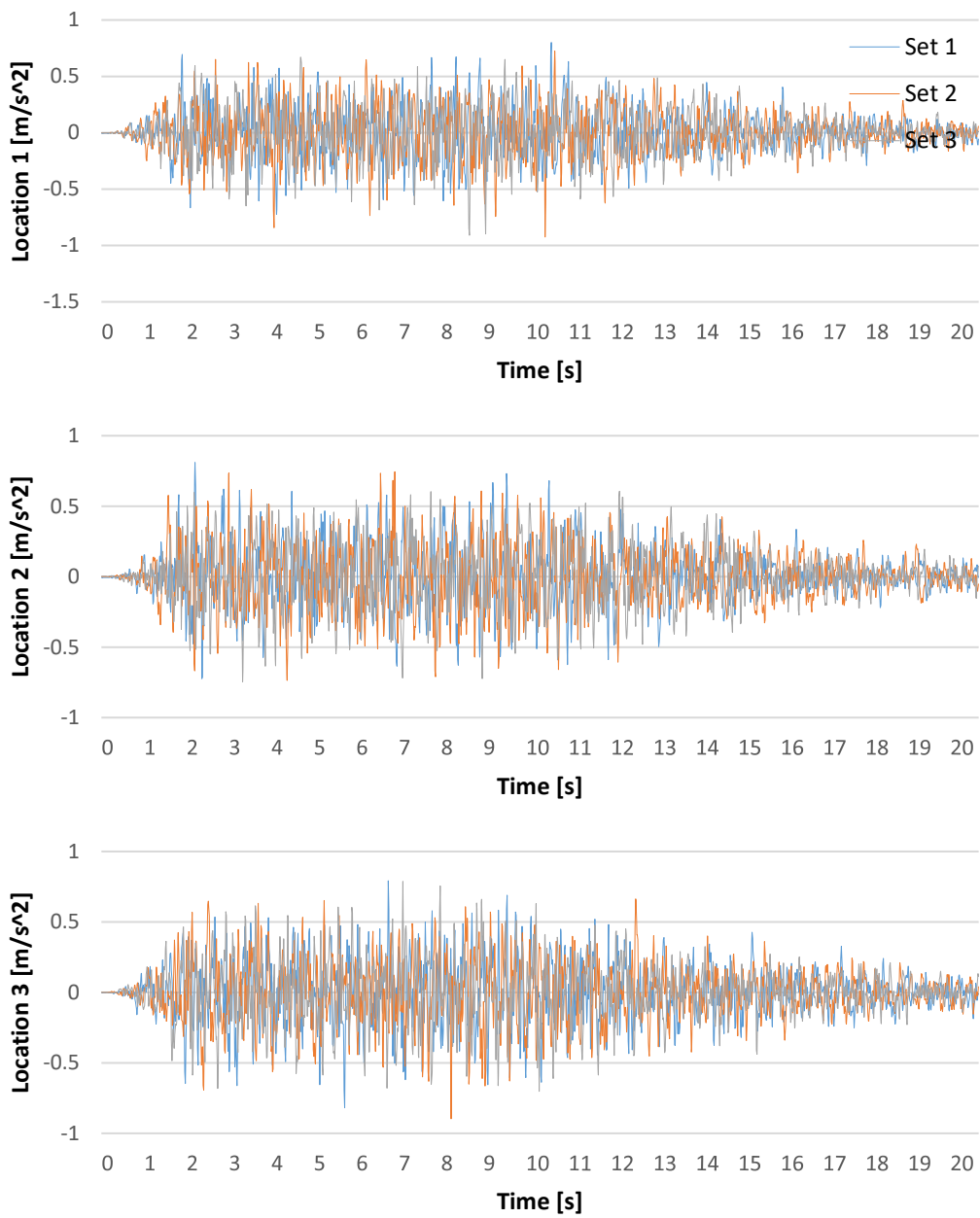
Figure B- 5: Generated ground motion in z-direction: Acceleration; Location 1-3

Figure B- 6: Generated ground motion in z-direction: Acceleration; Location 4-6
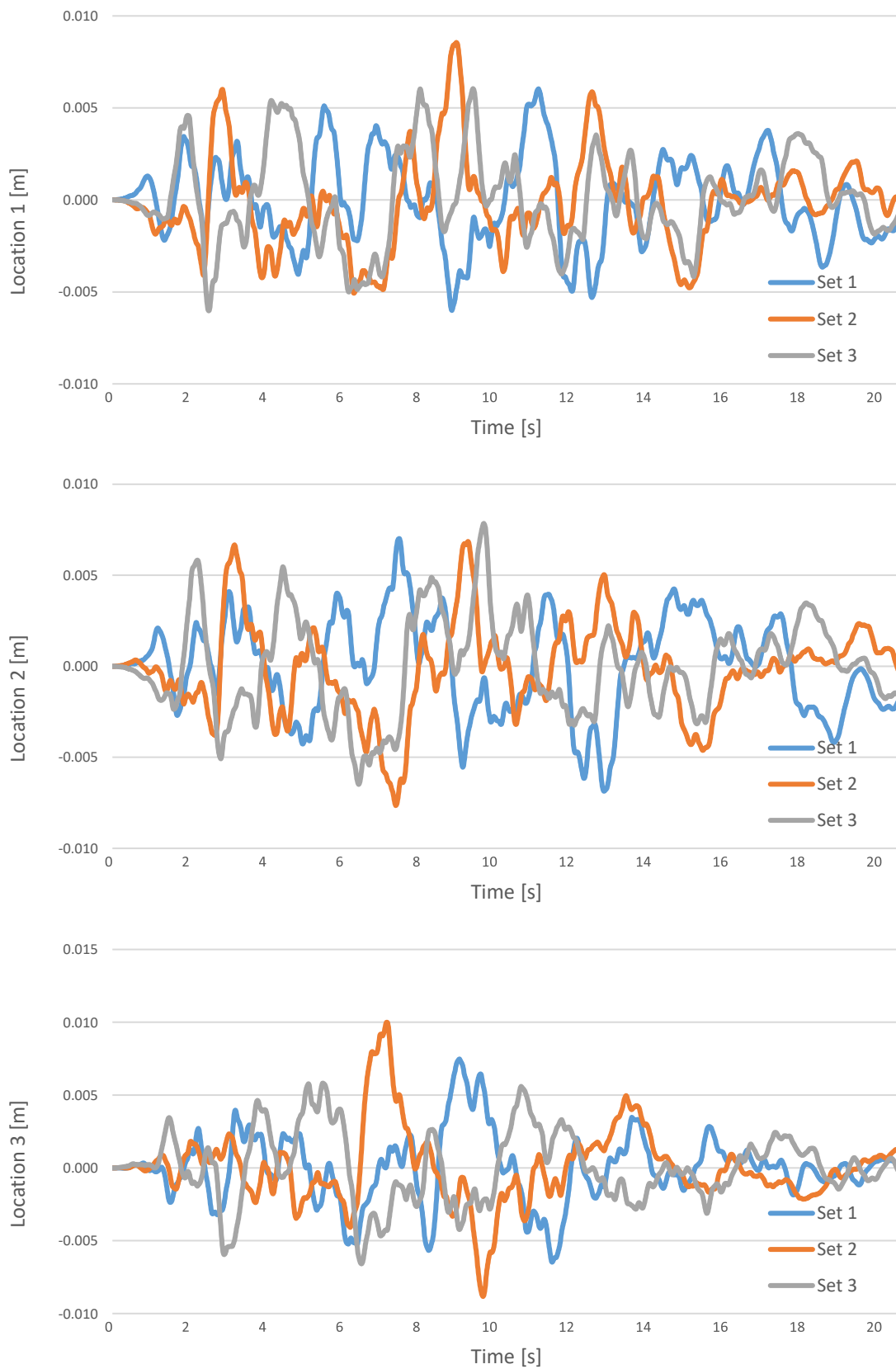
X-direction ground motion displacement

Figure B- 7: Generated ground motion in x-direction: Displacment; Location 1-3

Figure B- 8: Generated ground motion in x-direction: Displacment; Location 4-6

Y-direction ground motion displacement

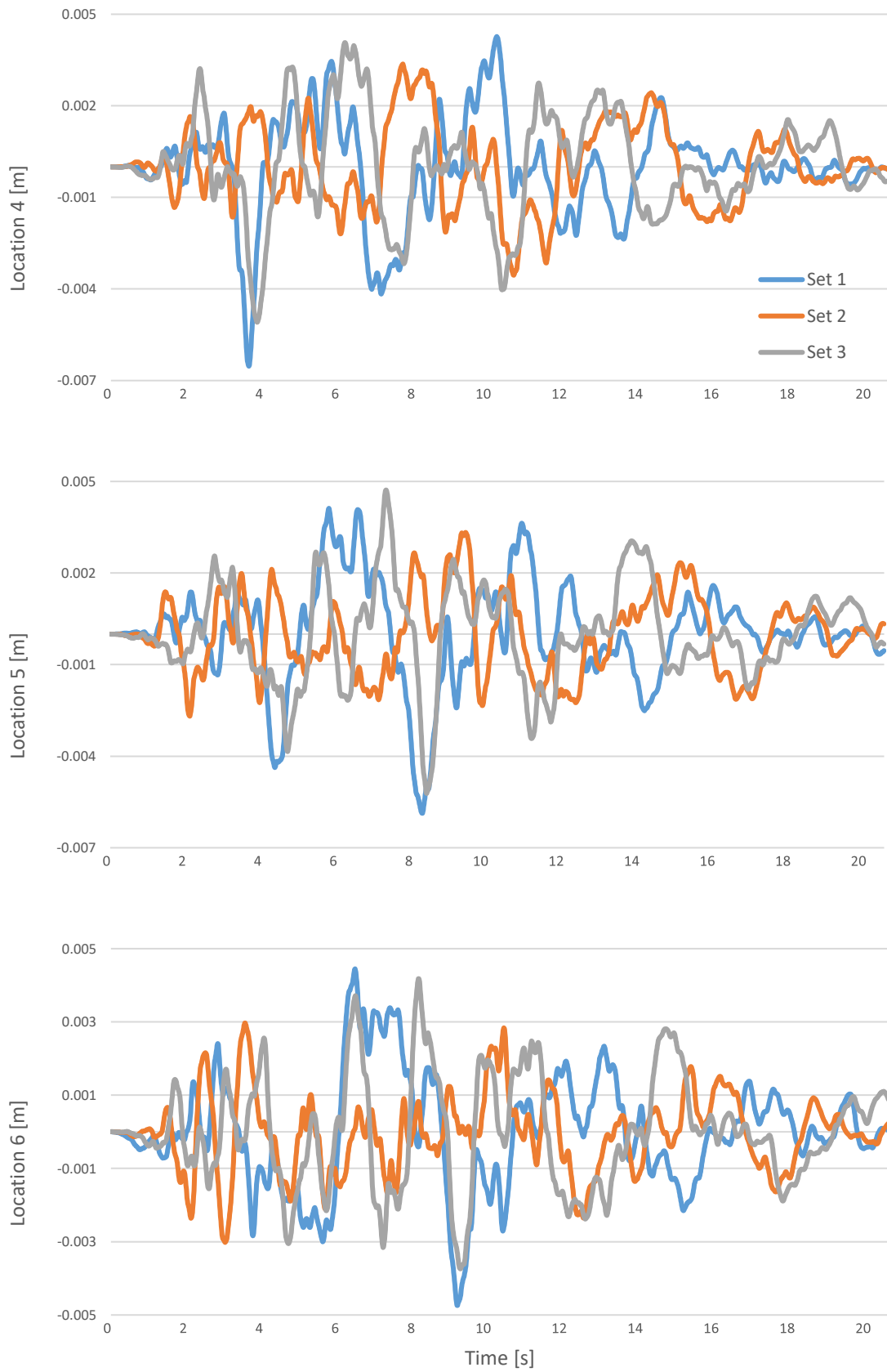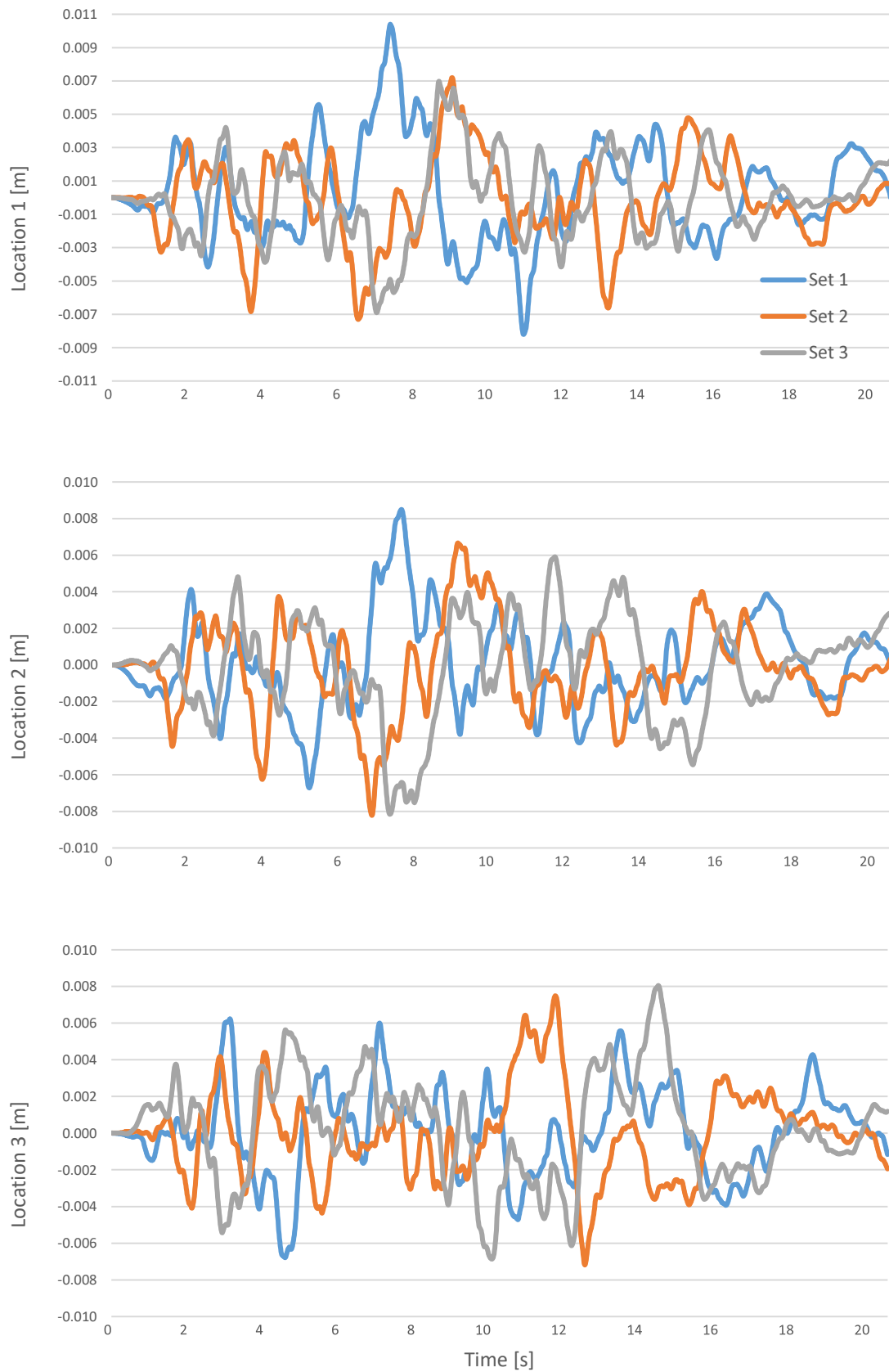**_Figure B- 9: Generated ground motion in y-direction: Displacment; Location 1-3_**

Figure B- 10: Generated ground motion in y-direction: Displacment; Location 4-6

Z-direction ground motion displacement

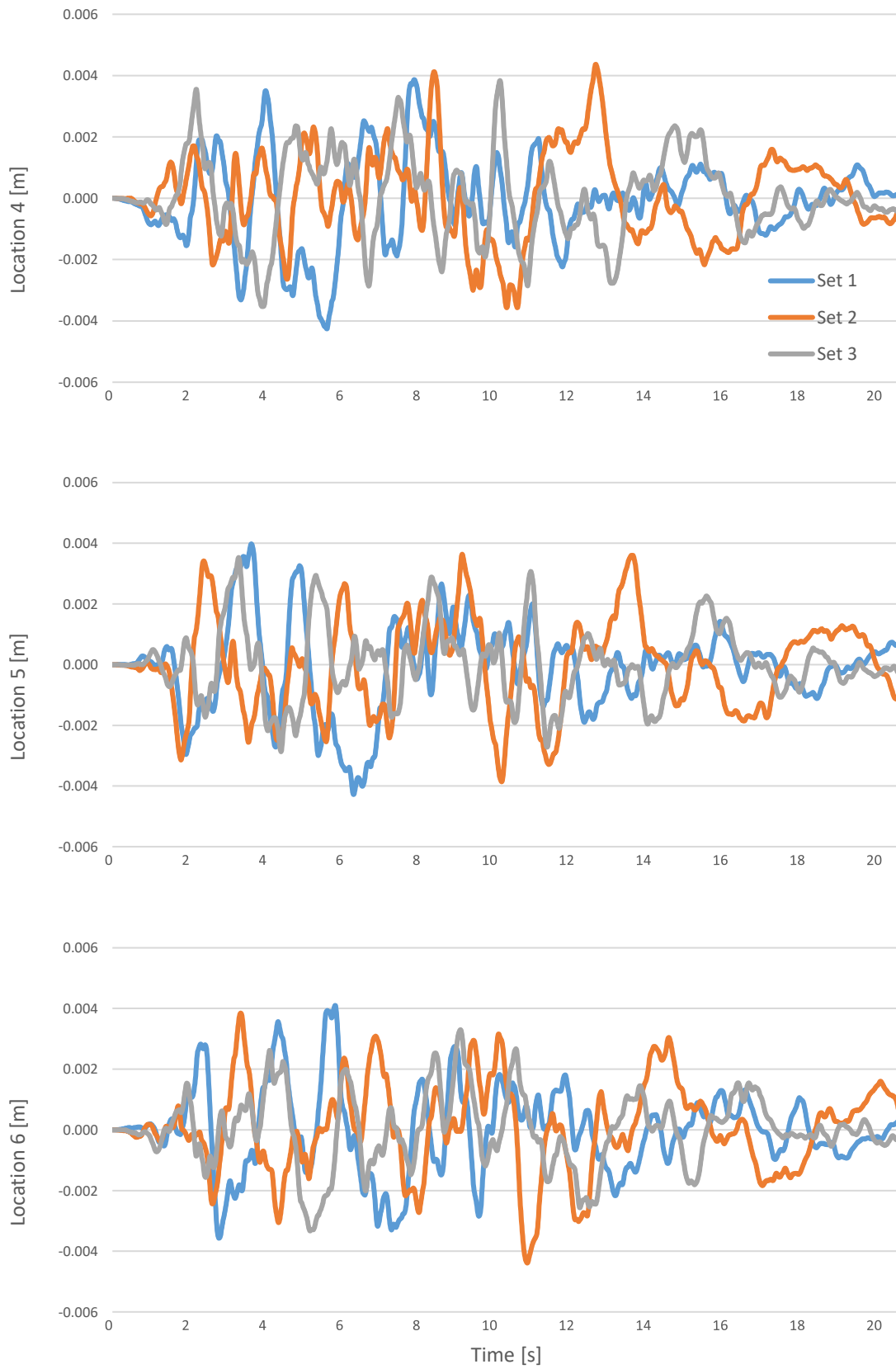**Figure B- 11: Generated ground motion in z-direction: Displacment; Location 1-3**

Figure B- 12: Generated ground motion in z-direction: Displacment; Location 4-6